Relativistic Effects in Gravitational Quantum States

(重力場中の量子状態における相対論的効果)

Ar Rohim

A thesis submitted to

Department of Physical Science

Graduate School of Science

Hiroshima University

December 2021

Abstract

In this thesis, we consider quantum states in an external gravitational field. The quantum nature is important on a microscopic level, whereas the gravity is important on a large scale. There are at present few examples in which the two important physics are simultaneously involved. The gravity is treated as a classical field so that our approach is semi-classical. However, the subject is of interest for theories and experiments in the future. We explicitly study the quantum states of a particle in an external gravitational field and bouncing on the floor of a perfectly reflecting mirror from the classical perspective. The gravitational acceleration is constant, such that the potential is linear with respect to distance. We focus upon the relativistic effects in gravitational quantum states from the perspective of the equivalence principle under appropriate boundary conditions. We investigate the problem for free Klein–Gordon, Dirac, and Majorana particles repeatedly bounced off by a uniformly accelerated mirror in Minkowski space. For the Klein–Gordon particle, we adopt the Dirichlet boundary condition of a vanishing scalar field at the mirror surface. The boundary condition for Dirac and Majorana particles is nontrivial. As an alternative, we use the boundary condition from the MIT bag model. The results show that the transition frequencies between the two energy eigenstates of all relativistic bouncing particles exceed their nonrelativistic limits, and the relativistic corrections to the transition frequencies of Dirac and Majorana bouncers exceed those of a Klein–Gordon bouncer. To further our understanding of the roles of boundary conditions, we also revisit the system of a Dirac particle confined in a 1D box in the absence of a gravitational field, using the chiral MIT boundary conditions. We discuss how the system depends on the boundary condition parameterized by the chiral angle. We find that the boundary condition for a Dirac particle in some specific initial spin orientations can generate the asymmetric distributions of the probability and scalar densities of a Dirac particle inside a box.

Articles

The content of this thesis is primarily based on the following two articles:

(1) Relativistic quantum bouncing particles in a homogeneous gravitational field
Ar Rohim, Kazushige Ueda, Kazuhiro Yamamoto, and Shih-Yuin Lin
Int. J. Mod. Phys. D **30**, 2150098 (2021)
doi:10.1142/S021827182150098X

(2) Effects of chiral MIT boundary conditions for a Dirac particle in a box
Ar Rohim and Kazuhiro Yamamoto
Prog. Theor. Exp. Phys. **2021**, 113B01 (2021)
doi:10.1093/ptep/ptab122

Contents

List of Figures

List of Tables

Chapter 1

Introduction

The interplay of quantum physics and gravity is of considerable interest. One remarkable example of this interplay is Hawking radiation [1]: By considering quantum fields on a Schwarzschild black-hole spacetime, Hawking demonstrated that a black hole emits thermal radiation with a temperature depending on its mass. A similar effect arises in uniformly accelerated systems; that is, the accelerated observer sees the Minkowski vacuum as a thermal state with a temperature [2]. Thus, studies on quantum effects under the influence of gravitational fields are challenging; furthermore, very few phenomena can be observed or tested in the laboratory. One example system that can be tested in experiments is the quantum bouncer; this comprises a particle trapped in a linear gravitational potential, bouncing on the fixed floor of an ideal mirror. Theoretical analysis of the quantum bouncer has been presented and explored in many literatures (see, e.g., Refs. [3–13]). Interestingly, the gravitational quantum states have been experimentally checked using ultracold neutrons (UCNs) [14] (see also, e.g., Refs. [15–20]).

In realistic situations, the potential surrounding the glass mirror is described by a Fermi-pseudo potential. This potential is considerably larger than the transversal energy of the particle, where the lowest energy of neutrons quantum bouncer is of the order of peV (see, e.g., Ref. [21]); thus, we can approximate that the bouncing particle sees an infinite potential around the mirror surface. In a nonrelativistic treatment of the quantum bouncer, the wave function should vanish at the boundary surface because the particle is perfectly reflected by an infinite potential barrier, such that the stationary bound states exhibit discrete energy levels associated with the normalizable wave function. An observer attached to the mirror would experience the effect as a gravitational field. In this approach, which is based on the equivalence principle of relativity [22], we investigate the quantum bouncer problem for

relativistic bouncing particles under appropriate mirror boundary conditions. Namely, a particle bouncing on a fixed mirror under the influence of a gravitational field is equivalent to a free particle repeatedly bounced off by a uniformly accelerated mirror in Minkowski space. To describe the trajectory of the uniformly accelerated mirror, we introduce Rindler coordinates. We primarily discuss the relativistic effects in gravitational quantum states by solving the quantum bouncer problem for Klein–Gordon and Dirac equations in Rindler coordinates under the mirror boundary conditions. Note that the system of a Klein-Gordon bouncing particle under a uniformly accelerated ideal mirror has been previously investigated by Ref. [24]. The study was extended to a Dirac bouncing particle in Ref. [23]. In the nonrelativistic limit, the energy levels of Klein–Gordon and Dirac bouncing particles reduce to familiar eigen-energies for the Schrödinger equation in a gravitational field under the Dirichlet boundary condition of an ideal mirror, as has been shown by Ref. [23].

To investigate the bound state of a Klein–Gordon bouncer, we follow Ref. [24] to use the Dirichlet boundary condition of a vanishing scalar field at the mirror surface; this is applicable because the particle approximately sees an infinite Fermi pseudo-potential barrier. As noted in Ref. [23], the extension to a Dirac bouncing particle is nontrivial. Imposing the Dirichlet boundary condition on the Dirac equation causes the Dirac wave function to vanish everywhere trivially [23]. Therefore, Ref. [23] used an alternative boundary condition to discuss the problem for the Dirac bouncing particle (cf. Refs. [25–27]). In this thesis, we follow Ref. [25] to use the boundary condition given in the MIT bag model (BC-MIT) [28, 29] (see also Ref. [30] for a review) as an alternative for the Dirac equation to represent the description of the Fermi pseudo-potential barrier of the mirror while avoiding the Klein paradox problem [31]. The BC-MIT ensures the vanishing of the normal probability current and scalar densities at the boundary surface [32]. The probability density of a Dirac particle does not vanish around the boundary surface (see Ref. [26] for the confinement system). This behavior implies that the chiral symmetry is broken. To resolve this issue, Ref. [33] introduced the chiral bag model (see also Refs. [34–42]), which restores the symmetry breaking via a pion field outside the bag [37, 43]. However, in our mirror model for the UCN, the boundary thickness is of the order of 0.1 nm, far larger than the size of a hadron. Hence, we choose to adopt the BC-MIT rather than boundary condition given in the chiral (or little/cloudy) bag model [33–42], even though the chiral bag model is more realistic than the MIT bag model for hadrons.

The neutron can also be presented as a Majorana fermion when neutron-antineutron oscillation exists [44–51]. Therefore, it is also essential to discuss the UCN quantum bouncer problem using a Majorana particle under an appropriate mirror boundary condition for

the complementary. In this study, the Majorana wave function is obtained from a linear combination of the Dirac wave function and its charge conjugation [49] under an additional condition (i.e., that the charge conjugation of the Majorana wave function is the same as itself), which ensures that the Majorana wave function also satisfies the Dirac equation. A similar problem to that of the Dirac particle occurs at the boundary condition for the Majorana particle; that is, the Dirichlet boundary condition cannot be applied to investigate the bound system. Instead, we use the BC-MIT [28–30] as an alternative boundary condition for the Majorana particle, as we apply for the Dirac particle.

Alongside the above approximations, we investigate the energy levels and transition frequencies between two energy eigenstates for all relativistic bouncing particles. We compare the results for relativistic bouncing particles with their nonrelativistic limits. This comparison indicates the presence of relativistic corrections. Then, we apply the relativistic corrections thereby obtain to the transition frequencies for the UCN. In our system, the boundary conditions play a critical role because the precise properties of the wave function cannot be discussed without an appropriate boundary condition. We further discuss how the boundary condition affects the density functions, namely, the particle localization probability, current density in the normal direction, and scalar densities.

The likelihood of experimental observations of gravitationally quantum bound states of Ps atoms has been discussed in Refs. [52, 53] (cf. Refs. [54, 55] for the discussion on the feasibility of the gravitational free-fall experiment of Rydberg Ps atom). Compared to the UCN, the Ps atom has a lighter mass; thus, the energy levels of the Ps atom quantum bouncer are smaller than those of the UCN. In contrast, the relativistic corrections to the Ps atom transition frequencies exceed those of the UCN. In this thesis, we also apply the analytical results for the Ps atom.

The Foldy–Wouthuysen transformation [56] (see also Refs. [57–59]) for the Hamiltonian of the Dirac equation in Rindler coordinates (see, e.g., Refs. [23, 60–62][1]) can be used to investigate the relativistic corrections of the energy levels of relativistic particles [23]. Using this transformation, the relativistic Hamiltonian from the Dirac equation reduces to the nonrelativistic one. We can perform a perturbation approximation to obtain the relativistic corrections to the energy level [23]. Using this approximation, we find that the first-order relativistic energy level corrections obtained from the lowest order of the Foldy–Wouthuysen transformed Hamiltonian coincide with those of the Klein–Gordon bouncing particle under the Dirichlet boundary condition of a vanishing field at the mirror surface. This condition

---

[1]Refs. [23, 60–62] have computed the Foldy–Wouthuysen transformation for the Hamiltonian of the Dirac equation in Rindler coordinates using the metric first given in Ref. [63].

may give an additional hint that the boundary condition would be essential to investigate the energy level of bouncing particles.

The authors of Refs. [34] introduced the general form of the BC-MIT, which keeps ensuring a vanishing normal probability current density at the boundary surface. The general form of the BC-MIT conditions that includes the contribution of the chiral angle is referred to as the chiral MIT boundary conditions (BC-chiral MIT) [34, 64, 65]. The energy levels of a particle under these boundary conditions may depend on the chiral angle [65]. Several studies have applied the BC-chiral MIT, e.g., Refs. [66–69] used it to confine Dirac fermions in a rotating system. Interestingly, the author of Ref. [25] reported that the BC-chiral MIT could be used to analyze the change of spin orientations; there, the wave function was written as a linear combination of the incident and reflected wave components associated with their spin orientations.

To further our understanding of the roles of boundary conditions, we also revisit the system of a Dirac particle confined in a 1D box in the absence of a gravitational field, using the BC-chiral MIT to describe the properties of the walls or mirrors [70]. Such systems have been discussed in Ref. [26] (cf. Ref. [27] for a discussion of the system in a 3D box); however, they there used the BC-MIT as an alternative boundary condition to avoid the Klein-paradox problem. Other previous studies into confined relativistic particles can be found in, e.g., Refs. [43, 71–78]. Along with this analysis, we investigate how the discrete momenta and energy levels of a Dirac particle behave under boundary conditions. Then, we discuss how the spin orientations change, owing to reflections at the mirrors. Because the boundary conditions relate to the behaviors of density functions, we recast our analysis of the quantum bouncer to analyze the behavior of the probability, normal probability current, and scalar densities of a Dirac particle inside a box. Our calculation for this system is limited to one dimension; however, our study may facilitate exploration of related topics on finite-size effects and chiral symmetry breaking, although this subject has already been considered in, e.g., Refs. [66, 67] (cf. Ref. [79] for a discussion on the Nambu–Jona-Lasinio (NJL) model using the BC-MIT).

The remainder of this thesis is organized as follows. In Chap. 2, we briefly review the bound states of a nonrelativistic bouncing particle in a homogeneous gravitational field with an ideal mirror boundary condition; here, we also briefly review the properties of UCNs and Ps atoms. In Chap. 3, we discuss the bound states of a Klein–Gordon bouncing particle under the Dirichlet boundary condition of a vanishing scalar field at the mirror surface. In Chap. 4, we investigate the bound states of Dirac and Majorana bouncing particles under the BC-MIT in the case of arbitrary spin orientations. In Chap. 5, we discuss the roles of boundary

conditions in the quantum states of bouncing particles in a homogeneous gravitational field, by comparing the energy levels and transition frequencies between two energy eigenstates for all bouncing particles, as well as discussing their density functions (especially around the mirror surface); in this chapter, we also discuss the Foldy–Wouthuysen transformation for the Dirac equation in Rindler Coordinates, and we investigate relativistic corrections to the energy levels, using the perturbation approximations. In Chap. 6, we analyze the roles of the BC-chiral MIT on the system of a Dirac particle confined in a 1D box in the absence of a gravitational field. We discuss how the discrete momenta and energy levels depend on the chiral angle parameters. We also analyze how the reflections with the boundary surface under the BC-chiral MIT generate changes of the spin orientations, and we discuss the behaviors of the density functions with respect to the chiral angle and initial spin orientation. In Chap. 7, we provide our summary and conclusions. In Appendix A, we briefly review the solution to the Dirac equation in Minkowski coordinates. In Appendix B, we briefly review the two alternative boundary conditions that we apply to the Dirac equation: the BC-MIT and BC-chiral MIT. Throughout this thesis, we use units of $c = \hbar = 1$.

Chapter 2

Gravitational Quantum States of a Bouncing Particle in Nonrelativistic Quantum Mechanics

In this chapter, we primarily learn the well-known feature of the quantum bouncer, which is the existence of the bound states of a particle trapped in a gravitational field and bouncing above a perfectly reflecting mirror in the viewpoint of nonrelativistic quantum mechanics. We explicitly discuss the quantum bouncer problem by investigating the Schrödinger equation in a linear gravitational potential with an ideal mirror. We start with a brief review of the properties of UCNs and Ps atoms. Then, we discuss the bound state under the Dirichlet boundary condition of a vanishing wave function at the mirror surface. We will show that the quantum bouncer exhibits discrete energy levels, as demonstrated in the literatures (see, e.g., Refs. [3–12]). We also briefly discuss the applications of the analytic solution of energy levels to UCN and Ps atoms.

2.1 Ultracold Neutrons and Positronium Atoms

2.1.1 Ultracold Neutrons

The research on neutron optics has been discussed and reported, e.g., in Refs. [80–89]; see also Ref. [90] for the discussion on the transmission of the electromagnetic wave through an accelerated dielectric slab. The observation of the gravitational quantum states of UCNs

[14–20] is an application of neutron optics under the influence of a gravitational field, in which the particle bouncing above a reflecting mirror and exhibits discrete energy levels; see also Refs. [91, 92] for the observation of UCNs. Another quantum bouncer system, namely, the centrifugal quantum states near the cylindrical mirror is discussed in Refs. [93, 94]. In such a system, the particle experiences a centrifugal force. UCNs are neutrons with kinetic energy lower than the step barrier of the Fermi pseudo-potential of materials [95]. Under this condition, UCNs can be totally reflected by appropriate materials at arbitrary incidence angles. The mass of neutron is approximately 0.94 GeV [96]. The neutron lifetime is longer than the observational time of the quantum bouncer under the gravitational field [14]. Along with the mentioned properties and neutrality of neutrons, they can be successfully used as an experimental object to observe gravitationally quantum bound states [14] (see also Refs. [15–20]), for which a reflecting mirror must be used to trap the particle in a linear gravitational potential [14].

2.1.2 Positronium Atom

As mentioned in the introduction, the possibility of observing the gravitationally quantum bound states of Ps atoms has been discussed in Refs. [52, 53]. Ps atom consists of an electron and positron (matter and antimatter); it has a total mass of approximately 1 MeV, which is roughly around 10^3 times smaller than neutron mass. Furthermore, the lifetime of a Ps atom is shorter than the observation time. To increase its lifetime, Ps atom should be placed in the Rydberg state n'; this can increase its lifetime by a factor of n'^3 [52, 54].

2.2 Quantum Mechanical Description of a Bouncing Particle in a Gravitational Field

In the following, we review the quantum mechanical description of the quantum bouncer in 1+1D system. We consider a particle bouncing on a rest floor under the influence of a linear gravitational potential

$$V(z) = \begin{cases} maz, & \text{for } z > 0, \\ \infty, & \text{for } z \leq 0. \end{cases} \tag{2.1}$$

Here, m and $a = g$ denote the mass and uniform (gravitational) acceleration of the particle, respectively. In this system, we take the approximation in which the potential around the mirror surface at $z = 0$ is infinite; hence, the particle can only move in the region of $z > 0$.

2.2.1 Schrödinger Equation in a Gravitational Field

The dynamics of a particle bouncing above a perfectly reflecting mirror in a linear gravitational potential (2.1) can be described by the time-dependent Schrödinger equation, as follows

$$i\frac{\partial}{\partial t}\Psi(z,t) = -\frac{1}{2m}\frac{\partial^2\Psi(z,t)}{\partial z^2} + maz\Psi(z,t). \tag{2.2}$$

By introducing the following general solution

$$\Psi(z,t) = e^{-iE_n t}\psi_n(z), \tag{2.3}$$

we find that the wave function $\psi_n(z)$ satisfies the time-independent Schrödinger equation, as follows

$$-\frac{1}{2m}\frac{d^2\psi_n(z)}{dz^2} + maz\psi_n(z) = E_n\psi_n(z). \tag{2.4}$$

To solve the above equation, it is more convenient to introduce the parameter of $\zeta = z/\mathcal{B}$, where $\mathcal{B}$ is the gravitational length scale explicitly given by [7]

$$\mathcal{B} = \left(2m^2a\right)^{-1/3}. \tag{2.5}$$

Then, the above time-independent Schrödinger equation (2.4) can be written as follows

$$-\frac{d^2\psi_n(\zeta)}{d\zeta^2} + (\zeta - \zeta_n)\psi_n(\zeta) = 0. \tag{2.6}$$

Here, ζ_n is defined as $\zeta_n = E_n/(ma\mathcal{B})$. The second-order differential equation (2.6) is the Airy differential equation, which takes a solution consisting of a linear combination of Airy function $\mathrm{Ai}(\zeta - \zeta_n)$ and Airy function $\mathrm{Bi}(\zeta - \zeta_n)$ [97]. The Airy function $\mathrm{Ai}(\zeta - \zeta_n)$ converges goes to zero as ζ goes to infinity. By contrast, the Airy function $\mathrm{Bi}(\zeta - \zeta_n)$ diverges goes to infinity with the growth of ζ (see Fig. 2.1). In the quantum bouncer, the wave function vanishes under the increases of height $z(\equiv \mathcal{B}\zeta)$, which is described by the boundary conditions $\psi(z \to \infty) = 0$. Therefore, the Airy function Bi cannot be used as a
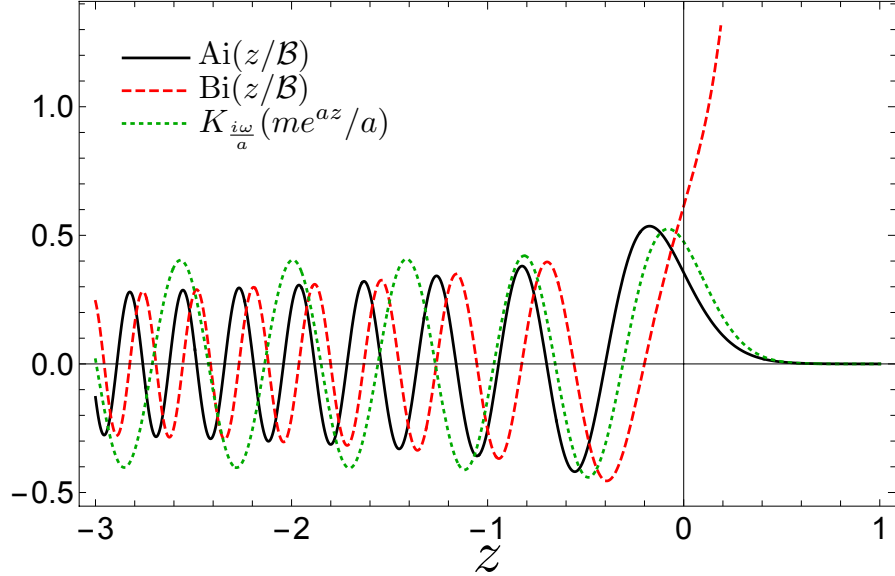
FIGURE 2.1: The solid black line is Airy function $\text{Ai}(z/\mathcal{B})$, the dashed red line is Airy function $\text{Bi}(z/\mathcal{B})$, and the dotted green line is second kind of the modified Bessel function $K_{\frac{i\omega}{a}}(me^{az}/a)$. Here, we used mass $m = 10$, uniform acceleration $a = 1$, $\omega = 11$, and $\mathcal{B}$ is the length scale defined in Eq. (2.5). Both the Airy function Ai and modified Bessel function converges goes to zero as the increases of z. In contrast, the Airy function Bi diverges goes to infinite as the increases of z. This figure is reproduced from Ref. [31].

solution, and an appropriate solution for the equation (2.6) can be given by Airy function $\text{Ai}(\zeta - \zeta_n)$ only; this is explicitly given as

$$\psi_n(\zeta) = \mathcal{N}_n \text{Ai}(\zeta - \zeta_n). \tag{2.7}$$

Here, $\mathcal{N}_n$ is the normalization constant, defined as

$$\int_0^\infty |\Psi_n(t, z)|^2 dz = \int_0^\infty |\psi_n(z)|^2 dz = \int_0^\infty \mathcal{B}|\mathcal{N}_n|^2 \left[\text{Ai}(\zeta - \zeta_n)\right]^2 d\zeta = 1, \tag{2.8}$$

where we have used the relation of $z = \mathcal{B}\zeta$ with the parameter values ζ_n are determined by the boundary condition, as we will show below.

2.2.2 Bound States of a Bouncing Particle in a Gravitational Field

As mentioned above, in a realistic system, the contact potential around the glass mirror is finite and may depend on the momentum of the bouncing particle [98, 99]. However, the potential around the mirror is considerably much larger than the energy of the UCN [21]. Under this condition, we can assume that a bouncing particle sees an infinite potential at

the mirror surface; thus, the Dirichlet boundary condition of a vanishing wave function at the floor is sufficient to investigate the bound system. Imposing this Dirichlet boundary condition to the wave function (2.7) at the reflecting mirror located at $z = 0$ leads to the following condition [7]

$$\mathrm{Ai}(-\zeta_n) = 0, \quad n = 1, 2, 3, \dots . \tag{2.9}$$

From the boundary condition (2.9), we can see that $-\zeta_n$ refers to the zeros of the Airy function, which takes negative and discrete values (see Fig. 2.1). Hence, the value of parameter ζ_n is discrete positive. The essential feature from the boundary condition (2.9) is that the energy of a bouncing particle for states n is also discrete and explicitly given by

$$E_n = ma\mathcal{B}\zeta_n, \tag{2.10}$$

where its values are also always positive; see Table 2.1 for the lowest few energy levels of a neutron.

It is well-known that the analytical expression of the zeros of the Airy function $-\zeta_n$ cannot be found exactly in an analytic way. However, the Wentzel-Kramers-Brillouin (WKB) approximation gives a high precision; approximately, it is given as [5, 7]

$$\zeta_n^{\mathrm{WKB}} \simeq \left[\frac{3\pi}{2} \left(n - \frac{1}{4} \right) \right]^{2/3}, \tag{2.11}$$

and the normalization constant under the WKB approximation is approximately given by (see Ref. [7])

$$\sqrt{\mathcal{B}}\mathcal{N}_n^{\mathrm{WKB}} \simeq \left[\frac{8\pi^2}{3(4n-1)} \right]^{1/6}. \tag{2.12}$$

The turning point of a classical particle is given by [17, 20]

$$z_n = \mathcal{B}\zeta_n, \tag{2.13}$$

which is also discrete. From the above derivations, we can see that the mass dependences of the energy level (2.10) and the turning point (2.13) appear in the factors $m^{1/3}$ and $m^{-2/3}$, respectively. Therefore, the energy level and turning point of the Ridberg Ps atom are 10 times smaller [52] and 10^2 times higher than for those of the UCN at the same state n, respectively.

TABLE 2.1: The first six values of the parameters ζ_n (left column) in comparison with those of ζ_n^{WKB} (middle column). Here, we also provides the first six values of the energy level E_n (right column) of a neutron with mass $m \approx 0.94$ GeV and uniform acceleration $a \approx 2.15 \times 10^{-32}$ GeV.

n	ζ_n	ζ_n^{WKB}	E_n (peV)
1	2.338	2.320	1.406
2	4.088	4.082	2.458
3	5.521	5.517	3.319
4	6.787	6.784	4.080
5	7.944	7.942	4.776
6	9.023	9.021	5.424

Table 2.1 provides the first six values of the parameter ζ_n and the energy level E_n for the neutron with mass $m \approx 0.94$ GeV [96] and acceleration $a \approx 2.15 \times 10^{-32}$ GeV. From this table, we can also see that the values of parameter ζ_n^{WKB} obtained from WKB approximation approaches to the value of parameter ζ_n as the increases of the state n.

Chapter 3

Gravitational Quantum States of a Klein–Gordon Bouncing Particle

In this chapter, we discuss the bound states of a Klein–Gordon bouncer in the viewpoint of the equivalence principle of relativity. We analyze the problem by investigating the Klein–Gordon equation in Rindler coordinates under the boundary condition of an ideal mirror. We begin by briefly deriving the solution to the Klein–Gordon equation in Rindler coordinates [100] (cf. Ref. [101]). Then, we follow Ref. [24] to use the Dirichlet boundary condition of the vanishing scalar field at the mirror surface to derive the energy eigenstates of a Klein–Gordon bouncer. From the obtained boundary condition, we proceed to express the energy level using the approximation formula given in Ref. [102]. The application of this solution to the UCN and Ps atom, as well as the comparison with the energy levels of the other bouncing particles, will be discussed in Chap. 5.

3.1   Rindler Coordinates

Rindler coordinates (η, x, y, ξ) describe a uniformly accelerated observer in Minkowski coordinates (t, x, y, z); these two coordinate systems can be related via the following transformation:

$$t = \frac{e^{a\xi}}{a} \sinh a\eta \quad \text{and} \quad z = \frac{e^{a\xi}}{a} \cosh a\eta. \tag{3.1}$$

Here, a denotes a uniform acceleration in the z-direction. The line element in Minkowski coordinates is given by

$$ds^2 = \eta_{\mu\nu}dx^\mu dx^\nu = dt^2 - dx^2 - dy^2 - dz^2, \tag{3.2}$$

where in the present thesis we use $\eta_{\mu\nu} = \text{diag.}(1, -1, -1, -1)$. Using the transformations given in Eq. (3.1), the line element in Rindler coordinates can be expressed as [103, 104]

$$ds^2 = g_{\mu\nu}dx^\mu dx^\nu = e^{2a\xi}(d\eta^2 - d\xi^2) - dx^2 - dy^2, \tag{3.3}$$

where $g_{\mu\nu} = \text{diag.}(e^{2a\xi}, -1, -1, -e^{2a\xi})$.

3.2 Klein–Gordon Equation in Rindler Coordinates

We consider a free massive scalar field ϕ in curved spacetime, with an action given by

$$S = \frac{1}{2} \int d^4x \sqrt{-g} \left(g^{\mu\nu} \partial_\mu \phi \partial_\nu \phi - m^2 \phi^2 \right), \tag{3.4}$$

where m is the mass of the scalar field. Taking the variation of the above action, we obtain the Klein–Gordon equation in curved spacetime, as follows

$$\frac{1}{\sqrt{-g}} \partial_\mu \left(\sqrt{-g} g^{\mu\nu} \partial_\nu \phi \right) + m^2 \phi = 0. \tag{3.5}$$

Using the Rindler metric (3.3), the Klein–Gordon equation in Rindler coordinates reads

$$\left(\frac{\partial^2}{\partial\eta^2} - \frac{\partial^2}{\partial\xi^2} - e^{2a\xi} \frac{\partial^2}{\partial\boldsymbol{x}_\perp^2} \right) \phi + m^2 e^{2a\xi} \phi = 0, \tag{3.6}$$

where $\boldsymbol{x}_\perp \equiv (x, y)$ denotes the coordinates perpendicular to the direction of the uniform acceleration a. To proceed, we introduce the ansatz for the positive-frequency solution as

$$\phi_{\omega\boldsymbol{k}_\perp} = f^{\text{KG}}_{\omega\boldsymbol{k}_\perp} e^{i\boldsymbol{k}_\perp \cdot \boldsymbol{x}_\perp - i\omega\eta}, \tag{3.7}$$

where $\boldsymbol{k}_\perp = \sqrt{k_1^2 + k_2^2}$ is the momentum perpendicular to the direction of the uniform acceleration a. Substituting the positive-frequency ansatz solution (3.7) into the Klein–Gordon equation (3.6), we obtain a differential equation, known as the modified Bessel differential

equation, as follows

$$\frac{1}{a^2}\frac{\partial^2}{\partial\xi^2}f^{\mathrm{KG}}_{\omega\boldsymbol{k}_\perp} = \left[(m^2+\boldsymbol{k}_\perp^2)\frac{1}{a^2}e^{2a\xi}+\left(\frac{i\omega}{a}\right)^2\right]f^{\mathrm{KG}}_{\omega\boldsymbol{k}_\perp}. \tag{3.8}$$

The solution of the modified Bessel differential equation consists of a linear combination of the second kind of modified Bessel function $K_\nu(z)$ and the first kind of modified Bessel function $I_\nu(z)$; $I_\nu(z)$ diverges to infinity as the parameter z increases; meanwhile, $K_\nu(z)$ converges to zero under z increases [97] (see also Fig. 2.1). Therefore, the solution to the above differential equation (3.8) consists of the second kind of modified Bessel function $K_\nu(z)$ only, and is given as (see, e.g., Ref. [100])

$$\phi_{\omega\boldsymbol{k}_\perp}(\eta,\xi,\boldsymbol{x}_\perp) = \mathcal{N}^{\mathrm{KG}}_{\omega\boldsymbol{k}_\perp} K_{\frac{i\omega}{a}}\left(\frac{\kappa}{a}e^{a\xi}\right)e^{i\boldsymbol{k}_\perp\cdot\boldsymbol{x}_\perp-i\omega\eta}, \tag{3.9}$$

where $\kappa=\sqrt{m^2+\boldsymbol{k}_\perp^2}$ and $\mathcal{N}^{\mathrm{KG}}_{\omega\boldsymbol{k}_\perp}$ is a normalization constant determined depending on the boundary condition. We will see that ω should be discrete in the presence of the mirror boundary condition. In contrast, ω will takes the continuous values $0\leq\omega<\infty$ in the absence of the mirror.

3.3 Bound States of a Klein–Gordon Bouncing Particle

Similar to the above solution of the Schödinger equation, the infinite potential around the mirror for the scalar field (3.9) can be represented via the Dirichlet boundary condition of the vanishing scalar field at the boundary surface, which implies that [24]

$$K_{\frac{i\omega}{a}}\left(\frac{\kappa}{a}\right)=0, \tag{3.10}$$

and leads that ω in the condition of Eq. (3.10) must be discrete. The boundary condition (3.10) can be written in the first kind of a Hankel function [97, 102]; explicitly, this is written as $H^{(1)}_{\frac{i\omega}{a}}\left(\frac{\kappa}{a}e^{i\pi/2}\right)=0$ [23].

Here, we discuss the bound system for the case of a suppressed perpendicular momentum; that is, where $\boldsymbol{k}_\perp=0$. In this case, $\kappa=m$ and the boundary condition of the bouncing Klein–Gordon particle leads to

$$H^{(1)}_{\frac{i\omega}{a}}(i\mu)=0, \tag{3.11}$$

where $\mu \equiv m/a$. To explicitly obtain the zeros of the first kind of the Hankel function in the boundary condition (3.11), we use the approximation formula given in Ref. [102], taking advantage of the expansion of μ in the case of $\omega/a \gg 1$. We obtain the solution of the discrete ω_n for a Klein–Gordon bouncer; this is explicitly as

$$\frac{\omega_n}{a} \approx \mu + \zeta_n 2^{-1/3} \mu^{1/3} + \frac{\zeta_n^2}{60} 2^{1/3} \mu^{-1/3} + \left(\frac{1}{70} - \frac{\zeta_n^3}{700} \right) \mu^{-1} + \mathcal{O}(\mu^{-5/3}), \tag{3.12}$$

where ζ_n can be obtained from the zeros of the Airy function.

The solution of the energy level of a Klein–Gordon bouncer can be directly found using the relation of $\omega_n = \mathcal{E}_n + m$ for Eq. (3.12). Then, we can see that in the nonrelativistic limit, the energy level of a Klein–Gordon bouncer reduces to the eigen-energy for the Schrödinger equation in a linear gravitational potential under the Dirichlet boundary condition, which appears at the second term on the right-hand side of Eq. (3.12). The remaining terms on the right-hand side can be understood as relativistic corrections to the energy levels of a Klein–Gordon bouncer determined by the Dirichlet boundary conditions. Thus, we can write the energy level of a Klein–Gordon bouncer as

$$\mathcal{E}_n^{\mathrm{KG}} = \mathcal{E}_n^{\mathrm{NR}} + \Delta\mathcal{E}_n^{\mathrm{KG}}, \tag{3.13}$$

where $\mathcal{E}_n^{\mathrm{NR}}(\equiv E_n)$ is the energy level in the nonrelativistic limit given by Eq. (2.10) and $\Delta\mathcal{E}^{\mathrm{KG}}$ is the relativistic correction to the energy level of a Klein–Gordon bouncer.

Chapter 4

Gravitational Quantum States of Dirac and Majorana Bouncing Particles

In this chapter, we expand upon the previous discussion of Dirac and Majorana bouncing particles under appropriate mirror boundary conditions [31]; see also Ref. [23] for an earlier discussion on the Dirac bouncing particle. We start with the derivation of the Dirac wave function from the Dirac equation in Rindler coordinates, which have been studied in many previous works. Here, we follow the procedure given in Refs. [100, 103–108] to obtain the solution to the Dirac equation in Rindler coordinates; this procedure uses the Dirac representation. In the present study, we initially derive the solution to the Dirac equation written in the Majorana representation [109, 110]. Then, the obtained solution is directly transformed to that written in the Dirac representation using the unitary matrix [109, 110]. From the obtained Dirac wave function, we solve for the Majorana wave function by taking a linear combination of the Dirac wave function and its charge conjugation [49] so that the Majorana wave function consists of positive- and negative-energy components. We apply the condition that the charge conjugation of the Majorana wave function is the same as itself. To obtain the energy eigenstates, we adopt the BC-MIT [28–30] (instead of the Dirichlet boundary condition) as alternative boundary conditions for Dirac and Majorana bouncing particles. Then, we calculate the analytic energy eigenstate solutions for Dirac and Majorana bouncers in the nonrelativistic limit using the approximation formula given in Ref. [102]. In this chapter, we also briefly discuss the application of the BC-chiral MIT for the Dirac bouncing particle in the particular case.

4.1 Dirac Bouncing Particle in a Homogeneous Gravitational Field

As mentioned above, we here discuss the bound states of Dirac and Majorana bouncers in the viewpoint of equivalence principle of relativity. We analyze the bouncer problems by investigating the Dirac equations in Rindler coordinates under appropriate mirror boundary conditions.

4.1.1 Dirac Equation in Rindler Coordinates

The Dirac equation for a Dirac wave function $\tilde{\psi}^{\mathrm{D}}$ written in the Majorana representation in Rindler coordinates is given by [104]

$$\left[i\tilde{\gamma}_{\mathrm{R}}^{\mu} \left(\frac{\partial}{\partial x^{\mu}} + \tilde{\Gamma}_{\mu} \right) - m \right] \tilde{\psi}^{\mathrm{D}} = 0, \tag{4.1}$$

where m is the rest mass of the particle, $\tilde{\Gamma}_{\mu}$ is the spin connection written in the Majorana representation, $\tilde{\gamma}_{\mathrm{R}}^{\mu}$ are gamma matrices in the Rindler coordinates written in the Majorana representation, and σ represents the spin orientation. In Rindler coordinates, the spin connection is given by $\tilde{\Gamma}_{\mu} = (\frac{a}{2}\tilde{\gamma}^{0}\tilde{\gamma}^{3}, 0, 0, 0)$.

The gamma matrices in Minkowski and in Rindler coordinates written in the Majorana representation satisfy the anti-commutation relations $\{\tilde{\gamma}^{\mu}, \tilde{\gamma}^{\nu}\} = 2\eta^{\mu\nu}$ and $\{\tilde{\gamma}_{\mathrm{R}}^{\mu}, \tilde{\gamma}_{\mathrm{R}}^{\nu}\} = 2g^{\mu\nu}$, respectively. From these anti-commutation relations, the gamma matrices in Minkowski coordinates can be related to those in the Rindler coordinates as follows

$$\tilde{\gamma}_{\mathrm{R}}^{0} = e^{-a\xi}\tilde{\gamma}^{0}, \quad \tilde{\gamma}_{\mathrm{R}}^{1} = \tilde{\gamma}^{1}, \quad \tilde{\gamma}_{\mathrm{R}}^{2} = \tilde{\gamma}^{2}, \quad \tilde{\gamma}_{\mathrm{R}}^{3} = e^{-a\xi}\tilde{\gamma}^{3}. \tag{4.2}$$

The gamma matrices in Minkowski coordinates written in the Majorana representation $\tilde{\gamma}^{\mu}$ can be obtained from those written in the Dirac representation γ^{μ} by using the following relation [109, 110]

$$\tilde{\gamma}^{\mu} = U\gamma^{\mu}U^{\dagger}. \tag{4.3}$$

In this thesis, we use the gamma matrices γ^{μ} given in Refs. [111, 112] as

$$\gamma^{0} = \begin{pmatrix} I & 0 \\ 0 & -I \end{pmatrix}, \quad \gamma^{i} = \begin{pmatrix} 0 & \sigma_{i} \\ -\sigma_{i} & 0 \end{pmatrix}, \quad i = 1, 2, 3, \tag{4.4}$$

where I is a 2×2 identity matrix and σ_i are Pauli matrices that satisfy anti-commutation relations $\{\sigma_i, \sigma_j\} = 2\delta_{ij}I$. The detail expression of the Pauli matrices are given by

$$\sigma_1 = \begin{pmatrix} 0 & 1 \\ 1 & 0 \end{pmatrix}, \quad \sigma_2 = \begin{pmatrix} 0 & -i \\ i & 0 \end{pmatrix}, \quad \sigma_3 = \begin{pmatrix} 1 & 0 \\ 0 & -1 \end{pmatrix}. \tag{4.5}$$

The above gamma matrices satisfy anti-commutation relations $\{\gamma^\mu, \gamma^\nu\} = 2\eta^{\mu\nu}$, where in the present study we adopt $\eta^{\mu\nu} = \text{diag.}(1, -1, -1, -1)$. To use the transformation in Eq. (4.3), we adopt the unitary matrix U as [109]

$$U = U^\dagger = U^{-1} = \frac{1}{\sqrt{2}} \begin{pmatrix} I & \sigma_2 \\ \sigma_2 & -I \end{pmatrix}. \tag{4.6}$$

In the Majorana representation, we can obtain a real solution for the Dirac equation [110]. Applying the unitary transformation (4.3) to the gamma matrices written in Dirac representation γ^μ (4.4), we obtain Majorana representation counterparts $\tilde{\gamma}^\mu$ as [109][1]

$$\tilde{\gamma}^0 = \begin{pmatrix} 0 & \sigma_2 \\ \sigma_2 & 0 \end{pmatrix}, \quad \tilde{\gamma}^1 = \begin{pmatrix} i\sigma_3 & 0 \\ 0 & i\sigma_3 \end{pmatrix}, \quad \tilde{\gamma}^2 = \begin{pmatrix} 0 & -\sigma_2 \\ \sigma_2 & 0 \end{pmatrix}, \quad \tilde{\gamma}^3 = \begin{pmatrix} -i\sigma_1 & 0 \\ 0 & -i\sigma_1 \end{pmatrix}. \tag{4.7}$$

See also Ref. [110] for the other set of gamma matrices written in the Majorana representation. From their expressions given in Eq. (4.7), we can see that the gamma matrices written in the Majorana representation satisfy [110]

$$(\tilde{\gamma}^\mu)^* = -\tilde{\gamma}^\mu, \tag{4.8}$$

which explicitly means that the gamma matrices written in the Majorana representation $\tilde{\gamma}^\mu$ are purely imaginary [109, 110].

4.1.2 Dirac Wave Function in Rindler Coordinates

We represent the wave function for the UCN as the positive-frequency solution of the Dirac equation (4.1) [112]. Then, we introduce an ansatz of the positive-energy solution for the Dirac equation as

$$\tilde{\psi}^D_{\omega \boldsymbol{k}_\perp \sigma} \equiv \tilde{f}^D_{\omega \boldsymbol{k}_\perp \sigma}(\xi) e^{i\boldsymbol{k}_\perp \cdot \boldsymbol{x}_\perp} e^{-i\omega\eta}, \tag{4.9}$$

---

[1]The choice of the gamma matrices written in the Majorana representation is not limited to Eq. (4.7) because there is an infinite choice of the gamma matrices in the Dirac representation [110].

where $\tilde{f}^{\mathrm{D}}_{\omega \boldsymbol{k}_\perp \sigma}(\xi)$ denotes a four-component Dirac spinor written in the Majorana representation. To further proceed, we here follow the procedure in Refs. [100, 105–108]. Inserting the ansatz (4.9) into Eq. (4.1), the Dirac equation reads

$$\omega \tilde{f}^{\mathrm{D}}_{\omega \boldsymbol{k}_\perp \sigma}(\xi) = \left[m e^{a\xi} \tilde{\beta} - i\frac{a}{2} \tilde{\alpha}_3 - i\tilde{\alpha}_3 \frac{\partial}{\partial \xi} + k_1 e^{a\xi} \tilde{\alpha}_1 + k_2 e^{a\xi} \tilde{\alpha}_2 \right] \tilde{f}^{\mathrm{D}}_{\omega \boldsymbol{k}_\perp \sigma}(\xi), \qquad (4.10)$$

where $\tilde{\beta} \equiv \tilde{\gamma}^0$ and $\tilde{\alpha}_j \equiv \tilde{\gamma}^0 \tilde{\gamma}^j$ are explicitly given by

$$\tilde{\beta} = \begin{pmatrix} 0 & \sigma_2 \\ \sigma_2 & 0 \end{pmatrix}, \quad \tilde{\alpha}_1 = \begin{pmatrix} 0 & -\sigma_1 \\ -\sigma_1 & 0 \end{pmatrix}, \quad \tilde{\alpha}_2 = \begin{pmatrix} I & 0 \\ 0 & -I \end{pmatrix}, \quad \tilde{\alpha}_3 = \begin{pmatrix} 0 & \sigma_3 \\ -\sigma_3 & 0 \end{pmatrix}. \quad (4.11)$$

Next, we decompose the four-component Dirac spinor $\tilde{f}^{\mathrm{D}}_{\omega \boldsymbol{k}_\perp \sigma}(\xi)$ into the upper two-component spinor $\tilde{\chi}_1(\xi)$ and lower two-component spinor $\tilde{\chi}_2(\xi)$, as follows

$$\tilde{f}^{\mathrm{D}}_{\omega \boldsymbol{k}_\perp \sigma}(\xi) = \begin{pmatrix} \tilde{\chi}_1(\xi) \\ \tilde{\chi}_2(\xi) \end{pmatrix}. \qquad (4.12)$$

Inserting the form of the four-component Dirac spinor (4.12) into the Dirac equation (4.10), we have

$$\omega \tilde{\chi}_1(\xi) = m e^{a\xi} \sigma_2 \tilde{\chi}_2(\xi) + i\frac{a}{2}\sigma_3 \tilde{\chi}_2(\xi) + i\sigma_3 \frac{\partial \tilde{\chi}_2(\xi)}{\partial \xi} - e^{a\xi} k_1 \sigma_1 \tilde{\chi}_2(\xi) + e^{a\xi} k_2 \tilde{\chi}_1(\xi), \quad (4.13)$$

$$\omega \tilde{\chi}_2(\xi) = m e^{a\xi} \sigma_2 \tilde{\chi}_1(\xi) + i\frac{a}{2}\sigma_3 \tilde{\chi}_1(\xi) + i\sigma_3 \frac{\partial \tilde{\chi}_1(\xi)}{\partial \xi} - e^{a\xi} k_1 \sigma_1 \tilde{\chi}_1(\xi) - e^{a\xi} k_2 \tilde{\chi}_2(\xi). \quad (4.14)$$

Further calculation yields

$$\frac{1}{a^2}\frac{\partial^2}{\partial \xi^2}\tilde{\chi}_1 = \left[\left(m^2 + \boldsymbol{k}_\perp^2\right) \frac{1}{a^2} e^{2a\xi} + \frac{1}{4} - \frac{\omega^2}{a^2} \right] \tilde{\chi}_1 + \frac{i\omega}{a}\sigma_3 \tilde{\chi}_2, \qquad (4.15)$$

$$\frac{1}{a^2}\frac{\partial^2}{\partial \xi^2}\tilde{\chi}_2 = \left[\left(m^2 + \boldsymbol{k}_\perp^2\right) \frac{1}{a^2} e^{2a\xi} + \frac{1}{4} - \frac{\omega^2}{a^2} \right] \tilde{\chi}_2 + \frac{i\omega}{a}\sigma_3 \tilde{\chi}_1. \qquad (4.16)$$

From Eqs. (4.13) and (4.14) or Eqs. (4.15) and (4.16), we see that the two-component spinors $\tilde{\chi}_1$ and $\tilde{\chi}_2$ are coupled each other. The Dirac equation is a first-order differential equation; therefore, we cannot use the Dirichlet boundary condition of a vanishing wave function at the boundary surface [26], and we employ an alternative boundary condition to compute the bound states of a Dirac particle. We introduce another two-component spinor as follows

$$\tilde{\phi}^\pm = \tilde{\chi}_1 \mp \tilde{\chi}_2 = \begin{pmatrix} \tilde{\vartheta}^\pm(\xi) \\ \tilde{\varsigma}^\pm(\xi) \end{pmatrix}. \qquad (4.17)$$

Then, Eqs. (4.15) and (4.16) yield

$$\frac{1}{a^2}\frac{\partial^2}{\partial \xi^2}\tilde{\vartheta}^{\pm}(\xi) = \left[(m^2 + \boldsymbol{k}_\perp^2)\frac{1}{a^2}e^{2a\xi} + \left(\frac{i\omega}{a} \mp \frac{1}{2}\right)^2\right]\tilde{\vartheta}^{\pm}(\xi), \tag{4.18}$$

$$\frac{1}{a^2}\frac{\partial^2}{\partial \xi^2}\tilde{\varsigma}^{\pm}(\xi) = \left[(m^2 + \boldsymbol{k}_\perp^2)\frac{1}{a^2}e^{2a\xi} + \left(\frac{i\omega}{a} \pm \frac{1}{2}\right)^2\right]\tilde{\varsigma}^{\pm}(\xi), \tag{4.19}$$

respectively. Both Eqs. (4.18) and (4.19) are Bessel differential equations (cf. Eq. (3.8)). The solutions to these differential equations are given by the modified Bessel function of the second kind, as (see, e.g., Refs. [100, 105–108])

$$\tilde{\vartheta}^{\pm}(\xi) = A_\pm K_\mp(\xi), \quad \tilde{\varsigma}^{\pm}(\xi) = B_\pm K_\pm(\xi), \tag{4.20}$$

where $K_\pm(\xi) = K_{i\frac{\omega}{a}\pm\frac{1}{2}}(\frac{\kappa}{a}e^{a\xi})$. Here, $A_\pm$ and $B_\pm$ are complex coefficients which store the information of spin orientations. From the two-component spinor in Eq. (4.17), the upper two-component spinor $\tilde{\chi}_1(\xi)$ can be rewritten as

$$\tilde{\chi}_1(\xi) = \frac{1}{2}(\tilde{\phi}^+ + \tilde{\phi}^-) = \frac{1}{2}\begin{pmatrix}\tilde{\vartheta}^+(\xi) + \tilde{\vartheta}^-(\xi) \\ \tilde{\varsigma}^+(\xi) + \tilde{\varsigma}^-(\xi)\end{pmatrix}, \tag{4.21}$$

while the lower two-component spinor $\tilde{\chi}_2(\xi)$ reads

$$\tilde{\chi}_2(\xi) = \frac{1}{2}(-\tilde{\phi}^+ + \tilde{\phi}^-) = \frac{1}{2}\begin{pmatrix}-\tilde{\vartheta}^+(\xi) + \tilde{\vartheta}^-(\xi) \\ -\tilde{\varsigma}^+(\xi) + \tilde{\varsigma}^-(\xi)\end{pmatrix}. \tag{4.22}$$

Then, by using the solution in Eq. (4.20), we obtain the Dirac spinor in Rindler coordinates written in the Majorana representation, as follows

$$\tilde{f}^{\mathrm{D}}_{\omega \boldsymbol{k}_\perp \sigma} = \frac{1}{2}\begin{pmatrix}\tilde{\vartheta}^+ + \tilde{\vartheta}^- \\ \tilde{\varsigma}^+ + \tilde{\varsigma}^- \\ -\tilde{\vartheta}^+ + \tilde{\vartheta}^- \\ -\tilde{\varsigma}^+ + \tilde{\varsigma}^-\end{pmatrix} = \frac{1}{2}\begin{pmatrix}A_+ K_-(\xi) + A_- K_+(\xi) \\ B_+ K_+(\xi) + B_- K_-(\xi) \\ -A_+ K_-(\xi) + A_- K_+(\xi) \\ -B_+ K_+(\xi) + B_- K_-(\xi)\end{pmatrix}. \tag{4.23}$$

From the Dirac spinor (4.23), we obtain the positive-frequency solution to the Dirac equation written in the Majorana representation for an arbitrary spin orientation expressed in terms of coefficients $A_\pm$ and $B_\pm$.

To physically interpret the coefficients $A_\pm$ and $B_\pm$, we next substitute back the solution of the Dirac spinor (4.23) into the Dirac equations (4.13) or (4.14). Thus, we obtain

that the coefficients $A_\pm$ and $B_\pm$ satisfy the relations in the following four equations (cf. Ref. [108] for expression in the Dirac representation)

$$i\kappa A_+ + k_2 A_- + (im + k_1)B_+ = 0, \quad (im - k_1)A_- + k_2 B_+ + i\kappa B_- = 0, \quad (4.24)$$

$$k_2 A_+ - i\kappa A_- - (im + k_1)B_- = 0, \quad (im - k_1)A_+ + i\kappa B_+ - k_2 B_- = 0. \quad (4.25)$$

From the above relations, the coefficients $B_\pm$ can be written in terms of the coefficients $A_\pm$; then, the four-component Dirac spinor in Rindler coordinates written in the Majorana representation can be written in terms of the coefficients $A_\pm$ only, as follows

$$\tilde{f}^{\mathrm{D}}_{\omega \boldsymbol{k}_\perp \sigma} = \frac{1}{2} \begin{pmatrix} A_+ K_-(\xi) + A_- K_+(\xi) \\ -\frac{i\kappa A_+ + k_2 A_-}{(im+k_1)} K_+(\xi) + \frac{k_2 A_+ - i\kappa A_-}{(im+k_1)} K_-(\xi) \\ -A_+ K_-(\xi) + A_- K_+(\xi) \\ \frac{i\kappa A_+ + k_2 A_-}{(im+k_1)} K_+(\xi) + \frac{k_2 A_+ - i\kappa A_-}{(im+k_1)} K_-(\xi) \end{pmatrix}. \quad (4.26)$$

In the previous discussion, we successfully obtained the solution to the Dirac equation in the Rindler coordinates written in the Majorana representation. Here, we discuss the solution in the Dirac representation. The Dirac wave function in the Dirac representation $\psi^{\mathrm{D}}_{\omega \boldsymbol{k}_\perp \sigma}$ can be obtained by applying a unitary transformation $\psi^{\mathrm{D}}_{\omega \boldsymbol{k}_\perp \sigma} = U \tilde{\psi}^{\mathrm{D}}_{\omega \boldsymbol{k}_\perp \sigma}$ [109, 110], which is explicitly given as

$$\psi^{\mathrm{D}}_{\omega \boldsymbol{k}_\perp \sigma} = \frac{\mathcal{N}^{\mathrm{D}}_{\omega \boldsymbol{k}_\perp \sigma}}{(im + k_1)} \begin{pmatrix} \mathcal{P}K_+(\xi) + \mathcal{Q}K_-(\xi) \\ \mathcal{R}K_+(\xi) + \mathcal{S}K_-(\xi) \\ -\mathcal{P}K_+(\xi) + \mathcal{Q}K_-(\xi) \\ \mathcal{R}K_+(\xi) - \mathcal{S}K_-(\xi) \end{pmatrix} e^{i\boldsymbol{k}_\perp \cdot \boldsymbol{x}_\perp} e^{-i\omega\eta}, \quad (4.27)$$

where the details of coefficients $\mathcal{P}, \mathcal{Q}, \mathcal{R}$, and $\mathcal{S}$ are given as follows

$$\mathcal{P} = \left[\kappa A_+ + (im + k_1 - ik_2)A_- \right], \quad \mathcal{Q} = \left[(im + k_1 - ik_2)A_+ - \kappa A_- \right], \quad (4.28)$$

$$\mathcal{R} = \left[-i\kappa A_+ - (m - ik_1 + k_2)A_- \right], \quad \mathcal{S} = \left[(m - ik_1 + k_2)A_+ - i\kappa A_- \right], \quad (4.29)$$

with the unitary matrix U given in Eq. (4.3) [109]. Here, $\mathcal{N}^{\mathrm{D}}_{\omega \boldsymbol{k}_\perp \sigma}$ is a normalization constant determined depending on the boundary condition, as shown later in Sec. 5.5. The general solution to the Dirac equation in the Rindler coordinates for the case of general momentum and arbitrary spin orientations (written in the Dirac representation) has been calculated and discussed elsewhere (e.g., Refs. [107, 108]; see also the solution provided in Ref. [113]).

Interestingly, the coefficients $\mathcal{P}, \mathcal{Q}, \mathcal{S}$, and $\mathcal{R}$ in the solution (4.27) can be seen as

c_1, c_2, c_3, c_4 of Ref. [108]², respectively. From this fact, we have the relations between the coefficients $A_\pm$, $B_\pm$ and c_1, c_2, c_3, c_4 of Ref. [108]. This relation indicates that it is also acceptable to operate using other representations because they can be transformed into each other using a specific unitary matrix [109, 110]. We can set these coefficients to obtain the solution in a specific direction of spin orientation (see Refs. [107, 108]). However, in the present study, we discuss the system in the general spin orientation, which is expressed via the coefficients $A_\pm$.

In the following, we consider the Dirac solution for a simpler case: that of suppressed perpendicular momentum $\boldsymbol{k}_\perp = 0$. In this case, $\kappa = m$ and the Dirac wave function in Rindler coordinates written in the Dirac representation (4.27) reduces to the following form:

$$\psi^{\mathrm{D}}_{\omega\sigma} = \mathcal{N}^{\mathrm{D}}_{\omega\sigma} \begin{pmatrix} (-iA_+ + A_-)K_{i\frac{\omega}{a}+\frac{1}{2}}(\frac{m}{a}e^{a\xi}) + (A_+ + iA_-)K_{i\frac{\omega}{a}-\frac{1}{2}}(\frac{m}{a}e^{a\xi}) \\ (-A_+ + iA_-)K_{i\frac{\omega}{a}+\frac{1}{2}}(\frac{m}{a}e^{a\xi}) - (iA_+ + A_-)K_{i\frac{\omega}{a}-\frac{1}{2}}(\frac{m}{a}e^{a\xi}) \\ (iA_+ - A_-)K_{i\frac{\omega}{a}+\frac{1}{2}}(\frac{m}{a}e^{a\xi}) + (A_+ + iA_-)K_{i\frac{\omega}{a}-\frac{1}{2}}(\frac{m}{a}e^{a\xi}) \\ (-A_+ + iA_-)K_{i\frac{\omega}{a}+\frac{1}{2}}(\frac{m}{a}e^{a\xi}) + (iA_+ + A_-)K_{i\frac{\omega}{a}-\frac{1}{2}}(\frac{m}{a}e^{a\xi}) \end{pmatrix} e^{-i\omega\eta}. \quad (4.30)$$

When $A_+ = \pm iA_-$, the Dirac wave function (4.30) has a spin orientation in the $\pm z$-direction; see Refs. [100, 105, 106] for the explicit form of the Dirac wave function in the case of $\boldsymbol{k}_\perp = 0$ with spin orientation is in the $\pm z$-direction. Below we will discuss the bound system for an arbitrary spin orientation.

4.1.3 Bound States of a Dirac Bouncing Particle in a Homogeneous Gravitational Field

Here, we discuss the bound states of a Dirac bouncing particle in the case of suppressed perpendicular momentum. We here utilize the BC-MIT [28–30] as the boundary condition for the Dirac wave function in Rindler coordinates ψ^{D} at $\xi = 0$, given by (see Appendix B for a brief review)

$$iN_\mu\gamma^\mu_{\mathrm{R}}\psi^{\mathrm{D}}\big|_{\xi=0} = \psi^{\mathrm{D}}\big|_{\xi=0}, \quad (4.31)$$

where an inward normal unit vector to the boundary is given by $N_\mu = (0, 0, 0, e^{a\xi})$. By decomposing the Dirac wave function into upper and lower two-component spinors $\psi^{\mathrm{D}} =$

---

²The coefficients in Ref. [108] are originally denoted by $c_1^n, c_2^n, c_3^n, c_4^n$, where n in that reference denotes the direction of the spin state.

$(\chi_1, \chi_2)^{\mathrm{T}}$, the boundary condition (4.31) yields

$$i\sigma_3\chi_1|_{\xi=0} + \chi_2|_{\xi=0} = 0. \tag{4.32}$$

Imposing the boundary condition (4.32) to the Dirac wave function in Rindler coordinates for the case of $\boldsymbol{k}_\perp = 0$ (4.30), we obtain

$$K_{\frac{i\omega}{a}+\frac{1}{2}}\left(\frac{m}{a}\right) + K_{\frac{i\omega}{a}-\frac{1}{2}}\left(\frac{m}{a}\right) = 0. \tag{4.33}$$

See our work in Ref. [31] for the boundary condition of a Dirac bouncing particle in the case of general momentum. We can see that the boundary condition in Eq. (4.33) does not depend on the spin orientation; thus, the boundary condition (4.33) holds for all spin orientations.

The boundary condition (4.33) leads ω must be discrete, for which the analytical solution for the case of $\omega/a \gg 1$ can be found using the approximation formula in Ref. [102]; the discrete solutions ω_n are approximately given by

$$\begin{aligned}
\frac{\omega_n}{a} &\approx \mu + \zeta_n 2^{-1/3}\mu^{1/3} - \frac{1}{2} + \frac{\zeta_n^2}{60}2^{1/3}\mu^{-1/3} + \frac{\zeta_n}{6}2^{-1/3}\mu^{-2/3} + \left(\frac{1}{70} - \frac{\zeta_n^3}{700} - \frac{1}{12}\right)\mu^{-1} \\
&\quad + \mathcal{O}(\mu^{-4/3}),
\end{aligned} \tag{4.34}$$

where $\mu = m/a$. Similar to the Klein–Gordon bouncer, the energy level of a Dirac bouncer in Eq. (4.34) can be found using $\omega_n = \mathcal{E}_n^{\mathrm{D}} + m$. The results show that, in the nonrelativistic limit, the energy levels of a Dirac bouncer also reduce to eigen-energies for the Schrödinger equation in a linear gravitational potential with an ideal mirror. This can be seen from the second term of the right-hand side of the energy levels of a Dirac bouncer in Eq. (4.34). The remaining terms on the right-hand side can be understood as a relativistic effect of the bouncing Dirac particle associated with the BC-MIT. Thus, we can write the energy level of a Dirac bouncer as

$$\mathcal{E}_n^{\mathrm{D}} = \mathcal{E}_n^{\mathrm{NR}} + \Delta\mathcal{E}_n^{\mathrm{D}}, \tag{4.35}$$

where $\mathcal{E}_n^{\mathrm{NR}}(\equiv E_n)$ is the energy level in the nonrelativistic limit given by Eq. (2.10) and shared with the Klein–Gordon bouncer in the same limit. Here, $\Delta\mathcal{E}_n^{\mathrm{D}}$ is the relativistic correction to the energy level of a Dirac bouncer.

Here, we briefly discuss the bound states of a Dirac bouncing particle under the BC-chiral MIT. Similar to the previous discussion, we here compute the case of a suppressed

perpendicular momentum $\boldsymbol{k}_\perp = 0$. The BC-chiral MIT [64] for the Dirac wavefunction in the Rindler coordinates at $\xi = 0$ is given by (see Appendix B for a brief review)

$$iN_\mu\gamma_R^\mu\psi^D\big|_{\xi=0} = e^{-i\gamma^5\Theta}\,\psi^D\big|_{\xi=0}, \tag{4.36}$$

where $\gamma^5 = i\gamma^0\gamma^1\gamma^2\gamma^3$ and the inward normal unit vector to the boundary is given by $N_\mu = (0,0,0,e^{a\xi})$ and shared with that of the BC-MIT (4.31). The BC-chiral MIT (4.36) can be decomposed into two equations, as follows:

$$i(\sigma_3 + \sin\Theta I)\chi_2\big|_{\xi=0} - \cos\Theta\chi_1\big|_{\xi=0} = 0, \tag{4.37}$$

$$i(\sigma_3 - \sin\Theta I)\chi_1\big|_{\xi=0} + \cos\Theta\chi_2\big|_{\xi=0} = 0. \tag{4.38}$$

Here, both boundary conditions (4.37) and (4.38) are equivalent: The two-component Dirac spinors in Eq. (4.37) trivially satisfy Eq. (4.38).

Imposing the boundary condition (4.37) to the Dirac wave function in the case of a suppressed perpendicular momentum (4.30), we obtain two equations that can be rewritten in the form of a multiplication between two matrices as

$$\begin{pmatrix} \mathcal{T} & \mathcal{U} \\ \mathcal{V} & \mathcal{W} \end{pmatrix}\begin{pmatrix} A_+ \\ A_- \end{pmatrix} = \begin{pmatrix} 0 \\ 0 \end{pmatrix}, \tag{4.39}$$

where

$$\mathcal{T} = (1 + \sin\Theta)(K_+(0) + iK_-(0)) + i\cos\Theta(-K_+(0) + iK_-(0)), \tag{4.40}$$

$$\mathcal{U} = (1 + \sin\Theta)(-iK_+(0) - K_-(0)) + i\cos\Theta(iK_+(0) - K_-(0)), \tag{4.41}$$

$$\mathcal{V} = (-1 + \sin\Theta)(-iK_+(0) - K_-(0)) + i\cos\Theta(-iK_+(0) + K_-(0)), \tag{4.42}$$

$$\mathcal{W} = (-1 + \sin\Theta)(-K_+(0) + iK_-(0)) + i\cos\Theta(-K_+(0) - iK_-(0)). \tag{4.43}$$

For the arbitrary non-zero coefficients $A_\pm$, we require the vanishing of the determinant of the 2×2 matrix in Eq. (4.39); this implies the following condition:

$$K_{\frac{i\omega}{a} - \frac{1}{2}}\left(\frac{m}{a}\right) + e^{-i\Theta}K_{\frac{i\omega}{a} + \frac{1}{2}}\left(\frac{m}{a}\right) = 0. \tag{4.44}$$

The presence of the chiral angle in Eq. (4.44) determines the explicit structure of the boundary conditions. For example, in the non-chiral case ($\Theta = 0$), the boundary condition (4.44) generated by the BC-chiral MIT reduces to the boundary condition (4.33). For the case of

chiral angle $\Theta = \pi$, one has the following boundary condition

$$K_{\frac{i\omega}{a} - \frac{1}{2}}\left(\frac{m}{a}\right) - K_{\frac{i\omega}{a} + \frac{1}{2}}\left(\frac{m}{a}\right) = 0. \tag{4.45}$$

Both the boundary conditions in Eqs. (4.33) and (4.45) coincide with the boundary condition in Ref. [23].

The authors of Ref. [23] showed that the behavior of the lowest few energy eigenstates energy obtained from the boundary conditions differed from those of the Klein–Gordon bouncing particle (3.11). In Chap. 5, we restrict our discussion to the non-chiral case ($\Theta = 0$) applicable for realistic UCN systems, and we compare the energy levels and transition frequencies of a nonrelativistic bouncer with those of a Klein–Gordon bouncer. Meanwhile, we also compare the results against those of Ps atoms, using the analytic Klein–Gordon bouncer solution. In addition, the study of the effects of chiral angle on the confinement system has been discussed in Ref. [70], as we will also present in this thesis.

4.2 Majorana Bouncing Particle in a Homogeneous Gravitational Field

Here, we turn to discuss the quantum bouncer problem for the Majorana particle in the viewpoint of the equivalence principle. We investigate a Majorana solution of the Dirac equation in Rindler coordinates under appropriate mirror boundary condition. Here, we adopt the condition that the mirror properties are described by the BC-MIT so that the normal probability current and scalar densities of a Majorana bouncing particle vanish at the mirror surface. We start with a derivation of the Majorana wave function in Rindler coordinates. There are several ways to obtain the solution of the Majorana wave function (see, e.g., Refs. [49, 109, 110, 114]). In the present study, we follow the procedure given in Ref. [49], in which the Majorana wave function is constructed using a linear combination of the Dirac wave function and its charge conjugation. We use an additional condition for the Majorana particle. Namely, the charge conjugation of the Majorana wave function is the same as itself. Then, we apply the boundary condition to the Majorana wave function to discuss its bound state.

4.2.1 Majorana wave function in Rindler Coordinates

The Majorana wave function in Rindler coordinates written in the Dirac representation is given by [49]

$$\psi^{\mathrm{M}}_{\omega \boldsymbol{k}_\perp \sigma} = \frac{1}{\sqrt{2}} \left[\psi^{\mathrm{D}}_{\omega \boldsymbol{k}_\perp \sigma} + \lambda (\psi^{\mathrm{D}}_{\omega \boldsymbol{k}_\perp \sigma})^C \right] = \lambda (\psi^{\mathrm{M}}_{\omega \boldsymbol{k}_\perp \sigma})^C, \qquad (4.46)$$

where $\lambda = \pm 1$ and $\psi^{\mathrm{D}}_{\omega \boldsymbol{k}_\perp \sigma}$ is the positive-frequency Dirac wave function (4.27). Here, the charge conjugation is defined by $\psi^C = i\gamma^2 \psi^*$. We can see that the Majorana wave function (4.46) consists of positive- and negative-energy components. For the parameter $\lambda = +1$, the charge conjugation of the Majorana wave function is completely the same as itself and the components of the Majorana wave function satisfy

$$\psi^{\mathrm{M}} = \begin{pmatrix} \chi^{\mathrm{M}}_1 \\ -i\sigma_2 \chi^{\mathrm{M*}}_1 \end{pmatrix} = (\psi^{\mathrm{M}})^C. \qquad (4.47)$$

This means that one can obtain the complete solution of the Majorana wave function from the upper or lower two-components of the Majorana wave function only [110].

4.2.2 Bound States of a Majorana Bouncing Particle in a Homogeneous Gravitational Field

In the following, we consider the bound states of a Majorana particle in the case of a suppressed perpendicular momentum $\boldsymbol{k}_\perp = 0$ and arbitrary spin orientation. Because the Majorana wave function is derived from the same equation as the Dirac wave function, i.e., the Dirac equation, the same problem regarding boundary conditions also appears for the Majorana bouncing particle. Then, similar to the case of the Dirac bouncing particle, we here adopt the BC-MIT (4.31) for the Majorana wave function (4.46); this gives us the following boundary condition:

$$\left[K_{\frac{i\omega}{a} + \frac{1}{2}} \left(\frac{m}{a} \right) + K_{\frac{i\omega}{a} - \frac{1}{2}} \left(\frac{m}{a} \right) \right] \left[e^{-i\omega\eta} (A_+ + iA_-) + \lambda e^{i\omega\eta} (iA_+^* - A_-^*) \right] = 0. \qquad (4.48)$$

The solution of ω in the boundary condition (4.48) must satisfy for all η. Therefore, each term $e^{-i\omega\eta}$ and $e^{i\omega\eta}$ of the boundary condition (4.48) must vanish separately. From this requirement, we finally find that for both cases $\lambda = \pm 1$, the boundary condition of the Majorana bouncing particle (4.48) reduces to the boundary condition given in Eq. (4.33);

this yields the discrete ω_n as given in Eq. (4.34), where the solutions for both cases $\lambda = \pm 1$ are shared with those of the Dirac bouncing particle. This means that the energy levels of a Majorana bouncer and its relativistic correction are the same as those of a Dirac bouncer. In the following chapter, we will discuss the case of $\lambda = +1$ only.

Chapter 5

Roles of Boundary Conditions on Gravitational Quantum States of Bouncing Particles

In the previous chapters, we discussed the bound systems for four types of bouncing particles associated with the boundary conditions. We showed that the bound systems of all relativistic bouncing particles can be compared to their nonrelativistic limits. In this chapter, we discuss the roles of boundary conditions on the behaviors of bouncing particles in a homogeneous gravitational field by analyzing the energy levels, transition frequencies, and density functions using the results in Ref. [31].

5.1   Energy Levels of Quantum Bouncing Particles

We first summarize and compare the energy levels of four types of bouncing particles in the case of suppressed perpendicular momentum, which are derived and discussed in the previous chapters.

Nonrelativistic Particle.   The energy level of a nonrelativistic bouncing particle under the Dirichlet boundary condition of a vanishing wave function at the mirror surface is given from Eq. (2.10) as

$$\frac{\mathcal{E}_n^{\mathrm{NR}}}{a} = 2^{-1/3} \left(\frac{m}{a} \right)^{1/3} \zeta_n, \tag{5.1}$$

where m is the mass of the particle, a is uniform (gravitational) acceleration, $\mathcal{B}$ is the length scale defined by Eq. (2.5), and ζ_n is obtained from the zeros of the Airy function $\mathrm{Ai}(-\zeta_n) = 0$ (2.9).

Klein–Gordon Particle. The energy level of a Klein–Gordon bouncing particle under the Dirichlet boundary condition of a vanishing scalar field at the mirror surface is obtained as

$$\frac{\mathcal{E}_n^{\mathrm{KG}}}{a} \approx \frac{\mathcal{E}_n^{\mathrm{NR}}}{a} + \frac{\zeta_n^2}{60} 2^{1/3} \left(\frac{a}{m} \right)^{1/3} + \left(\frac{1}{70} - \frac{\zeta_n^3}{700} \right) \frac{a}{m} \tag{5.2}$$

from the analytic expansion given in Eq. (3.12) after inserting $\mu = m/a$ and $\omega_n = \mathcal{E}_n^{\mathrm{KG}} + m$. Using this approximation in the nonrelativistic limit, the energy levels of a Klein–Gordon bouncer (5.2) can be clearly compared with those of a nonrelativistic bouncer, where the energy levels of a Klein–Gordon bouncer has the additional terms approximately given as follows:

$$\frac{\Delta \mathcal{E}_n^{\mathrm{KG}}}{a} = \frac{\mathcal{E}_n^{\mathrm{KG}}}{a} - \frac{\mathcal{E}_n^{\mathrm{NR}}}{a} \approx \frac{\zeta_n^2}{60} 2^{1/3} \left(\frac{a}{m} \right)^{1/3} + \left(\frac{1}{70} - \frac{\zeta_n^3}{700} \right) \frac{a}{m}. \tag{5.3}$$

These additional terms can be understood as relativistic corrections to the energy levels generated by the Dirichlet boundary condition; their values are dominated by the first term of Eq. (5.3) and are positive. In other words, the energy levels of a Klein–Gordon bouncer always exceed those of the nonrelativistic bouncing particle for all states n. In Table 5.1, we shows an example of such properties of a Klein–Gordon bouncer for mass $m = 10$ and uniform acceleration $a = 1$. In addition, from Eq. (5.3), we can also see that the relativistic corrections to the energy levels go to zero in the large-mass and small-acceleration schemes.

Dirac and Majorana Particles. The energy levels of Dirac and Majorana bouncing particles under the BC-MIT are given by

$$\frac{\mathcal{E}_n^{\mathrm{D,M}}}{a} \approx \frac{\mathcal{E}_n^{\mathrm{NR}}}{a} - \frac{1}{2} + \frac{\zeta_n^2}{60} 2^{1/3} \left(\frac{a}{m} \right)^{1/3} + \frac{\zeta_n}{6} 2^{-1/3} \left(\frac{a}{m} \right)^{2/3} + \left(\frac{1}{70} - \frac{\zeta_n^3}{700} - \frac{1}{12} \right) \frac{a}{m}, \tag{5.4}$$

which is obtained from the analytic expansion given in Eq. (4.34) with $\mu = m/a$ and $\omega_n = \mathcal{E}_n^{\mathrm{D,M}} + m$. Comparing the energy levels of Dirac and Majorana bouncers in the nonrelativistic limit to those of a nonrelativistic bouncer, we find the extra terms approximately given as

$$\frac{\Delta \mathcal{E}_n^{\mathrm{D,M}}}{a} \approx -\frac{1}{2} + \frac{\zeta_n^2}{60} 2^{1/3} \left(\frac{a}{m} \right)^{1/3} + \frac{\zeta_n}{6} 2^{-1/3} \left(\frac{a}{m} \right)^{2/3} + \left(\frac{1}{70} - \frac{\zeta_n^3}{700} - \frac{1}{12} \right) \frac{a}{m}, \tag{5.5}$$

TABLE 5.1: Energy levels of quantum bouncers for the lowest six states. The left column is for a nonrelativistic bouncer, the middle column is for a Klein–Gordon bouncer, and the right column is for Dirac and Majorana bouncers. Here, we use mass $m = 10$, uniform acceleration $a = 1$, and each energy level is scaled by a factor $ma\mathcal{B}$ [31].

n	$\mathcal{E}_n^{\mathrm{NR}}/ma\mathcal{B}$	$\mathcal{E}_n^{\mathrm{KG}}/ma\mathcal{B}$	$\mathcal{E}_n^{\mathrm{D,M}}/ma\mathcal{B}$
1	2.338	2.369	2.103
2	4.088	4.179	3.931
3	5.521	5.683	5.446
4	6.787	7.028	6.800
5	7.944	8.270	8.049
6	9.023	9.438	9.223

which can be understood as relativistic corrections to energy levels. It can be seen that in the lowest few states, the correction is dominated by the first term of Eq. (5.5) and has a negative contribution. However, when the state n is sufficiently large, the correction gives a positive contribution. As an example, Table. 5.1 shows that the energy levels of Dirac and Majorana bouncers with mass $m = 10$ and uniform acceleration $a = 1$ are lower and higher than those of nonrelativistic bouncing particle for $n \leq 3$ and $n \geq 4$, respectively. Similar to the Klein–Gordon bouncer, the relativistic corrections from Dirac and Majorana bouncers also go to zero in the case of large-mass and small-acceleration. A comparison of the scaled energy level of a Dirac bouncer to those for a Klein–Gordon bouncer has previously been discussed in Ref. [23] (see Figs. 1 and 2 of Ref. [23]).

TABLE 5.2: The lowest six relativistic corrections to energy levels of quantum bouncers in Table 5.1. The left column is for a Klein–Gordon bouncer, and the middle column is for Dirac and Majorana bouncers. The right column provides the differences values of the transition frequencies between a Klein–Gordon bouncer and Dirac and Majorana bouncers. Here, we use mass $m = 10$, uniform acceleration $a = 1$, and each relativistic correction to the transition frequency is scaled by a factor $ma\mathcal{B}$.

n	$\Delta\mathcal{E}_n^{\mathrm{KG}}/ma\mathcal{B}$	$\Delta\mathcal{E}_n^{\mathrm{D,M}}/ma\mathcal{B}$	$(\Delta\mathcal{E}_n^{\mathrm{KG}} - \Delta\mathcal{E}_n^{\mathrm{D,M}})/ma\mathcal{B}$
1	0.031	-0.235	0.266
2	0.091	-0.157	0.248
3	0.162	-0.075	0.237
4	0.241	0.013	0.228
5	0.326	0.105	0.221
6	0.415	0.200	0.215

Table 5.2 provides the relativistic corrections to the energy levels of Klein–Gordon (left column) and Dirac and Majorana bouncers (middle column) for mass $m = 10$ and uniform acceleration $a = 1$. The results show that the relativistic corrections to the energy

levels of a Klein–Gordon bouncer are always positive for all states n. In contrast, those of Dirac and Majorana bouncers are negative for the lowest three states and positive for the higher states $n \geq 4$. This table also provides the lowest six scaled differences values of the transition frequencies between a Klein–Gordon bouncer and Dirac and Majorana bouncers (right column). The results show that, for the lowest few states, the differences give the smaller value as the increases of the state n.

In the realistic situation, where the mass of the neutron is $m \approx 0.94$ GeV [96] and the gravitational acceleration on the Earth's surface is $a = 9.8$ m/s$^2 \approx 2.15 \times 10^{-32}$ GeV, the first six energy levels of a nonrelativistic bouncer of the UCN are approximately given by $\mathcal{E}_n^{\mathrm{NR}} \approx 1.406, 2.458, 4.080, 4.776$, and 5.424 peV for $n = 1, 2, 3, 4, 5$, and 6, respectively (see the values in Table 2.1). The first term of the relativistic corrections to the energy levels of the Klein–Gordon bouncing particle (5.3), when compared with $\mathcal{E}_n^{\mathrm{NR}}/a$ is $\zeta_n(2a/m)^{2/3}/60$, which is about 4.984×10^{-23} for the lowest state of the UCN. We can see that the order is fairly small. Meanwhile, the first term of relativistic corrections to the energy levels of the Dirac and Majorana bouncers (5.5), compared with $\mathcal{E}_n^{\mathrm{NR}}/a$ is $-(a/4m)^{1/3}/\zeta_n$, which is about -7.339×10^{-12} for the lowest state of the UCN. This order is also fairly small.

As we mentioned above, observations of gravitational quantum states have recently been proposed not only for UCNs but also for Ps atoms [52, 53], whose masses are 10^{-3} times smaller. The dependence of the energy levels and first-order relativistic corrections to energy levels on the mass appear in the factors $m^{1/3}$ and $m^{-1/3}$, respectively. Therefore, the energy levels and the relativistic corrections to there for the Rydberg Ps atom are 10 times smaller [52] and 10 times larger than for those of UCNs at the same state n, respectively.

5.2   Relativistic Corrections to Energy Levels of a Classical Particle in Rindler Coordinates

In the previous section, we discussed how the energy levels behave under specific boundary conditions. To further our understanding of the boundary conditions, we calculate the relativistic corrections to the energy levels for a classical particle in Rindler coordinates by using a perturbation approximation (see, e.g., Refs. [23, 115, 116]). Below, we consider the first-order correction to the energy level. We start with the derivation of the nonrelativistic Hamiltonian of the Dirac equation in Rindler coordinates. The derivation is applicable for both Dirac and Majorana particles because we adopt that the Majorana wave function satisfies the Dirac equation, similar to the Dirac wave function.

5.2.1 Hamiltonian of Dirac equation in Rindler Coordinates

We start with the action of a relativistic particle of mass m in Rindler coordinates, as given by

$$S = -\int m \sqrt{e^{2a\xi}\left(1 - \dot{\xi}^2\right)}\, d\eta = \int L\, d\eta, \tag{5.6}$$

where $\dot{\xi} \equiv d\xi/d\eta$ and we have suppressed the transverse motion in the x and y directions. The Hamiltonian is defined as

$$H = P\dot{\xi} - L = me^{a\xi}\sqrt{\frac{P^2}{m^2 e^{2a\xi}} + 1}, \tag{5.7}$$

where P is the conjugate momentum given by

$$P = \frac{\delta S}{\delta \dot{\xi}} = \frac{me^{2a\xi}\dot{\xi}}{\sqrt{e^{2a\xi}(1 - \dot{\xi}^2)}}. \tag{5.8}$$

Using the expansion of $\sqrt{1 + x} = 1 + \frac{1}{2}x - \frac{1}{8}x^2 + \mathcal{O}(x^3)$ and $e^x = 1 + x + \frac{1}{2}x^2 + \mathcal{O}(x^3)$, we obtain

$$H \approx H_{\mathrm{NR}} \equiv m + \frac{P^2}{2m} + ma\xi + \frac{ma^2\xi^2}{2} - \frac{P^4}{8m^3} - \frac{a\xi P^2}{2m}. \tag{5.9}$$

The first term of Eq. (5.9) is the rest-mass, which can be excluded from the total Hamiltonian. The second and third terms of Eq. (5.9) describe the Hamiltonian of a particle in a linear gravitational field; this takes a solution in the form of the Airy function Ai, as we previously discussed in Sec. 2.2. Thus, the particle's energy from the Hamiltonian (5.9) can be calculated using the perturbation approximation, as we demonstrate in the following subsection; see also the calculation in Ref. [23].

5.2.2 Relativistic Corrections to Energy Levels

We classify the nonrelavitistic Hamiltonian (5.9) into two terms: perturbed and unperturbed Hamiltonians. That is,

$$H_{\mathrm{NR}} \equiv H^0 + H', \tag{5.10}$$

where the unperturbed Hamiltonian consists of the kinetic and potential terms explicitly given by

$$H^0 = \frac{P^2}{2m} + ma\xi, \tag{5.11}$$

which will form the nonrelativistic Hamiltonian if we replace the ξ here by the z given in Sec. 2.2; furthermore,

$$H' = \frac{ma^2\xi^2}{2} - \frac{P^4}{8m^3} - \frac{a\xi P^2}{2m} \tag{5.12}$$

is the relativistic correction, which is a perturbed terms in our approximation.

To obtain the relativistic corrections, we write ξ in the above Hamiltonians as the z in Sec. 2.2 and quantize the system by introducing $[z, P] = i$. With this parameter, we obtain the energy levels from the unperturbed Hamiltonian via

$$
\begin{aligned}
E_n^0 &= \langle\psi_n|H^0|\psi_n\rangle \\
&= \langle\psi_n|\frac{P^2}{2m} + maz|\psi_n\rangle \\
&= ma\mathcal{B}\zeta_n = \mathcal{E}_n^{\mathrm{NR}},
\end{aligned} \tag{5.13}
$$

which matches that of the energy levels of a nonrelativistic bouncer (2.10). Here, $|\psi_n\rangle$ is the nth energy eigenstate, whose wavefunction $\psi_n(z) = \langle z|\psi_n\rangle$ is in the function of the Airy function (2.7). Next, we discuss the first-order correction, which can be obtained using the perturbation approximation as

$$
\begin{aligned}
\tilde{\mathcal{E}}_n^{(1)} &\approx \langle\psi_n|H'|\psi_n\rangle \\
&= \frac{ma^2}{2}\langle z^2\rangle - \frac{1}{8m^3}\langle P^4\rangle - \frac{a}{2m}\langle zP^2\rangle.
\end{aligned} \tag{5.14}
$$

Here, all expectation values are taken with respect to the state $|\psi_n\rangle$. The second term of Eq. (5.14) gives

$$
\begin{aligned}
-\frac{1}{8m^3}\langle P^4\rangle &= -\frac{1}{8m^3}\langle 4m^2(E_n^2 - 2mazE_n + m^2a^2z^2)\rangle \\
&= -\frac{E_n^2}{2m} + aE_n\langle z\rangle - ma^2\langle z^2\rangle,
\end{aligned} \tag{5.15}
$$

where we have used the relation

$$P^2|\psi_n\rangle = 2m(E_n - maz)|\psi_n\rangle, \tag{5.16}$$

from the Schrödinger equation (2.4). Then, by exploiting Eq. (5.16), the commutation relation $[z, P^2] = 2iP$, and the fact that $\langle\psi_n|P|\psi_n\rangle = 0$, the last term of Eq. (5.14) can be

written as

$$-\frac{a}{2m}\langle zP^2\rangle = -aE_n\langle z\rangle + ma^2\langle z^2\rangle. \tag{5.17}$$

Combining Eqs. (5.15) and (5.17), the first-order correction (5.14) yileds

$$\tilde{\mathcal{E}}_n^{(1)} \approx -\frac{E_n^2}{2m} + ma^2\langle z^2\rangle. \tag{5.18}$$

The contribution of the first term of Eq. (5.18) is $-ma^2\beta^2\zeta_n^2/2$, which is obtained after inserting the explicit expression of the energy level $E_n(\equiv \mathcal{E}_n)$ given in Eq. (2.10). Meanwhile, the second term of Eq. (5.18) gives

$$\begin{aligned}
ma^2\langle z^2\rangle &= ma^2\mathcal{B}\int_0^\infty \psi_n^*(\zeta)z^2\psi_n(\zeta)d\zeta \\
&= ma^2\mathcal{B}^3\mathcal{N}_n^2\int_0^\infty \zeta^2(\text{Ai}(\zeta-\zeta_n))^2d\zeta \\
&= ma^2\mathcal{B}^2\frac{8}{15}\zeta_n^2, \tag{5.19}
\end{aligned}$$

where we have used $\zeta = z/\mathcal{B}$. Combining the first and second terms of Eq. (5.18), we obtain the total first-order correction as

$$\begin{aligned}
\tilde{\mathcal{E}}_n^{(1)} &\approx -\frac{1}{2}ma^2\mathcal{B}^2\zeta_n^2 + \frac{8}{15}ma^2\mathcal{B}^2\zeta_n^2 \\
&\approx \frac{1}{30}ma^2\mathcal{B}^2\zeta_n^2, \tag{5.20}
\end{aligned}$$

which matches that of a Klein–Gordon bouncer (5.3) and gives a positive correction. From this result, we learn that the boundary condition is important to analyze the bound system.

5.3   Foldy–Wouthuysen Transformed Hamiltonian for Dirac Equation in Rindler Coordinates

In this section, we apply the Foldy–Wouthuysen transformation [56–59] to the Hamiltonian of the relativistic spin-1/2 particle, to obtain its nonrelativistic approximation. The Hamiltonian for the Dirac equation in Rindler coordinates is given by [100, 113]

$$\begin{aligned}
H &= e^{a\xi}m\gamma^0 - i\frac{a}{2}\alpha_3 - i\alpha_3 P_\xi \\
&\simeq \gamma^0 m + \gamma^0 ma\xi + \gamma^0\frac{m}{2}a^2\xi^2 - i\frac{a}{2}\alpha_3 + \alpha_3 P_\xi, \tag{5.21}
\end{aligned}$$

where we have used the expansion of $e^x = 1 + x + \frac{1}{2}x^2 + \mathcal{O}(x^3)$, $-i\frac{\partial}{\partial\xi} \equiv P_\xi$, and we have suppressed the coordinates perpendicular to the direction of acceleration a. The Hamiltonian (5.21) can be classified into three terms as

$$H = \beta m + \varepsilon + O \tag{5.22}$$

with $\beta \equiv \gamma^0$. Here, ε and O are even and odd operators that satisfy

$$\beta\varepsilon = \varepsilon\beta, \quad \beta O = -O\beta, \tag{5.23}$$

respectively. We classify the even and odd operators for the relativistic Hamiltonian (5.21) as follows

$$\varepsilon = ma\xi\beta + \frac{1}{2}ma^2\xi^2\beta, \quad O = -i\frac{a}{2}\alpha_3 + \alpha_3 P_\xi. \tag{5.24}$$

The Foldy–Wouthuysen Hamiltonian is given by [56, 57]

$$H_{\text{FW}} \simeq \beta\left(m + \frac{O^2}{m^2} - \frac{O^4}{8m^3}\right) + \varepsilon - \frac{1}{8m^2}\big[O, [O, \varepsilon]\big]. \tag{5.25}$$

Inserting Eq. (5.24) into Eq. (5.25), we obtain the lowest order of the Foldy–Wouthuysen Hamiltonian transformation for Eq. (5.21), as follows:

$$H_{\text{FW}} \simeq \beta\left[m + \frac{P^2}{2m} + ma\xi + \frac{ma^2\xi^2}{2} - \frac{P^4}{8m^3} - \frac{a\xi P^2}{2m}\right]. \tag{5.26}$$

It can be seen that the Foldy–Wouthuysen transformed Hamiltonian consists of positive and negative eigenvalues under gamma matrix $\beta(\equiv \gamma^0)$ (see Eq. (4.4) for the detail expression of the gamma matrices). Here, we discuss the positive eigenvalues only. Then, the results show that the lowest orders of the Foldy–Wouthuysen transformed Hamiltonian (5.26) coincides with the nonrelativistic Hamiltonian (5.9) after replacing the ξ here by the z. Thus, Foldy–Wouthuysen transformed Hamiltonian give the same first-order correction as Eq. (5.20). Note that our Hamiltonian (5.26) was obtained using the Rindler metric given in Eq. (3.3). When one uses the metric first given in Ref. [63], expressed as

$$ds^2 = (1 + au)^2 dt^2 - dx^2 - dy^2 - du^2, \tag{5.27}$$

the Hamiltonian is given by

$$H = \beta m + \beta mgu + \alpha_3 P_u + \alpha_3 au P_u, \tag{5.28}$$

where the perpendicular coordinates $\boldsymbol{x}_\perp \equiv (x, y)$ are supressed. The odd and even operators of the Hamiltonian (5.28) are given by $\varepsilon = \beta mgu$ and $O = \alpha_3 P_u + \alpha_3 auP_u$, respectively. Then, the lowest order of the Foldy–Wouthuysen transformed Hamiltonian is given by (see, e.g., Refs. [23, 60–62])

$$H_{\mathrm{FW}} \simeq \beta \left[m + \frac{P^2}{2m} + maz + \frac{azP^2}{2m} - \frac{P^4}{8m^3} \right], \tag{5.29}$$

after treating u as z. Comparing to the lowest order of the Foldy–Wouthuysen transformed Hamiltonian given in Eq. (5.29), we can see that our Hamiltonian (5.26) is not exactly identical, because we use the metric given in Ref. [103], which is suitable for uniformly accelerated observers at $\xi = 0$ [117]. However, taking the advantage of the Hamiltonian of the Schrödinger equation as the unperturbed Hamiltonian of (5.26) and (5.29), both the perturbed terms of their Hamiltonian give the same correction, as we will see below. Note that the relativistic correction from the Hamiltonian has also been previously discussed in Ref. [23] using the metric given in Ref. [63]. The first-order correction from Hamiltonian (5.29) under the perturbartion approximation is given as follows

$$
\begin{aligned}
\mathcal{E}_n^{(1)} &\approx \frac{a}{2m} \langle zP^2 \rangle - \frac{1}{8m^3} \langle P^4 \rangle \\
&\approx 2aE_n \langle z \rangle - \frac{3}{2} ma^2 \langle z^2 \rangle - \frac{E_n^2}{2m} \\
&\approx \frac{1}{30} ma^2 \mathcal{B}^2 \zeta_n^2,
\end{aligned}
\tag{5.30}
$$

which is identical to our first-order correction to energy levels of a Klein–Gordon bouncer given in the first term of Eq. (5.3). The relativistic correction is also identical to Eq. (5.20).

The above obtained Foldy–Wouthuysen transformed Hamiltonian is applicable for both Dirac and Majorana particles because both Dirac and Majorana wave functions satisfy the Dirac equation. Thus, the relativistic corrections for the energy level of the Dirac bouncer also apply to the Majorana one.

5.4   Transition Frequencies between Two Energy Eigenstates of Bouncing Particles

In the previous section, we presented the bouncing particles' energy levels and their relativistic corrections. Unfortunately, the parameter of the shift of energy spectrum is not

detectable in the laboratory. However, the parameter of the transition frequencies between the energy eigenstates of the two quantum states can be observed, e.g., by using gravitational resonance spectroscopy [118–122]. The transition (angular) frequency between the two energy eigenstates $\mathcal{E}_{n'}$ and $\mathcal{E}_n$ is given by

$$\omega_{n,n'} = \mathcal{E}_{n'} - \mathcal{E}_n, \tag{5.31}$$

where we have used $\hbar \equiv 1$. Below, we compare the transition frequencies for four types of bouncing particles.

Nonrelativistic Particle. The transition frequency between the two energy eigenstates $\mathcal{E}_{n+1}^{\mathrm{NR}}$ and $\mathcal{E}_n^{\mathrm{NR}}$ for a nonrelativistic bouncer is given by

$$\omega_{n,n+1}^{\mathrm{NR}} = ma\mathcal{B}(\zeta_{n+1} - \zeta_n) = \left(\frac{ma^2}{2}\right)^{1/3}(\zeta_{n+1} - \zeta_n). \tag{5.32}$$

From the property of the zeros of the Airy function, the value of $\zeta_{n+1} > \zeta_n$ guarantees that the transition frequencies of a nonrelativistic bouncer (5.32) remain positive for all states n. However, its value goes to zero when the states n increase.

Klein–Gordon Particle. The transition frequency between the two energy eigenstates $\mathcal{E}_{n+1}^{\mathrm{KG}}$ and $\mathcal{E}_n^{\mathrm{KG}}$ for a Klein–Gordon bouncer is approximately given by

$$\omega_{n,n+1}^{\mathrm{KG}} \approx \omega_{n,n+1}^{\mathrm{NR}} + \frac{1}{60}\left(\frac{2a^4}{m}\right)^{1/3}(\zeta_{n+1}^2 - \zeta_n^2) - \frac{1}{700}\frac{a^2}{m}(\zeta_{n+1}^3 - \zeta_n^3). \tag{5.33}$$

The first term on the right hand side of Eq. (5.33) is the transition frequency of a nonrelativistic bouncer, while the remaining terms can be understood as relativistic corrections to the transition frequency of a Klein–Gordon bouncer, given by

$$\Delta\omega_{n,n+1}^{\mathrm{KG}} = \omega_{n,n+1}^{\mathrm{KG}} - \omega_{n,n+1}^{\mathrm{NR}} \approx \frac{1}{60}\left(\frac{2a^4}{m}\right)^{1/3}(\zeta_{n+1}^2 - \zeta_n^2) - \frac{1}{700}\frac{a^2}{m}(\zeta_{n+1}^3 - \zeta_n^3). \tag{5.34}$$

From Eq. (5.34), we can see that the relativistic corrections to transition frequency are dominated by the first term and give the positive values, where we here have used the case of $\omega/a \gg 1$. The relativistic corrections to the transition frequencies of a Klein–Gordon bouncer go to zero in the large-mass and small-acceleration schemes, which is similar to those of the energy levels of a Klein–Gordon bouncer. In addition, the analytic relativistic corrections of the transition frequencies of a Klein–Gordon bouncer are quite small when we

apply for the realistic parameters of the UCN and Ps atom, as we see below.

Dirac and Majorana Particles.   The transition frequencies between the two energy eigenstates $\mathcal{E}_{n+1}^{\mathrm{D,M}}$ and $\mathcal{E}_{n}^{\mathrm{D,M}}$ of Dirac and Majorana bouncers are given by

$$
\begin{aligned}
\omega_{n,n+1}^{\mathrm{D,M}} \quad \approx \quad & \omega_{n,n+1}^{\mathrm{NR}} + \frac{1}{60}\left(\frac{2a^4}{m}\right)^{1/3}(\zeta_{n+1}^2 - \zeta_n^2) + \frac{1}{6}\left(\frac{a^5}{2m^2}\right)^{1/3}(\zeta_{n+1} - \zeta_n) \\
& - \frac{1}{700}\frac{a^2}{m}(\zeta_{n+1}^3 - \zeta_n^3),
\end{aligned} \tag{5.35}
$$

and the relativistic corrections to the transition frequencies of a nonrelativistic bouncer are given by

$$
\Delta\omega_{n,n+1}^{\mathrm{D,M}} \approx \frac{1}{60}\left(\frac{2a^4}{m}\right)^{1/3}(\zeta_{n+1}^2 - \zeta_n^2) + \frac{1}{6}\left(\frac{a^5}{2m^2}\right)^{1/3}(\zeta_{n+1} - \zeta_n) - \frac{1}{700}\frac{a^2}{m}(\zeta_{n+1}^3 - \zeta_n^3). \tag{5.36}
$$

The contribution of $a/2$, responsible for the negative correction to the lowest few energy levels, is canceled in the transition frequencies. Thus, the relativistic corrections to the transition frequencies are dominated by the first term of Eq. (5.36) and give positive values. In other words, the obtained results show that the transition frequencies for all relativistic bouncing particles exceed those of a nonrelativistic one. As an example, we compare the transition frequencies for mass $m = 10$ and uniform acceleration $a = 1$ in Table 5.3. Compared to the results obtained for the Klein–Gordon particle, the relativistic corrections to transition frequencies of Dirac and Majorana particles feature one additional term, explicitly given in the second term of Eq. (5.36).

TABLE 5.3: The transition frequencies between the nth and $(n + 1)$th energy eigenstates of the bouncers in Table 5.1. The left column is for a nonrelativistic bouncer, the middle column is for a Klein–Gordon bouncer, and the right column is for Dirac and Majorana bouncers. Here, mass $m = 10$, uniform acceleration $a = 1$, and each transition frequency is scaled by a factor $ma\mathcal{B}$ [31].

n	$\omega_{n,n+1}^{\mathrm{NR}}/ma\mathcal{B}$	$\omega_{n,n+1}^{\mathrm{KG}}/ma\mathcal{B}$	$\omega_{n,n+1}^{\mathrm{D,M}}/ma\mathcal{B}$
1	1.750	1.810	1.828
2	1.433	1.504	1.515
3	1.266	1.345	1.354
4	1.157	1.242	1.249
5	1.079	1.168	1.174

Table 5.4 shows the relativistic corrections to the transition frequencies of a Klein–Gordon bouncer (left column) and Dirac and Majorana bouncers (middle column) from the obtained

TABLE 5.4: The relativistic corrections to the transition frequencies between the nth and $(n+1)$th energy eigenstates of the bouncers. The left column is for a Klein–Gordon bouncer and the middle column is for Dirac and Majorana bouncers. The right column is for the differences values of the scaled relativistic corrections to transition frequencies between a Klein–Gordon bouncer and Dirac and Majorana bouncers. Here, mass $m = 10$, uniform acceleration $a = 1$, and each relativistic correction to the transition frequency is scaled by a factor $ma\mathcal{B}$.

n	$\Delta\omega_{n,n+1}^{\text{KG}}/ma\mathcal{B}$	$\Delta\omega_{n,n+1}^{\text{D,M}}/ma\mathcal{B}$	$(\Delta\omega_{n,n+1}^{\text{D,M}} - \Delta\omega_{n,n+1}^{\text{KG}})/ma\mathcal{B}$
1	0.060	0.078	0.018
2	0.071	0.082	0.011
3	0.079	0.088	0.009
4	0.085	0.092	0.007
5	0.089	0.095	0.006

results in Table 5.3. We can see that that the relativistic corrections to the transition frequencies for all Klein–Gordon, Dirac, and Majorana particles increase under the increase of states n. This table also provides the differences values of the scaled relativistic corrections to transition frequencies between a Klein–Gordon bouncer and Dirac and Majorana bouncers (right column). The results show that, for the lowest few states, the differences decrease as the increase of states n.

In the realistic situation for UCNs, the relativistic corrections to the transition frequencies (5.34) and (5.36), $\Delta\nu_{n,n+1}^{\text{KG}} = \Delta\omega_{n,n+1}^{\text{KG}}/(2\pi)$ and $\Delta\nu_{n,n+1}^{\text{D,M}}$, are both on the order of 10^{-20} Hz for the lowest states, which are too small to be detected with the present technology. For comparison, the transition frequencies of UCNs in the lowest few states are approximately given by $\nu_{n,n+1}^{\text{NR}} \approx 254.44$, 208.31, 184.11, 168.30, and 156.82 Hz for $n = 1, 2, 3, 4$, and 5, respectively. The mass dependence of the first-order relativistic correction to transition-frequencies corrections also appears in the factor $m^{-1/3}$. Therefore, these relativistic corrections to transition frequencies for the Ps atom are 10 times larger than for the UCN, though still too small to be detected with the present technology.

5.5   Density Functions of Quantum Bouncing Particles

In this section, we discuss the density functions for bouncing particles in the case of suppressed perpendicular momentum $\boldsymbol{k}_\perp = 0$ [31]. We compare the probability, normal probability current, and scalar density of the bouncers. We may represent the functions in z or ξ using the relation of $az = e^{a\xi} - 1$.

5.5.1   Probability Density of Bouncing Particles

First, we discuss the comparison of the probability densities of four types of bouncing particles in the case of suppressed perpendicular momentum.

Nonrelativistic Particle.   The probability density of a nonrelativistic bouncer is given by

$$
\begin{aligned}
\rho^{\mathrm{NR}}(z) &= |\Psi_n(t,z)|^2 \\
&= |\mathcal{N}_n|^2 \left[\mathrm{Ai}\left(\frac{z}{\mathcal{B}} - \zeta_n \right) \right]^2,
\end{aligned}
\tag{5.37}
$$

where we have used the wave function in Eq. (2.3) with $\psi_n(z)$ as given in Eq. (2.7). Here, $\mathcal{B}$ is the gravitational length scale given in Eq. (2.5), $\mathcal{N}_n$ is the normalization constant determined by the condition in Eq. (2.8), and the parameter ζ_n is defined in Eq. (2.9). From the second line of Eq. (6.52), we can see that the probability density for a nonrelativistic bouncer is time-independent.

Klein–Gordon Particle.   The probability density of a Klein–Gordon bouncer is given by normalizing

$$
\begin{aligned}
\rho_\omega^{\mathrm{KG}}(\xi) &= i \left[\phi^*(\eta,\xi)\frac{\partial\phi(\eta,\xi)}{\partial\eta} - \phi(\eta,z)\frac{\partial\phi^*(\eta,\xi)}{\partial\eta} \right] \\
&= 2\omega \left| \mathcal{N}_\omega^{\mathrm{KG}} \right|^2 \left[K_{\frac{i\omega}{a}}\!\left(\frac{m}{a}e^{a\xi} \right) \right]^2,
\end{aligned}
\tag{5.38}
$$

where we have used the solution given in Eq. (3.9) with $\omega_n = \mathcal{E}_n^{\mathrm{KG}} + m$ determined by the boundary condition (3.10). Note that the probability density of a Klein–Gordon bouncer can also be written in the function of z by using the relation of $e^{a\xi} = az + 1$, as mentioned above. From Eq. (5.38), we can see that the probability density of a Klein–Gordon bouncer is time-independent, similar to the nonrelativistic one. Here, the normalization constant $\mathcal{N}_\omega^{\mathrm{KG}}$ is determined by the following condition

$$
\int_0^\infty \rho_\omega^{\mathrm{KG}}(\xi)e^{a\xi}d\xi = \int_0^\infty \rho_\omega^{\mathrm{KG}}(z)dz = 1
\tag{5.39}
$$

with $dz = e^{a\xi}d\xi$.

Dirac Particle.   The probability density of a positive-energy Dirac bouncing particle can

be obtained in a coordinate-independent way (see e.g., Ref. [123]) by normalizing

$$
\begin{aligned}
\rho^{\mathrm{D}}_{\omega\sigma}(\xi) &= n_0 \bar{\psi}^{\mathrm{D}}_{\omega\sigma}(\eta,\xi)\gamma^0_{\mathrm{R}}\psi^{\mathrm{D}}_{\omega\sigma}(\eta,\xi) \\
&= 8\left|\mathcal{N}^{\mathrm{D}}_{\omega\sigma}\right|^2 \left(|A_+|^2 + |A_-|^2\right)\left|K_{\frac{i\omega}{a}-\frac{1}{2}}(\frac{m}{a}e^{a\xi})\right|^2,
\end{aligned} \tag{5.40}
$$

which is obtained from the solution in Eq. (4.30) with $\omega_n = \mathcal{E}^{\mathrm{D,M}}_n + m$ determined by the boundary condition (4.33). The continuity equation of the Dirac equation in Rindler coordinates is given by $\partial_\mu(\sqrt{-g}\,\bar{\psi}\gamma^\mu_{\mathrm{R}}\psi) = \sqrt{-g}\,\nabla_\mu(\bar{\psi}\gamma^\mu_{\mathrm{R}}\psi) = 0$. Here, n_μ is the normal vector perpendicular to the constant time hypersurface. The normalization constant $\mathcal{N}^{\mathrm{D}}_{\omega\sigma}$ is determined by the following condition

$$
\int_0^\infty \rho^{\mathrm{D}}_{\omega\sigma}(\xi)e^{a\xi}d\xi = \int_0^\infty \rho^{\mathrm{D}}_{\omega\sigma}(z)dz = 1 \tag{5.41}
$$

with $dz = e^{a\xi}d\xi$. From Eq. (5.40), we can see that the probability density of a Dirac bouncing particle is time-independent, similar to the Klein–Gordon and nonrelativistic bouncing bouncers. In addition, the probability density of a Dirac bouncer does not depend on the spin orientation because the factor $(|A_+|^2 + |A_-|^2)$ gives real constant values that can be absorbed into the normalization constant.

Majorana Particle. We here define the probability density of a Majorana bouncer in the case of $\boldsymbol{k}_\perp = 0$ by normalizing

$$
\begin{aligned}
\rho^{\mathrm{M}}_{\omega\sigma}(\eta,\xi) &= n_0\bar{\psi}^{\mathrm{M}}_{\omega\sigma}(\eta,\xi)\gamma^0_{\mathrm{R}}\psi^{\mathrm{M}}_{\omega\sigma}(\eta,\xi) \\
&= 8\left|\mathcal{N}^{\mathrm{M}}_{\omega\sigma}\right|^2 \left(|A_+|^2 + |A_-|^2\right)\left\{\left|K_{\frac{i\omega}{a}-\frac{1}{2}}(\frac{m}{a}e^{a\xi})\right|^2 + 2\mathcal{A}(\eta)\,\mathrm{Re}\left[\left(K_{\frac{i\omega}{a}-\frac{1}{2}}(\frac{m}{a}e^{a\xi})\right)^2\right]\right\},
\end{aligned} \tag{5.42}
$$

from the Majorana wave function given in Eq. (4.46) with $\omega_n = \mathcal{E}^{\mathrm{D,M}}_n + m$ determined by the boundary condition (4.33) shared with the Dirac particle. Here, $\mathcal{N}^{\mathrm{M}}_{\omega\sigma}$ is the normalization constant of the Majorana wavefunction in the case of $\boldsymbol{k}_\perp = 0$, determined by the condition

$$
\int_0^\infty \rho^{\mathrm{M}}_{\omega\sigma}(\eta,\xi)e^{a\xi}d\xi = \int_0^\infty \rho^{\mathrm{M}}_{\omega\sigma}(\eta,z)dz = 1. \tag{5.43}
$$

In contrast to the Dirac bouncer, the behavior of the probability density for a Majorana bouncer depends on time η as well as spin orientation (determined by the values of $A_\pm$) via

the factor

$$\mathcal{A}(\eta) \equiv \frac{-\text{Im}\left[\left(A_+^2 + A_-^2\right) e^{-2i\omega\eta}\right]}{2\left(|A_+|^2 + |A_-|^2\right)}.$$
(5.44)

When the spin orientation is in the $\pm z$-direction ($A_+ = \pm iA_-$) [100, 105, 106], we have $\mathcal{A} = 0$ and the probability density of the Majorana bouncer exactly matches that of the Dirac bouncer. In the other spin orientations, we have $\mathcal{A} \neq 0$ in the last term of Eq. (5.42) that corresponds to the *Zitterbewegung*; it is explicitly given by

$$\rho_{\omega\sigma}^{\text{M,ZB}}(\eta, \xi) = -8\left|\mathcal{N}_{\omega\sigma}^{\text{M}}\right|^2 \text{Im}\left[\left(A_+^2 + A_-^2\right) e^{-2i\omega\eta}\right] \text{Re}\left[\left(K_{\frac{i\omega}{a} - \frac{1}{2}}\left(\frac{m}{a}e^{a\xi}\right)\right)^2\right].$$
(5.45)

This *Zitterbewegung* arises from the interference between the Dirac wavefunction and its charge conjugation, or from the positive- and negative-energy components of the Majorana wave function (4.46) [111]. However, this *Zitterbewegung* rapidly oscillates and might not be resolvable using experimental apparatus [31]. Thus, we can assume the vanishing of this factor; under this condition, the probability density of the Majorana bouncing particle exactly matches that of the Dirac bouncing particle (see Fig. 5.1 for the case of $\mathcal{A} = 0$).

Figure 5.1 shows the probability density of the nonrelativistic, Klein–Gordon, Dirac, and Majorana bouncers for the case of suppressed perpendicular momentum $\boldsymbol{k}_\perp = 0$ with mass $m = 10$ and uniform acceleration $a = 1$ for the ground, first-excited, and second-excited states. From this figure, we can see that the probability density of the nonrelativistic and Klein–Gordon bouncers vanishes around the boundaries $\xi = 0$ or $z = 0$. This property is associated with the Dirichlet boundary conditions. For a Dirac bouncer, the probability density under the BC-MIT does not vanish around the boundary surface for arbitrary coefficients $A_\pm$. For a Majorana bouncer, the behavior around the boundary surface depends on the coefficients $A_\pm$. This figure presents three cases for the probability density of a Majorana bouncer, which are presented for the three values of factor $\mathcal{A} = 0, +0.5,$ and -0.5. From this figure, we can see that at $\mathcal{A} = 0$, the probability density for both the Dirac and Majorana bouncing particles produce an identical pattern that does not vanish at the boundary. For $\mathcal{A} = +0.5$, the probability density of a Majorana bouncer vanishes around the boundary surface, which matches the behaviors of the nonrelativistic and Klein–Gordon bouncers around the boundary surface. However, their physical meaning differs: Both the nonrelativistic and Klein–Gordon cases are determined by the boundary conditions, whereas the Majorana one does not. In contrast, when $\mathcal{A} = -0.5$, the probability density of a Majorana bouncer does not vanish around the boundary surface and is higher than in other cases.
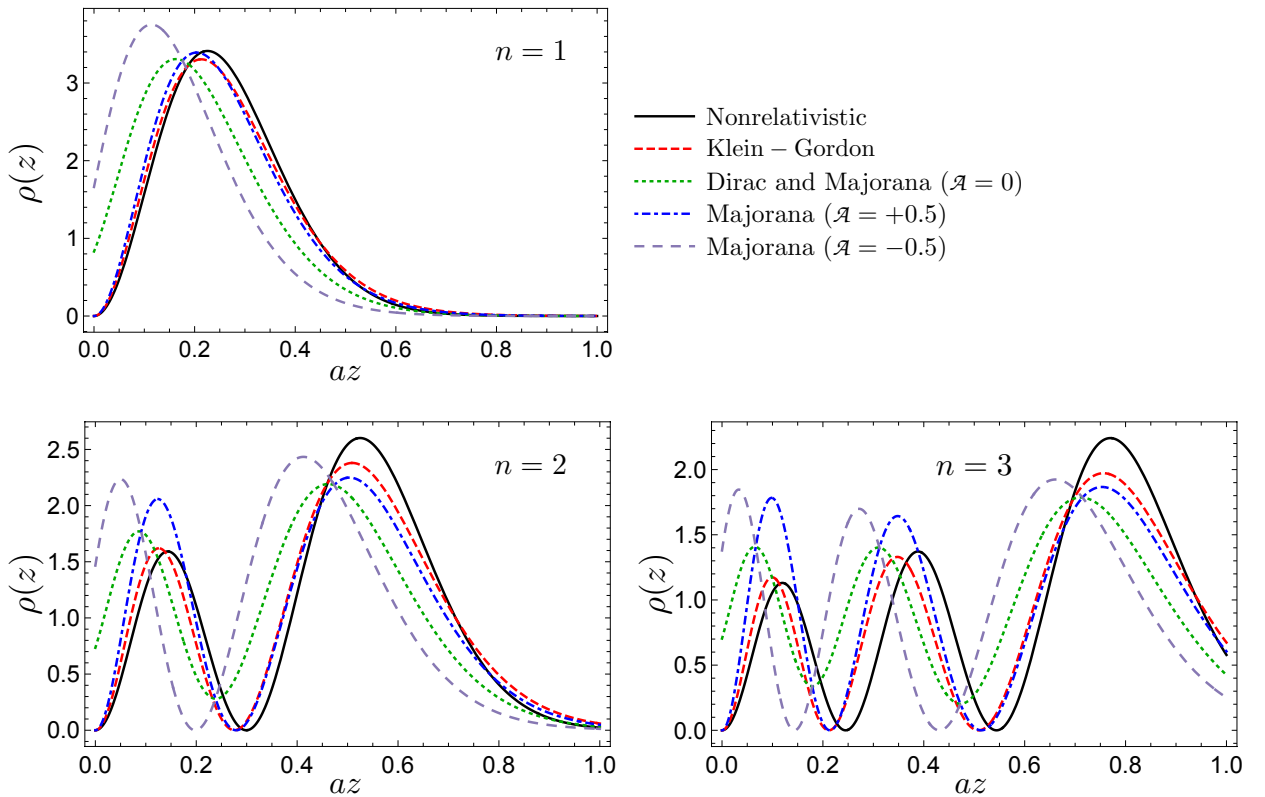
FIGURE 5.1: The probability densities of the bouncers with the transverse dimensions x and y suppressed. We demonstrate for the case of lowest three states: the ground state $n = 1$ (upper panel), first-excited state $n = 2$ (lower-left panel), and second-excited state $n = 3$ (lower-right panel). For the probability density of a Majorana bouncer, we depict three cases for various values of factor $\mathcal{A}$: $\mathcal{A} = 0$ is for the case of $A_+ = \pm i A_-$ (corresponding to the spin orientations in the $\pm z$-directions), $\mathcal{A} = +0.5$ is for the upper limit of $\mathcal{A} = +0.5 \sin(2\omega\eta)$ from purely real coefficients $A_\pm$ with $A_+ = A_-$, and $\mathcal{A} = +0.5$ is for the lower limit of $\mathcal{A} = -0.5 \sin(2\omega\eta)$ from purely imaginary coefficients $A_\pm$ with $A_+ = A_-$. Here, mass $m = 10$, uniform acceleration $a = 1$, and $az = e^{a\xi} - 1$. Both the probability densities of nonrelativistic and Klein–Gordon bouncers vanish around the boundary surface while a Dirac bouncer does not. For a Majorana bouncer, its behavior around the boundary surface depends on coefficients $A_\pm$. These figures are reproduced from Ref. [31].

Here, we discuss the physical interpretation or implications of the presence of the *Zitterbewegung*, which depends on the coefficients $A_\pm$ and oscillates in the function of time η. In the above discussion, we mentioned that the coefficients $A_\pm$ store the information regarding spin orientations. However, the presence of the *Zitterbewegung* in the probability density of a Majorana bouncer does not indicate a dependence of the *Zitterbewegung* on the spin orientation. As mentioned above, the BC-MIT requires vanishing the normal probability current density vanishes at the boundary surface. Therefore, the particle is perfectly reflected under all spin orientations [31] (cf. Ref. [25] for the reflection system, and see also the system

of a Dirac particle confined in a box, described in the next chapter).

5.5.2 Normal Probability Current Density for Dirac and Majorana Bouncing Particles

In this subsection, we turn to discuss the normal component of the probability current density $J_{N,\omega\sigma}(\eta,\xi) = \bar{\psi}_{\omega\sigma}(\eta,\xi)\gamma^3\psi_{\omega\sigma}(\eta,\xi)$ of Dirac and Majorana bouncers in arbitrary spin orientations, for the case of a suppressed perpendicular momentum $\boldsymbol{k}_\perp = 0$.

Dirac Particle. The normal probability current density for a Dirac bouncer vanishes everywhere; that is

$$
\begin{aligned}
J_{N,\omega\sigma}^{\mathrm{D}}(\xi) &= \bar{\psi}_{\omega\sigma}^{\mathrm{D}}(\eta,\xi)\gamma^3\psi_{\omega\sigma}^{\mathrm{D}}(\eta,\xi) \\
&= 0.
\end{aligned}
\tag{5.46}
$$

This can be mathematically explained in more detail as follows. The Dirac wavefunction consists of four components: $\psi^{\mathrm{D}} = (\psi_1^{\mathrm{D}}, \psi_2^{\mathrm{D}}, \psi_3^{\mathrm{D}}, \psi_4^{\mathrm{D}})^{\mathrm{T}}$. Thus, from the first line of Eq. (5.46), we have the summation of four terms: $\psi_3^{\mathrm{D}*}\psi_1^{\mathrm{D}} - \psi_4^{\mathrm{D}*}\psi_2^{\mathrm{D}} + \psi_1^{\mathrm{D}*}\psi_3^{\mathrm{D}} - \psi_2^{\mathrm{D}*}\psi_4^{\mathrm{D}}$. Substituting each component of the Dirac wavefunction (4.30) into those four terms, we find that the first and third terms cancel each other, likewise for the second and fourth terms. Finally, we find that the total contribution vanishes everywhere (see also the analysis in Ref. [23]). Here, we do not directly use the vanishing of the normal probability density as the boundary conditions for Dirac particle and further for Majorana particle to avoid the ambiguity of the chiral angle. If we apply this vanishing as the boundary condition, we have an extra result as given by Eq. (4.45).

Majorana Particle. In general, the normal component of the probability current density of a Majorana bouncer does not vanish; it is explicitly given by

$$
\begin{aligned}
J_{N,\omega\sigma}^{\mathrm{M}}(\eta,\xi) &= \bar{\psi}_{\omega\sigma}^{\mathrm{M}}(\eta,\xi)\gamma^3\psi_{\omega\sigma}^{\mathrm{M}}(\eta,\xi) \\
&= 8\left|\mathcal{N}_{\omega\sigma}^{\mathrm{M}}\right|^2 \mathrm{Re}\left[\left(A_-^2 + A_+^2\right)e^{-2i\omega\eta}\right]\mathrm{Im}\left[\left(K_{\frac{i\omega}{a}+\frac{1}{2}}(\frac{m}{a}e^{a\xi})\right)^2\right],
\end{aligned}
\tag{5.47}
$$

where $\mathcal{N}_{\omega\sigma}^{\mathrm{M}}$ is normalization constant determined by the condition in (5.43). We can see that the normal probability current of a Majorana bouncer is time-dependent. In addition,

it also depends on the coefficients $A_\pm$. These dependences corresponds to the *Zitterbewegung*, which are similar to that of the probability density. This *Zitterbewegung* arises from the contribution of the interference between the positive- and negative-energy components of the Majorana wavefunction (4.48). When the spin orientation is in the $\pm z$-directions (corresponding to the chosen values of the coefficients $A_+ = \pm i A_-$), the normal probability current density of a Majorana bouncer vanishes everywhere. In this condition, the normal probability current density of a Majorana bouncer is identical to the Dirac one. Discussions of the role of spin orientation on the probability density of a Majorana bouncer are limited. However, from the result in Ref. [25], we learn that the non-chiral case of the boundary conditions from the MIT bag model does not generate a change of spin orientation for a Dirac particle (see also our discussion in the next chapter). Furthermore, the BC-MIT requires the vanishing normal probability current density at the boundary surface. This property means that the particle is perfectly reflected for all spin orientations. Thus, the normal probability current density does not depend on the spin orientation.

5.5.3 Scalar Density of Dirac and Majorana Bouncing Particles

In the following, we discuss the scalar density $q(\eta, \xi) = \bar{\psi}(\eta, \xi)\psi(\eta, \xi)$ of Dirac and Majorana bouncers in arbitrary spin orientations, for the case of suppressed perpendicular momentum.

Dirac Particle. The scalar density of a Dirac bouncer is explicitly given by

$$
\begin{aligned}
q_{\omega\sigma}^{\mathrm{D}}(\xi) &= \bar{\psi}_{\omega\sigma}^{\mathrm{D}}(\eta, \xi)\psi_{\omega\sigma}^{\mathrm{D}}(\eta, \xi) \\
&= 8\left|\mathcal{N}_{\omega\sigma}^{\mathrm{D}}\right|^2 \left(|A_+|^2 + |A_-|^2\right) \mathrm{Im}\left\{\left[K_{\frac{i\omega}{a}+\frac{1}{2}}\left(\frac{m}{a}e^{a\xi}\right)\right]^2\right\},
\end{aligned}
\tag{5.48}
$$

obtained from the Dirac wave function given in Eq. (4.27), with $\omega_n = \mathcal{E}_n^{\mathrm{D,M}} + m$ determined by the boundary condition (4.33) and the normalization constant $\mathcal{N}_{\omega\sigma}^{\mathrm{D}}$ determined by the condition in Eq. (5.41). It can be seen that the scalar density of a Dirac bouncer does not depend on the spin orientation, because the contribution of $(|A_+|^2 + |A_-|^2)$ gives a real constants value that can be absorbed by the normalization constant. From this formalism, we can also see that the scalar density of a Dirac bouncer is time-independent.

Figure 5.2 depicts the scalar density of ground, first-excited, and second-excited states for a Dirac bouncer with mass $m = 10$, uniform acceleration $a = 1$, and arbitrary spin orientations σ, where the normalization constant is defined by the condition given in Eq. (5.41). The scalar density is plot as a function of z by using the relation of $az = e^{a\xi} - 1$. This figure
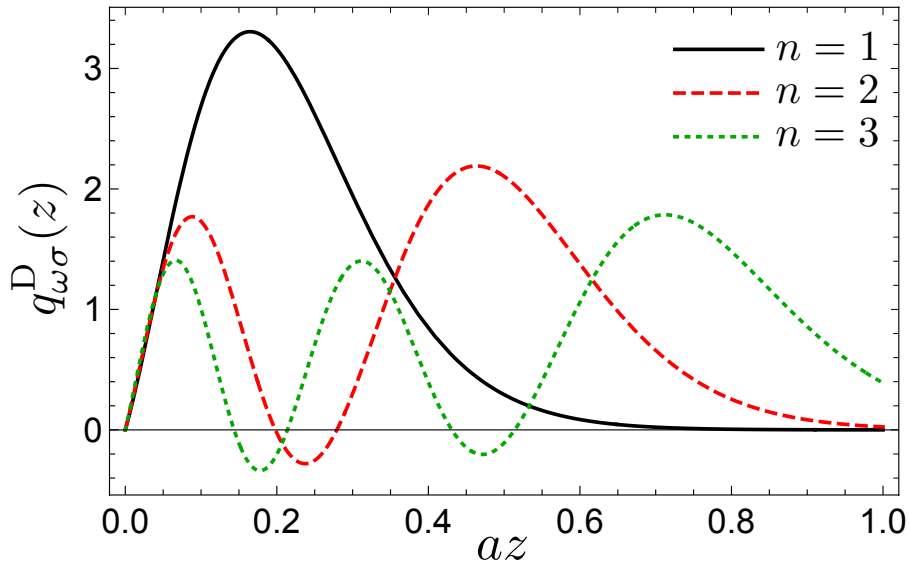
FIGURE 5.2:   The scalar density of a Dirac bouncer for arbitrary spin orientation and suppressed perpendicular momentum $\boldsymbol{k}_\perp = 0$. We demonstrate for the case of the lowest three states: the black solid curve is for the ground state $n = 1$, the red dashed curve is for the first-excited state $n = 2$, and the green dotted curve is for the second-excited states $n = 3$. Here, we use mass $m = 10$, uniform acceleration $a = 1$, and $az = e^{a\xi} - 1$. The scalar density for all states vanishes around the boundary surface, which is consistent with the property of the BC-MIT. This figure is reproduced from Ref. [31].

shows that the scalar density of a Dirac bouncer for all states n vanishes at the boundary surface $z = 0$ or $\xi = 0$. This property arises from the consequence of the usage of the mirror under the BC-MIT; see Eq. (B.2) for the non-chiral case $\Theta = 0$.

Majorana Particle.   The scalar density of a Majorana bouncer vanishes everywhere; that is,

$$
\begin{aligned}
q_{\omega\sigma}^{\mathrm{M}}(\eta,\xi) &= \bar{\psi}_{\omega\sigma}^{\mathrm{M}}(\eta,\xi)\psi_{\omega\sigma}^{\mathrm{M}}(\eta,\xi) \\
&= 0.
\end{aligned}
\tag{5.49}
$$

This vanishing occurs because the charge conjugation of the Majorana wave function is entirely the same as itself. This can be understood in more detail as follows. We write the Majorana wave function into four components as $\psi^{\mathrm{M}} = (\psi_1^{\mathrm{M}}, \psi_2^{\mathrm{M}}, -\psi_2^{\mathrm{M*}}, \psi_1^{\mathrm{M*}})^{\mathrm{T}}$ (see Eq. (4.47)), which satisfy the condition in Eq. (4.47). Inserting these four components into the first line of Eq. (5.49), we obtain four terms as $|\psi_1^{\mathrm{M}}|^2 + |\psi_2^{\mathrm{M}}|^2 - |\psi_2^{\mathrm{M}}|^2 - |\psi_1^{\mathrm{M}}|^2$. Then, it is clear that the total scalar density of a Majorana bouncer is zero everywhere.

Chapter 6

Roles of Chiral MIT Boundary Conditions on a Dirac Particle Confined in a 1D Box

In the previous chapters, we discussed the bound states of four types of bouncing particles in a gravitational field under the mirror boundary conditions. We utilized the Dirichlet boundary condition for nonrelativistic and Klein–Gordon bouncers, and used the BC-MIT to describe the property of the mirror for Dirac and Majorana bouncers while avoiding the Klein paradox problem. There, we discussed the relativistic effects generated by boundary conditions associated with types of relativistic bouncing particles. To further understand the roles of the boundary conditions, especially in the Dirac equation, we turn to discuss the system of a Dirac particle confined in a 1D box, though in the absence of a gravitational field [70]. To solve the problem, we first discuss the setup of the physical system, from which we derive the discrete momentum solution and its energy levels, by following the procedure in Ref. [26] but using the BC-chiral MIT [34, 64, 65] in describing the properties of the mirrors. In our setup, the presence of the mirrors under the BC-chiral MIT can be seen as an infinite mass of the particle at the boundary surfaces [25], as proposed for the MIT bag for hadron [28–30]. Thus, one can propose to write the mass in the function of position of the particle so that the problem of Klein paradox can be avoided [26, 27]. We investigate how the spin orientation changes under reflection. We review the spin orientation changes produced by the reflection at the first mirror by following Ref. [25] but using the chiral angle defined in Ref. [64]. Using the same procedure, we analyze the spin orientation change generated by the reflection at the second mirror. We also discuss the relation between the reflection at the first mirror and that of the second. At the end of the chapter, we demonstrate the density

functions for a Dirac particle in a 1D box, where the property of the boundary surface is described by the BC-chiral MIT, as we mentioned above.

6.1 Setup of a Dirac Particle in a Box

6.1.1 Total Dirac Wave Function

We consider a Dirac particle confined to a 1D box consisting of two perfectly reflecting mirrors under the BC-chiral MIT. The first mirror is placed at $z = 0$, while the second mirror is placed at $z = \ell$. In other words, the box size is ℓ. Inside the box, the particle moves with momentum k_3 along the z-axis, and the perpendicular momentum is suppressed. We set the total Dirac wave function to consist of a linear combination of left- and right-moving wave components, where each component is associated with a spin orientation. At the first mirror, the incident component is associated with the left-moving wave which propagates in the $-z$-direction; the reflecting component is associated with the right-moving wave component, which propagates in the $+z$-direction. At the second mirror, the reverse is true: The incident component is associated with the right-moving wave and the reflecting one is associated with the left-moving wave component. Note that the reflection system consisting of one perfectly reflecting mirror under the BC-chiral MIT has been previously discussed in Ref. [25]. There, the author of Ref. [25] discussed how the reflected spin orientation behaves owing to the reflection with the floor or wall. For the 1+1D Dirac equation, one can use the formalism on the basis of the 2×2 gamma matrices (see, e.g., Refs. [65, 73]). Using such formalism, one can clearly discuss the bound system as well as spin orientation. However, in the present study, we work in the basis of the 4×4 gamma matrices because it may be easier to extend the discussion for the more general cases (cf. Ref. [27]). From the above description, we propose the total wave function for a Dirac particle with the momentum k_3 inside the box, as

$$\psi_{k_3 s}(z) = B \begin{pmatrix} \xi_{R,s} \\ \frac{\sigma_3 k_3}{(m+E)} \xi_{R,s} \end{pmatrix} e^{ik_3 z} + C \begin{pmatrix} \xi_{L,s} \\ \frac{-\sigma_3 k_3}{(m+E)} \xi_{L,s} \end{pmatrix} e^{-ik_3 z}, \tag{6.1}$$

where the coefficients B and C are complex constants, m is the mass, and $E = \sqrt{m^2 + k_3^2}$ is the energy of the Dirac particle. Here, we use $\xi_{R,s}$ and $\xi_{L,s}$ to denote the two-component spinors of the right- and left-moving wave components, respectively, where s represents the spin orientation. Note that each component of the Dirac wave function $\Psi(t, z) = \psi(z)e^{-iEt}$ satisfies the Dirac equation in Eq. (A.1).

6.1.2   Initial Setup of Spin Orientation

As we mentioned above, the two-component spinor specifies the direction of the spin orientations. Thus, it is more convenient to decompose the two-component spinors $\xi_{L,s}$ and $\xi_{R,s}$ into

$$\xi_{L,s} = \begin{pmatrix} \alpha_{L,s} \\ \beta_{L,s} \end{pmatrix}, \qquad \xi_{R,s} = \begin{pmatrix} \alpha_{R,s} \\ \beta_{R,s} \end{pmatrix}. \tag{6.2}$$

In general, the two-component spinor $\xi_{L(R),s}$ consists of a linear combination of a two-component spinor with a spin-up ($+z$-direction) $\xi_{L(R),+z} = (1,0)^{\mathrm{T}}$ and a spin-down ($-z$-direction) $\xi_{L(R),-z} = (0,1)^{\mathrm{T}}$ as

$$\xi_{L(R),s} = \alpha\xi_{L(R),+z} + \beta\xi_{L(R),-z} = \begin{pmatrix} \alpha \\ \beta \end{pmatrix}, \tag{6.3}$$

where the normalized two-component spinor requires that $\xi_{L(R),s}^{\dagger}\xi_{L(R),s} = |\alpha|^{2}+|\beta|^{2} = 1$. The normalized two-component spinor $\xi_{L(R),s}$ with a spin orientation in some specific direction is given by

$$\xi_{L(R),+x} = \frac{1}{\sqrt{2}} \begin{pmatrix} 1 \\ 1 \end{pmatrix}, \qquad \xi_{L(R),-x} = \frac{1}{\sqrt{2}} \begin{pmatrix} 1 \\ -1 \end{pmatrix}, \tag{6.4}$$

$$\xi_{L(R),+y} = \frac{1}{\sqrt{2}} \begin{pmatrix} 1 \\ i \end{pmatrix}, \qquad \xi_{L(R),-y} = \frac{1}{\sqrt{2}} \begin{pmatrix} 1 \\ -i \end{pmatrix}. \tag{6.5}$$

In our setup, we first define the arbitrary spin orientation for the left-moving wave component, which is stored in the values of $\alpha_{L,s}$ and $\beta_{L,s}$. Owing to the interaction with the mirror, the two-component spinor $\xi_{L,s}$ can be related to the two-component spinor $\xi_{R,s}$. This relation is controlled by a rotation operator in the spin space [25].

6.2   Discrete Momenta and Energy Levels of a Dirac particle in a Box

At the first mirror, the incident component is associated with the left-moving wave, the reflected component is associated with the right-moving wave, and the inward normal unit vector to the boundary is given by $N_{\mu} = (0,0,0,1)$. Therefore, the BC-chiral MIT [64] for

the Dirac wave function $\psi = (\Phi_1, \Phi_2)^{\mathrm{T}}$ yields the following equations

$$i(\sigma_3 + \sin\Theta I)\Phi_2|_{z=0} - \cos\Theta\Phi_1|_{z=0} = 0, \tag{6.6}$$

$$i(\sigma_3 - \sin\Theta I)\Phi_1|_{z=0} + \cos\Theta\Phi_2|_{z=0} = 0. \tag{6.7}$$

Similar to the boundary conditions generated by the BC-MIT, both the boundary conditions (6.6) and (6.7) are equivalent, which indicates that we need only one of them [25]. One can simply check that both the two-component spinors in Eq. (6.6) trivially satisfy Eq. (6.7).

Imposing the boundary condition (6.6) on the Dirac wave function (6.1) at the first mirror $z = 0$, we have

$$B\left[i(I + \sin\Theta\sigma_3)\frac{k_3}{(m+E)} - \cos\Theta I\right]\xi_{R,s} = C\left[i(I + \sin\Theta\sigma_3)\frac{k_3}{(m+E)} + \cos\Theta I\right]\xi_{L,s}, \tag{6.8}$$

which can be rewritten in terms of a multipication between 2×2 and 2×1 matrices as

$$\left(\begin{bmatrix} \left[i(1 + \sin\Theta)\frac{k_3}{(m+E)} - \cos\Theta\right]\alpha_{R,s} & \left[-i(1 + \sin\Theta)\frac{k_3}{(m+E)} - \cos\Theta\right]\alpha_{L,s} \\ \left[i(1 - \sin\Theta)\frac{k_3}{(m+E)} - \cos\Theta\right]\beta_{R,s} & \left[-i(1 - \sin\Theta)\frac{k_3}{(m+E)} - \cos\Theta\right]\beta_{L,s} \end{bmatrix}\right)\begin{pmatrix} B \\ C \end{pmatrix} = 0, \tag{6.9}$$

after decomposing the two component-spinors $\xi_{R,s}$ and $\xi_{L,s}$ using Eq. (6.2). Note that the coefficients B or C cannot be zero because if one sets one or both of them are zero, the wave function will trivially vanish everywhere. As a consequence, we require the 2×2 matrix in Eq. (6.9) to vanish, which implies the following condition

$$(\alpha_{R,s}\beta_{L,s} - \beta_{R,s}\alpha_{L,s}) - \frac{ik_3\tan\Theta}{E}(\alpha_{R,s}\beta_{L,s} + \beta_{R,s}\alpha_{L,s}) = 0. \tag{6.10}$$

This condition indicates a relation between the incident and reflected spin orientations, expressed as a function of chiral angle Θ, where in the non-chiral case ($\Theta = 0$), the spin orientation does not change; the reflected spin orientation is the same as the incident one[1]. We will discuss this point in more detail later in Sec. 6.3. Meanwhile, from Eq. (6.8), we obtain the relation between coefficients B and C, given as

$$C = B\frac{i(1 + \sin\Theta)k_3/(m+E) - \cos\Theta}{i(1 + \sin\Theta)k_3/(m+E) + \cos\Theta}\frac{\alpha_{R,s}}{\alpha_{L,s}}, \tag{6.11}$$

$$C = B\frac{i(1 - \sin\Theta)k_3/(m+E) - \cos\Theta}{i(1 - \sin\Theta)k_3/(m+E) + \cos\Theta}\frac{\beta_{R,s}}{\beta_{L,s}}, \tag{6.12}$$

---

[1]In the non-chiral case, one can use the Dirac wave function given in Ref. [26], where the reflected and incident spin orientations are not distinguished.

where both relations in Eqs. (6.11) and (6.12) are equivalent, though Eq. (6.11) connects the coefficients $\alpha_{R,s}$ and $\alpha_{L,s}$ while Eq. (6.12) connects the coefficients $\beta_{R,s}$ and $\beta_{L,s}$. To obtain the solution of discrete momentum, it is necessary to proceed with the reflection at the second mirror under the BC-chiral MIT.

At the second mirror, the incident component is associated with the right-moving wave, the reflected component is associated with the left-moving wave, and the inward normal unit vector to the boundary is given by $N_\mu = (0, 0, 0, -1)$. Therefore, the BC-chiral MIT [64] for the Dirac wave function $\psi = (\Phi_1, \Phi_2)^{\mathrm{T}}$ reads

$$i(\sigma_3 - \sin\Theta I)\Phi_2|_{z=\ell} + \cos\Theta\Phi_1|_{z=\ell} = 0, \tag{6.13}$$

$$i(\sigma_3 + \sin\Theta I)\Phi_1|_{z=\ell} - \cos\Theta\Phi_2|_{z=\ell} = 0, \tag{6.14}$$

where both boundary conditions (6.13) and (6.14) are also equivalent. By imposing the boundary condition (6.13) upon the Dirac wave function (6.1) at the second mirror $z = \ell$, the relation between left- and right-moving waves can be obtained as

$$Be^{ik_3\ell}\left[i(I - \sin\Theta\sigma_3)\frac{k_3}{(m+E)} + \cos\Theta I\right]\xi_{R,s}$$
$$= Ce^{-ik_3\ell}\left[i(I - \sin\Theta\sigma_3)\frac{k_3}{(m+E)} - \cos\Theta I\right]\xi_{L,s}. \tag{6.15}$$

Decomposing the two-component spinors $\xi_{R,s}$ and $\xi_{L,s}$ as given in Eq. (6.2), the relation (6.15) gives

$$Be^{ik_3\ell}\left[i(1 - \sin\Theta)\frac{k_3}{(m+E)} + \cos\Theta\right]\alpha_{R,s}$$
$$= Ce^{-ik_3\ell}\left[i(1 - \sin\Theta)\frac{k_3}{(m+E)} - \cos\Theta\right]\alpha_{L,s}, \tag{6.16}$$

$$Be^{ik_3\ell}\left[i(1 + \sin\Theta)\frac{k_3}{(m+E)} + \cos\Theta\right]\beta_{R,s}$$
$$= Ce^{-ik_3\ell}\left[i(1 + \sin\Theta)\frac{k_3}{(m+E)} - \cos\Theta\right]\beta_{L,s}, \tag{6.17}$$

where both of these relations are also equivalent. Similar to the relations at the first mirror, the coefficients relation in Eq. (6.16) connects $\alpha_{R,s}$ and $\alpha_{L,s}$. Meanwhile, the coefficients relation in Eq. (6.17) connects $\beta_{R,s}$ and $\beta_{L,s}$. Taking the advantages of such properties, we can derive the discrete momentum solution.

6.2.1   Discrete Momenta of a Dirac Particle in a Box

Inserting the coefficients relation (6.11) into Eq. (6.16), we arrive at the following equation for the momentum k_3

$$-\frac{\tan(k_3\ell)}{k_3} = \frac{1}{m\cos\Theta}. \tag{6.18}$$

This requires the allowed momenta to be discrete. Note that we can also obtain the condition for discrete momenta by inserting the relation between coefficients B and C in Eq. (6.12) into Eq. (6.17). It is clear that the discrete momentum solutions (6.18) do not depend on spin orientation for all chiral angles Θ. This is because the contribution of spin orientation, which is stored in $\alpha_{R(L),s}$ or $\beta_{R(L),s}$ can be factorized out.
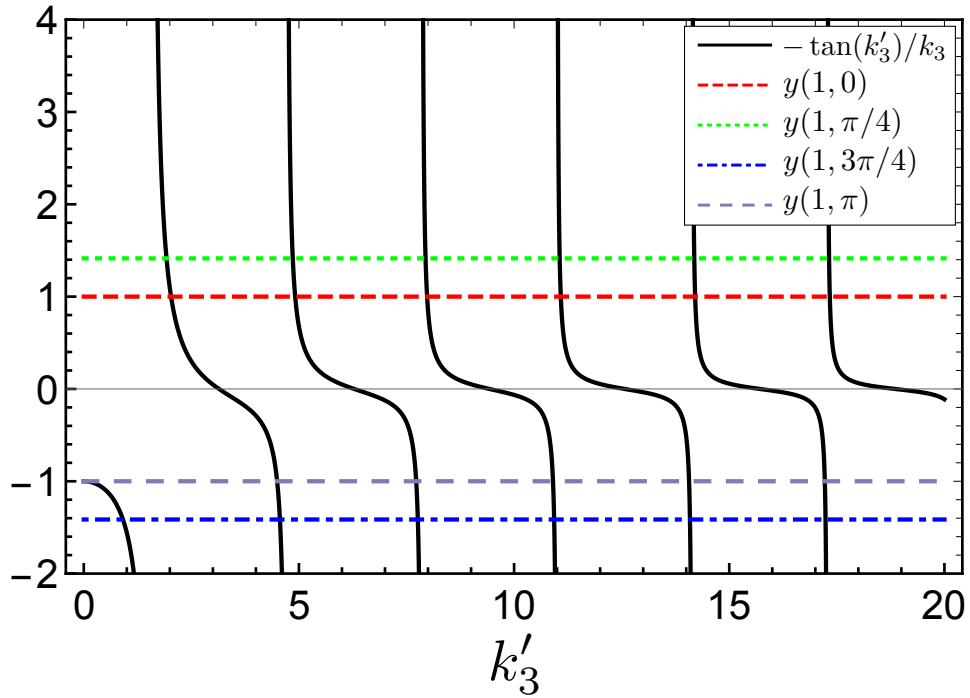
FIGURE 6.1: Plot of the curve $-\tan(k_3')/k_3'$ and the horizontal line $1/m'\cos\Theta \equiv y(m',\Theta)$ as a function of momentum k_3'. The intersection between the curve $-\tan(k_3')/k_3'$ and the horizontal line $y(m',\Theta)$ gives the solutions for the discrete momentum k_{3n}' with $k_{3n}' > 0$ and $n = 1, 2, 3, \dots$. Here, we adopt the parameter $m' = 1$ and four values of the chiral angle $\Theta = 0, \pi/4, \pi, 3\pi/4$. This figure is reproduced from Ref. [70].

To further discuss the discrete momentum, it is more convenient to introduce the following two new parameters

$$k_3' = k_3\ell, \qquad m' = m\ell. \tag{6.19}$$
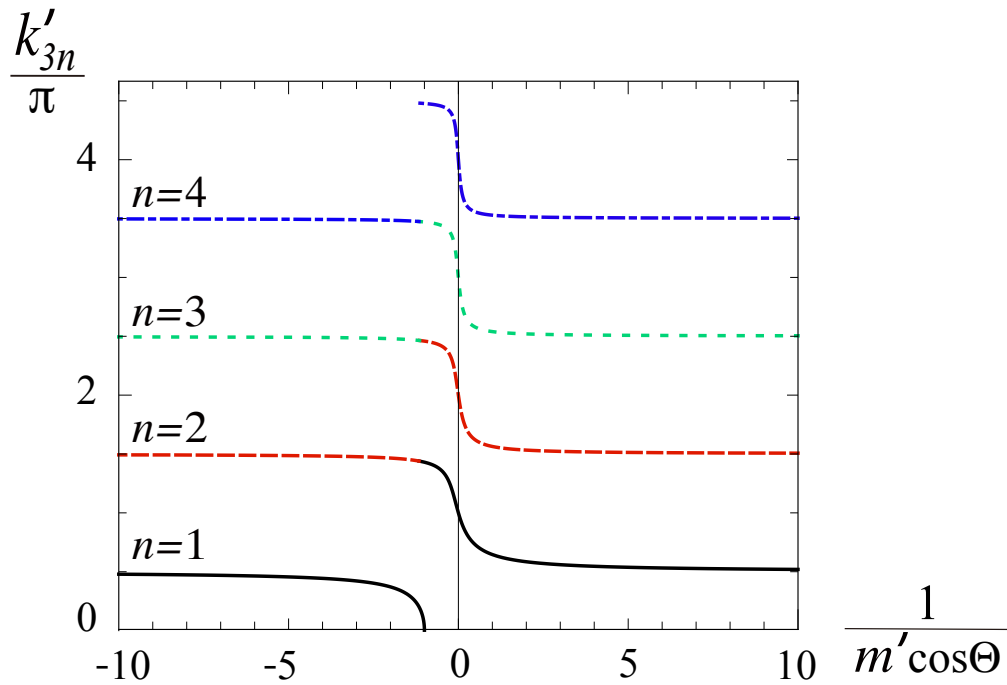
FIGURE 6.2: Discrete momentum solution k'_{3n} for Eq. (6.20) as a function of $1/m' \cos \Theta$. Each curved is normalized by a factor π. We demonstrate for the case of the lowest four states. The black solid curve is for $n = 1$, the dashed red curve is for $n = 2$, the green dotted curve is for $n = 3$, and the blue dash-dotted curve is for $n = 4$. This figure is reproduced from Ref. [70].

Thus, we have

$$-\frac{\tan(k'_3)}{k'_3} = \frac{1}{m' \cos \Theta}. \tag{6.20}$$

With these parameters, the discrete momentum solution k'_{3n} is expressed as a function of m' and chiral angle Θ. In other words, the discrete momentum depends on the mass m, chiral angle Θ, and box's size ℓ. Figure 6.1 plots the curves of $-\tan(k'_3)/k'_3$ and $1/m' \cos \Theta \equiv y(m', \Theta)$ as a function of momentum k'_3, where the intersection between the lines of $-\tan(k'_3)/k'_3$ and $1/m' \cos \Theta \equiv y(m', \Theta)$ provides the solution for discrete momentum k_{3n}, where n denotes the state. This figure demonstrates the various chiral angles with the fixed m'. The curves show that the solution for discrete momentum depends on the chiral angle, as expected. Figure 6.2 demonstrates the momentum solution k'_{3n} for Eq. (6.20), normalized by π as a function of $1/m' \cos \Theta$ for $n = 1, 2, 3$, and 4.

The authors of Refs. [26, 27] showed that the box's size determines whether the system behaves relativisticaly or approaches nonrelativistic or ultrarelativistic limits. Therefore, it

is also essential to discuss the nonrelativistic and ultrarelativistic limits of the discrete momentum. In the nonrelativistic limit $m' \gg 1$, the discrete momentum (6.20) approximately reduces to

$$k_{3n}'^{\mathrm{NR}} \simeq n\pi \left(1 - \frac{1}{m' \cos \Theta} \right), \tag{6.21}$$

where the dependence of the discrete momentum on the chiral angle is coupled to m' in the second term. The contribution of the second term increases under an increase in states n. In the ultrarelativistic limit $m' \ll 1$, the discrete momentum (6.20) approximately reduces to

$$k_{3n}'^{\mathrm{UR}} \simeq \frac{(2n-1)\pi}{2} + \frac{2m' \cos \Theta}{(2n-1)\pi}. \tag{6.22}$$

In the ultrarelativistic limit, the dependence of the discrete momentum on the chiral angle is coupled with the m' in the second term, similar to that in the nonrelativistic limit. However, the contribution of this second term decreases under the growth of states n. In the significantly nonrelativistic limit, the discrete momentum approximately reads $k_{3n}'^{\mathrm{NR}} \simeq n\pi$, which recovers the solution for that of the Schrödinger equation in an infinite potential well. While in the significantly ultrarelativistic limit, the discrete momentum approximately reads $k_{3n}'^{\mathrm{UR}} \simeq (2n-1)\pi/2$. In these two limits, the results are shared with those of under the BC-MIT at the same limits [26, 27], where the results do not depend on the chiral angle.

6.2.2   Energy Levels of a Dirac Particle in a Box

From the above discussion, it is clear that the mirrors under the BC-chiral MIT for the Dirac particle confined in a 1D box require the allowed momenta must be discrete. As a consequence, the energy of a Dirac particle in a 1D box under the BC-chiral MIT is also discrete; this is explicitly expressed as

$$E_n' = \sqrt{m'^2 + k_{3n}'^2}, \tag{6.23}$$

where $E_n' = E_n \ell$ and the momentum solution k_{3n}' satisfies Eq. (6.20). Similar to the discrete momentum, the energy level solution does not depend on the spin orientation but depends on mass m, chiral angle Θ, and the box's size ℓ.

We next discuss the nonrelativistic and ultrarelativistic limits of the energy level (6.23). In the ultrarelativistic limit, the energy level approximately reduces to

$$E_n'^{\text{UR}} \approx k_{3n}'^{\text{UR}} \simeq \frac{(2n-1)\pi}{2} + \frac{2m'\cos\Theta}{(2n-1)\pi}. \tag{6.24}$$

We can see that the energy level in the ultrarelativistic limit approximates that of the discrete momentum in the same limit, where the dependence of the energy level on the chiral angle appears in the second term and is coupled with the parameter m'. Here, the contribution of the second term decreases under an increase in states n. For the significantly ultrarelativistic limit, we find that the energy level does not depend on the chiral angle; it is approximately given by $E_n'^{\text{UR}} \simeq (2n-1)\pi/2$. Under this limit, the result corresponds to that of under the BC-MIT [26, 27]. In the nonrelativistic limit, the energy level approximately reduces to

$$E_n'^{\text{NR}} \approx m' + \frac{(k_{3n}'^{\text{NR}})^2}{2m'} \simeq m' + \frac{(n\pi)^2}{2m'}. \tag{6.25}$$

In this limit, the first and second terms of the energy level (6.25) do not depend on the chiral angle because their dependence are in higher order. For the significantly nonrelativistic limit, we find that the energy level of a Dirac particle confined in a 1D box is approximately given by the rest mass m', which does not depend on the chiral angle and is shared with that of under the BC-MIT [26, 27], similar to the behavior in the ultrarelativistic limit.

6.3   Changes of Spin Orientation due to Reflections at Both Boundaries of Mirrors

In this section, we discuss the changes of spin orientation owing to reflections with both the boundaries following the procedure in Ref. [25].

6.3.1   Changes of Spin Orientation at First Mirror

In the following, we discuss the spin orientation changes generated by the reflection at the first mirror located at $z = 0$, by following Ref. [25] and applying the BC-chiral MIT in Ref. [64]. To discuss the changes of spin orientation, it is more convenient to write the relation between the left- and right-moving wave components in Eq. (6.8) as

$$\xi_{R,s} = (Q_R^{(1)})^{-1} Q_L^{(1)} \xi_{L,s} = \mathcal{U}^{(1)} \xi_{L,s}, \tag{6.26}$$

where

$$Q_R^{(1)} = B\left[i(I + \sin\Theta\sigma_3)\frac{k'_{3n}}{(m' + E'_n)} - \cos\Theta I\right], \tag{6.27}$$

$$Q_L^{(1)} = C\left[i(I + \sin\Theta\sigma_3)\frac{k_{3n}}{(m' + E'_n)} + \cos\Theta I\right], \tag{6.28}$$

and $\mathcal{U}^{(1)}$ is the rotation operator in spin space, given as [25]

$$\mathcal{U}^{(1)} = e^{i\chi^{(1)}}\left[\cos(\frac{\varphi_n^{(1)}}{2})I - i\sin(\frac{\varphi_n^{(1)}}{2})\mathbf{\Upsilon}^{(1)}\cdot\boldsymbol{\sigma}\right]. \tag{6.29}$$

Here, $e^{i\chi^{(1)}}$, $\varphi_n^{(1)}$, and $\mathbf{\Upsilon}^{(1)}$ denote the pure phase, chiral angle, and rotation axis generated by the reflection at the first mirror, respectively. Inserting the coefficients in Eqs. (6.27) and (6.28) into Eq. (6.26), we obtain the relation between the incident and reflected spin orientations at the first mirror; this can be written as

$$\xi_{R,s} = \frac{C}{B}\frac{\cos\Theta}{(ik'_{3n} - m'\cos\Theta)}\left(E'_n I + ik'_{3n}\tan\Theta\sigma_3\right)\xi_{L,s}. \tag{6.30}$$

Decomposing two-component spinors in Eq. (6.30), the components of the right-moving wave can be connected with those of the left-moving wave, as follows

$$\begin{pmatrix}\alpha_{R,s}\\\beta_{R,s}\end{pmatrix} = \frac{C}{B}\frac{\cos\Theta}{(ik'_{3n} - m'\cos\Theta)}\begin{pmatrix}(E'_n + ik'_{3n}\tan\Theta)\alpha_{L,s}\\(E'_n - ik'_{3n}\tan\Theta)\beta_{L,s}\end{pmatrix}. \tag{6.31}$$

To obtain the explicit expression, we next take the equivalent expressions in Eq. (6.26) with Eqs. (6.29) and (6.30), which yields

$$e^{i\chi^{(1)}}\cos(\frac{\varphi_n^{(1)}}{2}) = \frac{C}{B}\frac{E'_n\cos\Theta}{(ik'_{3n} - m'\cos\Theta)}, \tag{6.32}$$

$$e^{i\chi^{(1)}}\sin(\frac{\varphi_n^{(1)}}{2})\mathbf{\Upsilon}^{(1)}\cdot\boldsymbol{\sigma} = -\frac{C}{B}\frac{k'_{3n}\sin\Theta}{(ik'_{3n} - m'\cos\Theta)}\sigma_3. \tag{6.33}$$

It is clear that the role of pure phase can be canceled, and we obtain the expression for the rotation angle and rotation axis at the first mirror as

$$\tan(\frac{\varphi_n^{(1)}}{2}) = -\frac{k'_{3n}\tan\Theta}{E'_n}, \quad \text{and} \quad \mathbf{\Upsilon}^{(1)} = \hat{z}, \tag{6.34}$$

respectively, where $\hat{z}$ is the unit vector in the direction of the z axis. Note that, from Eqs. (6.32) and (6.33), we may choose the rotation axis $\mathbf{\Upsilon}^{(1)} = -\hat{z}$ but with the opposite

sign of the rotation angle $\varphi_n^{(1)}$.

As mentioned above, the discussion for the system featuring one perfectly reflecting mirror under the BC-chiral MIT at $z = 0$ has been previously discussed in Ref. [25]. Our result for the rotation axis given in Eq. (6.34) matches that of Ref. [25]; however, our rotation angle has the opposite sign. The difference comes from the different definitions of chiral angle; here, we used the definition provided in Ref. [64].

6.3.2   Changes of Spin Orientation at Second Mirror

In this subsection, we consider the changes of the spin orientation generated by the reflection at the second mirror. The procedure at the second mirror matches that of the first mirror. Thus, it is more convenient to write the relation between the incident and reflected spin orientations produced by the reflection at the second mirror as

$$\xi_{L,s} = (Q_L^{(2)})^{-1} Q_R^{(2)} \xi_{R,s} = \mathcal{U}^{(2)} \xi_{R,s}, \tag{6.35}$$

where

$$Q_{L,s}^{(2)} = C e^{-ik'_{3n}} \left[i(I - \sin\Theta\sigma_3) \frac{k'_{3n}}{(m' + E'_n)} - \cos\Theta I \right], \tag{6.36}$$

$$Q_{R,s}^{(2)} = B e^{ik'_{3n}} \left[i(I - \sin\Theta\sigma_3) \frac{k'_{3n}}{(m' + E'_n)} + \cos\Theta I \right], \tag{6.37}$$

and $\mathcal{U}^{(2)}$ denotes the rotation operator for the reflection at the second mirror, which can be written as follows [25]

$$\mathcal{U}^{(2)} = e^{i\chi^{(2)}} \left[\cos(\frac{\varphi_n^{(2)}}{2})I - i\sin(\frac{\varphi_n^{(2)}}{2})\mathbf{\Upsilon}^{(2)} \cdot \boldsymbol{\sigma} \right]. \tag{6.38}$$

Here, we use $e^{i\chi^{(2)}}$, $\varphi_n^{(2)}$, and $\mathbf{\Upsilon}^{(2)}$ to denote the pure phase, rotation angle, and unit rotation axis generated by a reflection at the second mirror, respectively. Inserting the two parameters in Eqs. (6.36) and (6.37) into Eq. (6.35), the relation between the incident and reflected spin orientations at the second mirror can be written as

$$\xi_{L,s} = \frac{B e^{2ik'_{3n}}}{C} \frac{\cos\Theta}{(ik'_{3n} - m'\cos\Theta)} (E'_n I - ik'_{3n}\tan\Theta\sigma_3) \xi_{R,s}. \tag{6.39}$$

Decomposing the two-component spinor in Eq. (6.39), the relation between the incident and reflected spin orientations at the second mirror can be written as can be written explicitly

as

$$\begin{pmatrix} \alpha_{L,s} \\ \beta_{L,s} \end{pmatrix} = \frac{Be^{2ik'_{3n}}}{C} \frac{\cos\Theta}{(ik'_{3n} - m'\cos\Theta)} \begin{pmatrix} (E'_n - ik'_{3n}\tan\Theta)\alpha_{R,s} \\ (E'_n + ik'_{3n}\tan\Theta)\beta_{R,s} \end{pmatrix}. \tag{6.40}$$

Taking the equivalence expressions in Eq. (6.35) with Eqs. (6.38) and (6.39), we obtain the following relations

$$e^{i\chi^{(2)}}\cos(\frac{\varphi_n^{(2)}}{2}) = \frac{Be^{2ik'_{3n}}}{C} \frac{E'_n\cos\Theta}{(ik'_{3n} - m'\cos\Theta)}, \tag{6.41}$$

$$e^{i\chi^{(2)}}\sin(\frac{\varphi_n^{(2)}}{2})\mathbf{\Upsilon}^{(2)}\cdot\boldsymbol{\sigma} = \frac{Be^{2ik'_{3n}}}{C} \frac{k'_{3n}\sin\Theta}{(ik'_{3n} - m'\cos\Theta)}\sigma_3. \tag{6.42}$$

Similar to the reflection at the first mirror, the role of the pure phase $e^{i\chi^{(2)}}$ can be factorized out. The rotation angle and rotation axis at the second mirror are expressed as

$$\tan(\frac{\varphi_n^{(2)}}{2}) = -\frac{k'_{3n}\tan\Theta}{E'_n} \quad \text{and} \quad \mathbf{\Upsilon}^{(2)} = -\hat{z}, \tag{6.43}$$

respectively. Here, we choose the rotation axis at the second mirror as $\mathbf{\Upsilon}^{(2)} = -\hat{z}$ because we have chosen the rotation axis at the first mirror as $\mathbf{\Upsilon}^{(1)} = \hat{z}$ (6.34). The opposite direction of the rotation axis is derived from the normal unit vector N_μ opposite to the first and second mirrors. In addition, if we choose the rotation axis $\mathbf{\Upsilon}^{(1)} = -\hat{z}$, we can choose the rotation axis $\mathbf{\Upsilon}^{(2)} = \hat{z}$ with the opposite sign to the rotation angle $\varphi_n^{(2)}$.

6.3.3 Total Reflections inside a Box: Relations between Reflections at First and Second Mirrors

At the previous subsections, we discussed the changes of the spin orientation at both the mirrors. In the following, we discuss the relation between the reflections at the first and second mirrors. Inserting Eq. (6.31) into Eq. (6.40), we have

$$\begin{pmatrix} \alpha_{L,s} \\ \beta_{L,s} \end{pmatrix} = e^{i\Xi} \begin{pmatrix} \alpha_{L,s} \\ \beta_{L,s} \end{pmatrix}. \tag{6.44}$$

The phase factor $e^{i\Xi}$ in Eq. (6.44) is explicitly given by

$$e^{i\Xi} = \frac{e^{2ik'_{3n}}(-ik'_{3n} - m'\cos\Theta)}{(ik'_{3n} - m'\cos\Theta)}, \tag{6.45}$$

which equals 1 for the allowed momentum (6.20). This condition indicates that the reflected spin orientation at the second mirror matches the incident spin orientation at the first one; hence, we can use the Dirac wave function in Eq. (6.1) for this system.

From the reflection at the first mirror (6.31) and second mirror (6.40), we find that the normalized two-component spinor of the left-moving wave component $|\alpha_{RL,s}|^2 + |\beta_{L,s}|^2 = |C|^2/|B|^2$ implies that $|\alpha_{R,s}|^2 + |\beta_{R,s}|^2 = |C|^2/|B|^2$. In other words, the normalisation two-component spinor of the right-moving wave component $|\alpha_{R,s}|^2 + |\beta_{R,s}|^2 = 1$ entails that $|C|^2 = |B|^2$ (cf. Refs. [27, 74]). Comparing the obtained results in Eqs. (6.34) and (6.43), we obtain the relation for the parameters in both mirrors as

$$\varphi_n^{(2)} = \varphi_n^{(1)}, \quad \text{and} \quad \mathbf{\Upsilon}^{(2)} = -\mathbf{\Upsilon}^{(1)}, \tag{6.46}$$

which means that the rotation angles for reflection at both mirrors are identical but their rotation axes are in opposite directions[2]. From Eqs. (6.34) and (6.43), we can also see that the rotation angle depends on the momentum, mass, and chiral angle.

We next discuss the behavior of the rotation angle under the chiral angle in ultrarelativistic and nonrelativistic limits. In the ultrarelativistic limit, the rotation angle at the first and second mirror are approximately given by

$$\tan(\frac{\varphi_n^{(1),\text{UR}}}{2}) = \tan(\frac{\varphi_n^{(2),\text{UR}}}{2}) \simeq -\tan\Theta. \tag{6.47}$$

From this result, we can see that the rotation angle only depends on the chiral angle. More explicitly, the rotation angles are given by $\varphi_n^{(1),\text{UR}} = \varphi_n^{(2),\text{UR}} \simeq -2\Theta$. This indicates that the spin orientation does not change for chiral angle $\Theta = 0, \pi$. In the nonrelativistic limit, the rotation angles are approximately given by

$$\tan(\frac{\varphi_n^{(1),\text{NR}}}{2}) = \tan(\frac{\varphi_n^{(2),\text{NR}}}{2}) \simeq -\frac{n\pi}{m'}\tan\Theta. \tag{6.48}$$

For the significantly nonrelativistic limit, the spin orientation remains identical for all chiral angles; this is explicitly expressed by the condition of $\varphi_n^{(1),\text{NR}} = \varphi_n^{(2),\text{NR}} = 0$. Thus, the result corresponds to those of under the BC-MIT. In this case, we can adopt the total Dirac wave function given in Refs. [26, 27], where the incident and reflected two-component spinors are not distinguished.

---

[2]We may choose the conditions where the rotation axis for the reflection at both mirror are identical but their rotation angles are in opposite, as we mentioned in the previous subsections.

6.4 Density Functions of a Dirac Particle in a Box

In this section, we analyze the behavior of three types of density functions: the probability, normal probability current, and scalar densities [70]. Here, we use the parameter $z'(\equiv z/\ell)$; thus, the particle is confined to a box with a scaled size of $z' = 1$.

6.4.1 Probability Density of a Dirac Particle in a Box

First, we start the discussion of the density functions by considering the probability density of a Dirac particle confined in a 1D box, where the energy eigenstate and discrete momentum are determined by the BC-chiral MIT. To obtain the explicit expression for the probability density, we use the relations of normalized two-component spinors: $|\alpha_{L,s}|^2 + |\beta_{L,s}|^2 = 1$ and $|\alpha_{R,s}|^2 + |\beta_{R,s}|^2 = |C|^2/|B|^2 (= 1)$. Furthermore, we use the relation between coefficients B and C given in Eqs. (6.11) and (6.12). Then, we find that the probability density of a Dirac particle in a 1D box is given by

$$
\begin{aligned}
\rho_{k'_{3n},s}(z') &= \bar{\psi}^{\text{Box}}_{k'_{3n}s}(z')\gamma^0 \psi^{\text{Box}}_{k'_{3n}s}(z') \\
&= \frac{2|C|^2}{(m'+E'_n)}\left[2E'_n + (\mathcal{D}_n e^{-2ik'_{3n}z'} + \mathcal{D}_n^* e^{2ik'_{3n}z'})m'\right],
\end{aligned}
\tag{6.49}
$$

where the coefficient $\mathcal{D}_n$ is given by

$$
\mathcal{D}_n = \frac{(-E'_n \cos\Theta + ik'_{3n}\sin\Theta(|\alpha_{L,s}|^2 - |\beta_{L,s}|^2))}{(ik'_{3n} + m'\cos\Theta)}.
\tag{6.50}
$$

From the above expression, we can see that the probability density of a Dirac particle in a 1D box under the BC-chiral MIT depends on the chiral angle and spin orientation. This dependence appears in the second term of the numerator in Eq. (6.50). It arises from the interference between the left- and right-moving wave components. Here, the coefficient $|C|^2$ is determined using the following condition

$$
\int_0^1 \rho_{k'_{3n}s}(z')dz' = 1 .
\tag{6.51}
$$

We demonstrate the dependence of the probability density on the spin orientation in Figs. 6.3 and 6.4 for the parameters $m' = 10$ and $m' = 2$, respectively. Here, we use five values of the chiral angles as $\Theta = 0, \pi/4, \pi/2, 3\pi/4, \pi$. More specifically, in the top panel, we consider the case of a spin orientation in the $\pm x$- or $\pm y$-directions, where $|\alpha_{L,s}|^2 - |\beta_{L,s}|^2 = 0$.
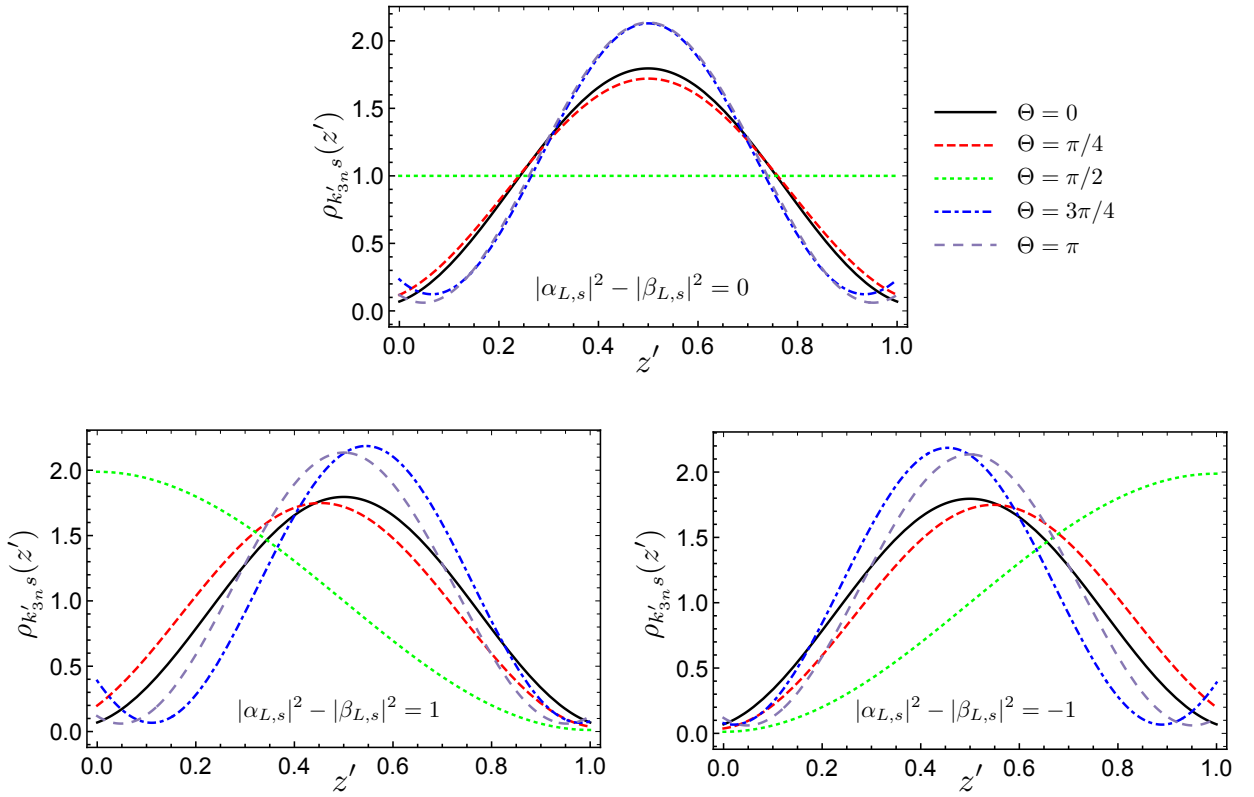
FIGURE 6.3: The probability densities of the ground state Dirac particle confined in a 1D box as a function of z' with the parameter $m' = 10$ and five values of the chiral angle $\Theta = 0, \pi/4, \pi/2, 3\pi/4, \pi$. We demonstrate three conditions for the spin orientation of the left-moving wave component. The upper panel corresponds to the condition in which the left-moving wave component has a spin orientation in the $\pm x$- or $\pm y$-direction ($|\alpha_{L,s}|^2 - |\beta_{L,s}|^2 = 0$), the lower-left panel corresponds to the $+z$-direction ($|\alpha_{L,s}|^2 - |\beta_{L,s}|^2 = 1$), and the lower-right panel corresponds to the $-z$-direction ($|\alpha_{L,s}|^2 - |\beta_{L,s}|^2 = -1$). These figures are reproduced from Ref. [70].

In these directions, we can see that the distributions of the probability density inside a box are symmetrical. In contrast, when the spin orientation is in the $+z$- or $-z$-directions, asymmetrical distributions are observed (see the lower panels). These properties correspond to the chiral angle and behavior of the spin direction at the first and second mirrors. It can be discussed in more detail as follows. From Eqs. (6.49) and (6.50), we can see that when "$\sin\Theta = 0$" and/or "$|\alpha_{L,s}|^2 - |\beta_{L,s}|^2 = 0$", the distributions will be symmetrical. When the chiral angle takes value $\Theta = 0, \pi$, the distributions will be symmetrical for all spin orientations. When we have "$|\alpha_{L,s}|^2 - |\beta_{L,s}|^2 = 0$" (e.g., when the spin orientation is in the $\pm x$- or $\pm y$-directions), the distributions inside a box will be symmetrical for all chiral angles. The condition of the spin orientation in the $\pm z$-directions related to the condition of "$|\alpha_{L,s}|^2 - |\beta_{L,s}|^2 \neq 0$". This may explain why we have asymmetrical distribution for the chiral angle $\Theta \neq 0, \pi$. Furthermore, when the incident spin orientation is in the $\pm z$-directions, the

reflected spin state has the same direction as the incident one.
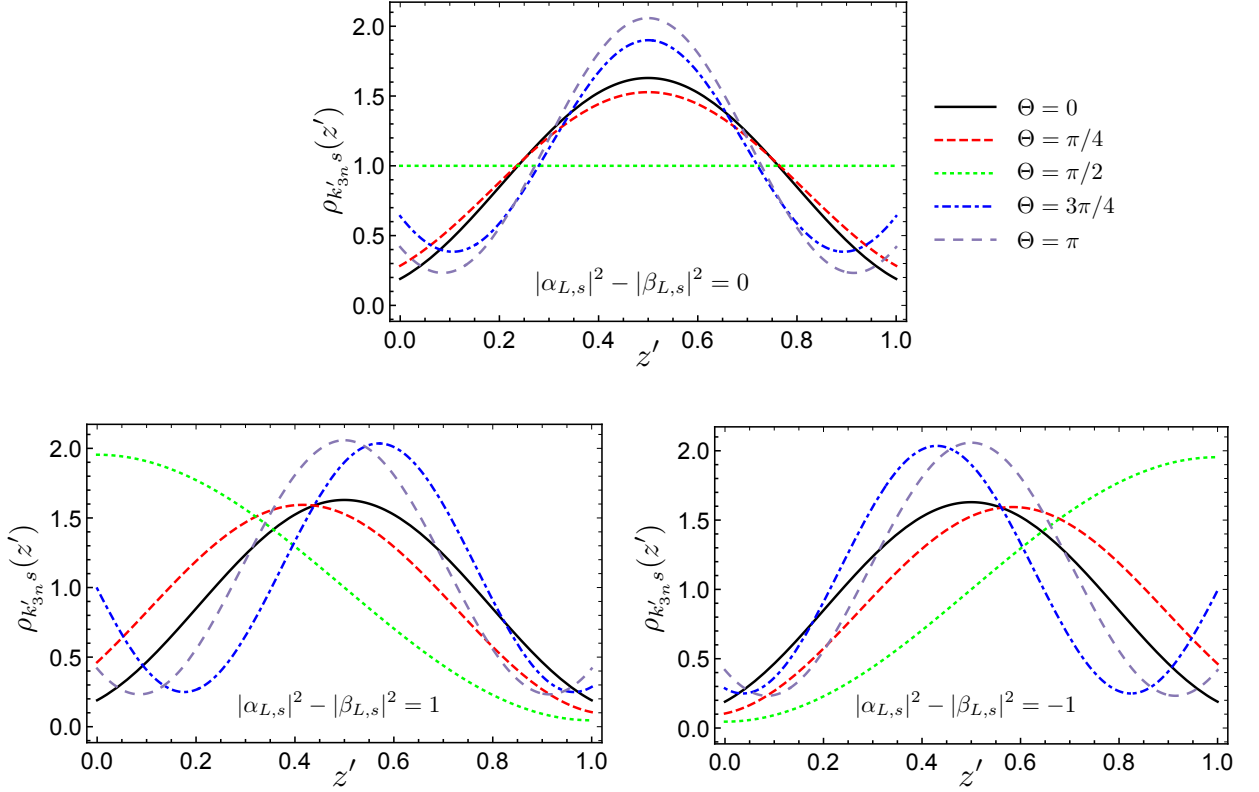
FIGURE 6.4: Similar to Fig. 6.3 but for the parameter $m' = 5$. The behaviors for each panel have similar properties to those of Fig. 6.3.

We next discuss the properties of the probability density as a function of the box's size. As has been shown by Refs. [26, 27], the box's size determines whether the system approach ultrarelativistic or nonrelativistic limits. In the nonrelativistic limit, the probability density for a Dirac particle in a box (6.49) approximately reduces to

$$\rho_{k_{3n}^{\prime\text{NR}}s}^{\text{NR}}(z') \simeq 2|C|^2 \left(1 + \mathcal{F}e^{-2ik_{3n}^{\prime\text{NR}}z'} + \mathcal{F}^*e^{2ik_{3n}^{\prime\text{NR}}z'} \right), \tag{6.52}$$

where we the coefficient $\mathcal{F}$ is approximately given by

$$\mathcal{F} \simeq \frac{-m'\cos\Theta - ik_{3n}^{\prime\text{NR}} + ik_{3n}^{\prime\text{NR}}\sin\Theta(|\alpha_{L,s}|^2 - |\beta_{L,s}|^2)}{2m'\cos\Theta}, \tag{6.53}$$

For the significantly nonrelativistic limit in the non-chiral case, we obtain the approximate probability density of a Dirac particle in a 1D box as $4|C|^2\sin^2(k_{3n}^{\prime\text{NR}}z')$. In this limit, we can see that the probability density reduces to the familiar probability density for the Schödinger equation in an infinite potential well or in a box. Furthermore, we can also see that the probability density does not depend on the spin orientation. In the ultrarelativistic limit,
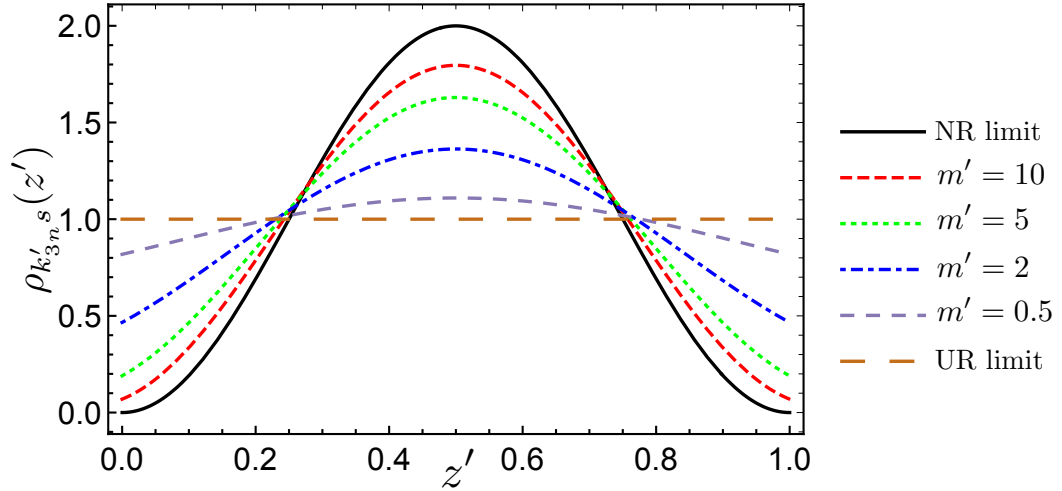
FIGURE 6.5: The probability density of the ground state Dirac particle confined in a 1D box with the values of the parameter $m' = 0.5, 2, 5$, and 10 in the non-chiral case in comparison with the nonrelativistic (NR) and ultrarelativistic (UR) limits. The probability density in the nonrelativistic limit vanishes at both the boundaries $z' = 0$ and $z' = 1$. In the ultrarelativistic limit, the probability density gives the constant value along z' inside the box. This figure is reproduced from Ref. [70].

the probability density for a Dirac particle in a box (6.49) approximately reduces to

$$\rho^{\mathrm{UR}}_{k'^{\mathrm{UR}}_{3n}s}(z') \simeq \frac{2|C|^2}{k'^{\mathrm{UR}}_{3n}} \left(2k'^{\mathrm{UR}}_{3n} - 2m' + \mathcal{G}e^{-2ik'^{\mathrm{UR}}_{3n}z'} + \mathcal{G}^*e^{2ik'^{\mathrm{UR}}_{3n}z'} \right), \tag{6.54}$$

where the coefficient $\mathcal{G}$ is approximately given by

$$\mathcal{G} \simeq im'\cos\Theta + m'\sin\Theta(|\alpha_{L,s}|^2 - |\beta_{L,s}|^2). \tag{6.55}$$

For the significantly ultrarelativistic limit in the non-chiral case, we obtain the approximate probability density of a Dirac particle in a 1D box as $4|C|^2$, which generates a constant distribution along z' inside the box. In addition, the probability density does not depend on the spin orientation, similar to the results obtained using the BC-MIT.

Figure 6.5 depicts the probability density for a Dirac particle confined in a box for the parameter $m' = 0.5, 2, 5$, and 10 in the non-chiral case, in comparison with the significantly nonrelativistic and ultrarelativistic cases. This figure shows that a smaller m' brings the probability density close to the ultrarelativistic limit. In contrast, a larger parameter m' brings the probability density close to the nonrelativistic one. From this figure, we can see that the different limits give different curves. For the nonrelativistic limit, the curve is proportional to $\sin^2 k'^{\mathrm{NR}}_{3n}z')$. While in the ultrarelativistic limit, the probability density is given by a constant along z', as we previously mentioned. Note that the value of $|C|^2$

is determined by the condition in Eq. (6.51). The authors of Ref. [26] have previously demonstrated the behavior of the probability density as a function of the box's size (see Fig. 5 of Ref. [26]); they showed that a larger box size pushes the probability density towards the nonrelativistic limit. From this figure, we can also see that the distribution for all parameters m' gives the symmetrical distribution. This is because we use the non-chiral case.

The different nature between the probability densities in the nonrelativistic and ultrarelativistic limits may be associated with the boundary conditions' roles at both limits. The BC-chiral MIT for the significantly nonrelativistic limit of the Dirac wave function approximately reduces to the Dirichlet boundary condition of a vanishing Dirac wave function at the boundary surface; this coincides with the Schrödinger equation in a box. In contrast, the BC-chiral MIT for the significantly ultrarelativistic limit does not reduce to the Dirichlet boundary condition. In this limit, the boundary condition remains to depend on the chiral angle. This kind of property does not appear for the nonrelativistic one. Later, we will show that the different properties at both limits also appear for the scalar density as well as rotation angle.

6.4.2 Normal Probability Current Density of a Dirac Particle in a Box

The normal component of the probability current density of a Dirac particle confined in a 1D box is expressed as

$$J_{N,k'_{3n}s}(z') = J^3_{k'_{3n}s}(z') = \bar{\psi}_{k'_{3n}s}(z')\gamma^3\psi_{k'_{3n}s}(z'), \tag{6.56}$$

which vanishes everywhere. This is similar to the case of a Dirac particle in Rindler coordinates [23, 31]. Note that to obtain complete results for the normal probability current, we use the same strategy as for probability density; that is, we use $|\alpha_L|^2 + |\beta_L|^2 = 1$, $|\alpha_R|^2 + |\beta_R|^2 = |C|^2/|B|^2(= 1)$, and the relation between B and C given in Eqs. (6.11) and (6.12).

The detailed contributions of each term are as follows: The contribution of the left-moving wave component to the normal probability current density is canceled by that of the right-moving one. The interference term between the left- and right-moving wave components vanishes everywhere. Finally, we find that the total normal probability density vanishes trivially everywhere as well. This indicates that we cannot directly use the vanishing normal probability current density at the boundary surface as a boundary condition for

our system. Furthermore, when we use this condition as the direct boundary condition, we lose the role of the chiral angle.

6.4.3 Scalar Density of a Dirac Particle in a Box

The scalar density of a Dirac particle in a 1D box as a function of z' is given by

$$
\begin{aligned}
q_{k'_{3n}s}(z') &= \bar{\psi}_{k'_{3n}s}(z')\psi_{k'_{3n}s}(z') \\
&= \frac{2|C|^2}{(E'_n + m')}\left[2m' + (\mathcal{D}_n e^{-2ik'_{3n}z'} + \mathcal{D}_n^* e^{2ik'_{3n}z'})E'_n\right],
\end{aligned} \tag{6.57}
$$

where $\mathcal{D}_n$ is given by Eq. (6.50) and shared with the probability density. Similar to the probability and normal probability current densities, to obtain the scalar density, we used $|\alpha_{L,s}|^2 + |\beta_{L,s}|^2 = 1$, $|\alpha_{R,s}|^2 + |\beta_{R,s}|^2 = |C|^2/|B|^2 (= 1)$, and the relation between B and C in Eq. (6.11). Here, the coefficient $|C|^2$ is determined by the condition given in Eq. (6.51).
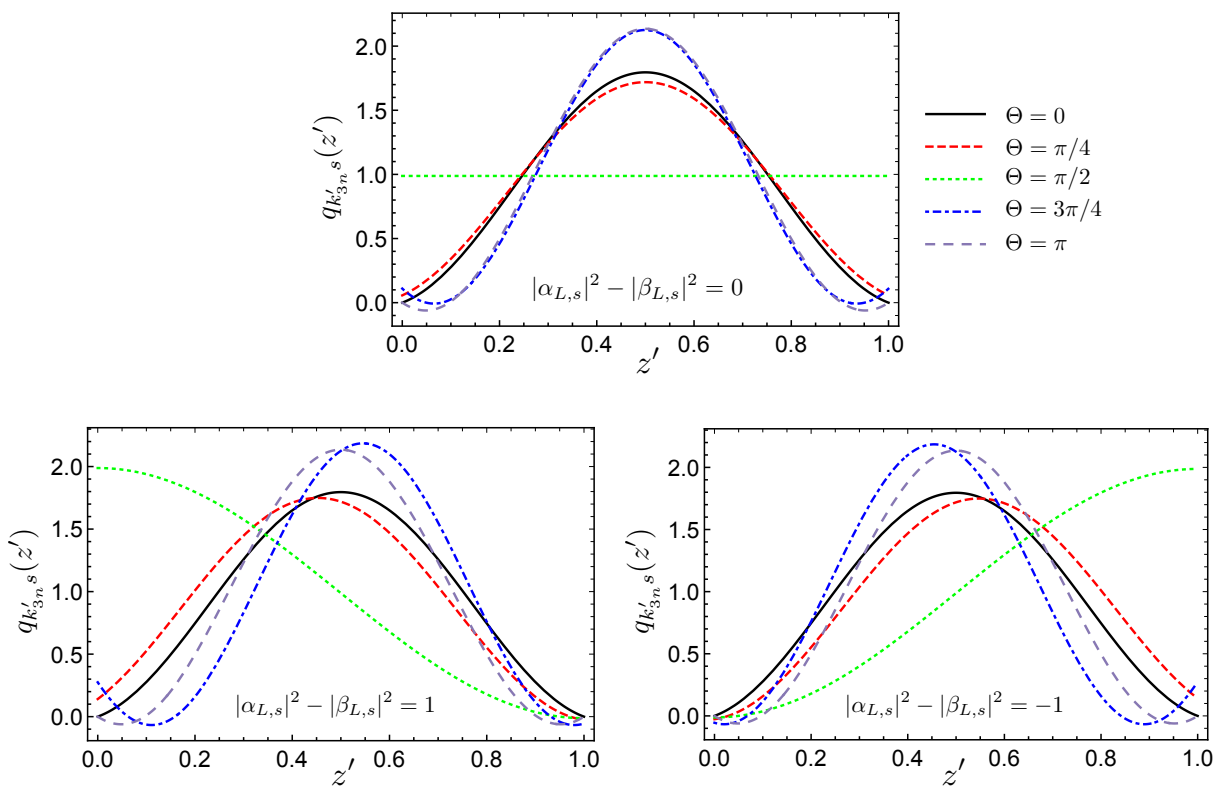
FIGURE 6.6: Scalar density for the ground state Dirac particle in a 1D box. Here, we used the same parameters for the chiral angle and spin orientation as those given in Fig. 6.3 for each panel. The scalar density for the case of the chiral angle $\Theta = 0, \pi$ vanishes at both the boundaries, as a consequence of the boundary condition. These figures are reproduced from Ref. [70].
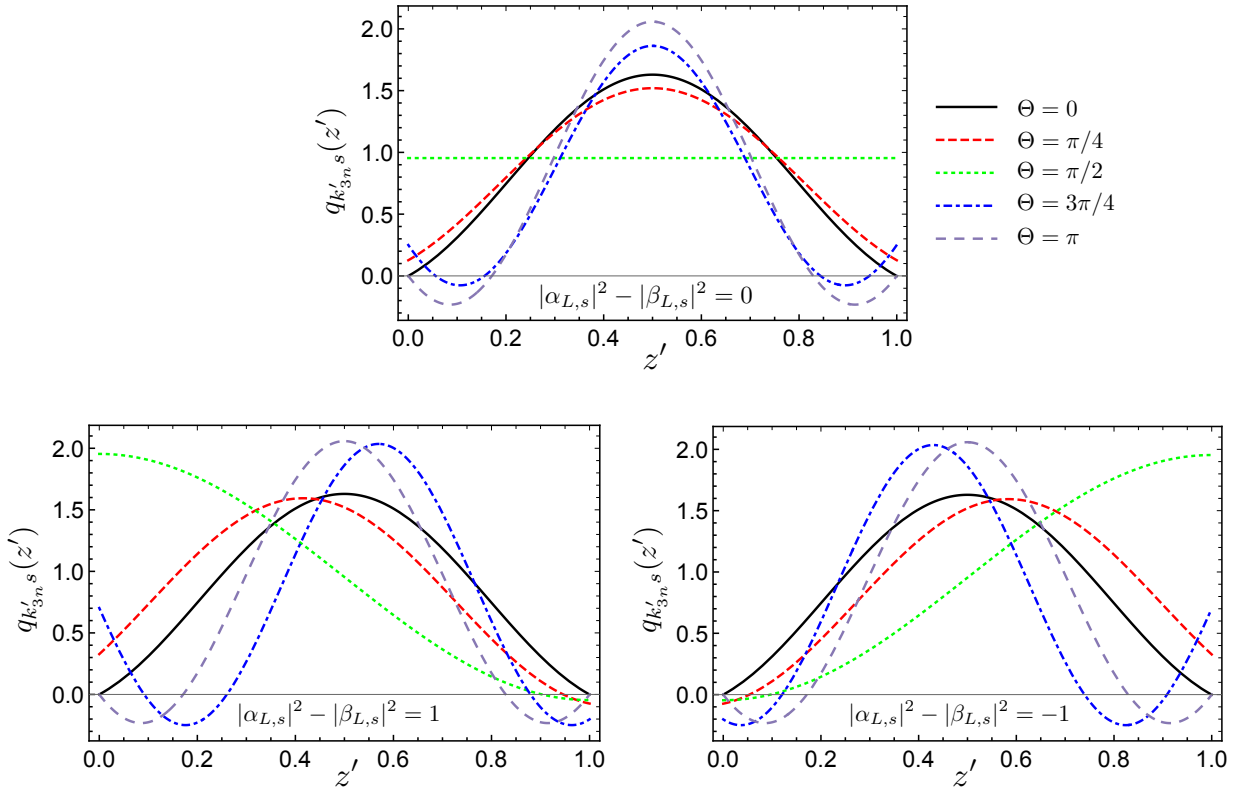
FIGURE 6.7: Similar to Fig. 6.6, but for the parameter $m' = 5$. The behaviors for each panel have similar properties to those of Fig. 6.6.

Figures 6.6 and 6.7 demonstrate the curves for the scalar density of the ground state Dirac particle in a 1D box for the parameters $m' = 10$ and $m' = 5$ with various chiral angles and spin orientation, respectively. The curves show that the scalar density vanishes at the boundary surface when the chiral angle takes the following two values as $\Theta = 0, \pi$. This behavior is consistent with the default properties of the boundary condition that we adopt (i.e., the BC-chiral MIT), which ensures a vanishing scalar density around the mirror for the chiral angle $\Theta = 0, \pi$. In these chiral angles, the scalar density does not depend on the spin orientation because the second term of the numerator in Eq. (6.50) becomes zero. The distributions inside a box in these chiral angles are symmetrical. Similar to the probability density, the scalar density for the Dirac particle in a box also depends on the chiral angle and spin orientation in general. For example, when the left-moving wave component has a spin orientation in the $\pm x$- or $\pm y$-directions (see the upper panel), the distribution of scalar density is symmetrical; however, when the left-moving wave component has a spin orientation in the $+z$- or $-z$-directions (see the lower panels), the distribution of the scalar density is asymmetrical. Similar to the probability density, this difference of behavior depends on the chiral angle and spin orientation.
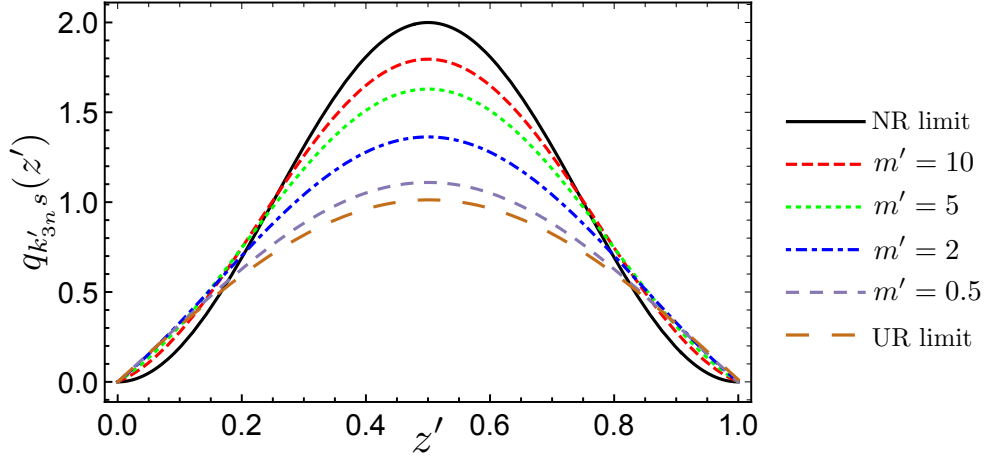
FIGURE 6.8: The scalar density of the ground state Dirac particle confined in a 1D box with the variational values of the parameter m' in the non-chiral case in comparison with the nonrelativistic and ultrarelativistic limits. The scalar density in the non-chiral case for all states n vanishes at both the boundary surfaces. This behavior is a consequence or requirement the boundary conditions. This figure is reproduced from Ref. [70].

In the ultrarelativistic limit, we have the approximation form for the scalar density of a Dirac particle in a 1D box as follows

$$q_{k'_{3n}s}^{\mathrm{UR}}(z') \simeq \frac{2|C|^2}{k'^{\mathrm{UR}}_{3n}} \left(2m' + \mathcal{P}e^{-2ik'^{\mathrm{UR}}_{3n}z'} + \mathcal{P}^*e^{2ik'^{\mathrm{UR}}_{3n}z'} \right), \tag{6.58}$$

where the coefficient $\mathcal{P}$ is given by

$$\mathcal{P} \simeq (im'\cos\Theta + k'^{\mathrm{UR}}_{3n} - m')(i\cos\Theta + \sin\Theta(|\alpha_{L,s}|^2 - |\beta_{L,s}|^2). \tag{6.59}$$

For the significantly ultrarelativistic limit in the non-chiral case, the scalar density approximately reduces to $4|C|^2\sin(2k'^{\mathrm{UR}}_3)$. In this condition, we can see that the scalar density does not depend on spin orientation. We can also see that its form differs from the probability density in the same limit. In the nonrelativistic limit, we obtain the approximate form for the scalar density as

$$q_{k'^{\mathrm{NR}}_{3n}s}^{\mathrm{NR}}(z') \simeq 2|C|^2 \left(1 + \mathcal{F}e^{-2ik'^{\mathrm{NR}}_{3n}z'} + \mathcal{F}^*e^{2ik'^{\mathrm{NR}}_{3n}z'} \right), \tag{6.60}$$

where $\mathcal{F}$ is given by (6.53), which is shared with the probability density of the nonrelativistic limit. For the significantly nonrelativistic limit in the non-chiral case, the scalar density of a Dirac particle in a 1D box is approximately given by $4|C|^2\sin^2(k'^{\mathrm{NR}}_{3n}z')$, which is shared with the probability density of a Dirac particle in the same limit and case.

Figure 6.8 shows the curves of scalar density for the ground state Dirac particle
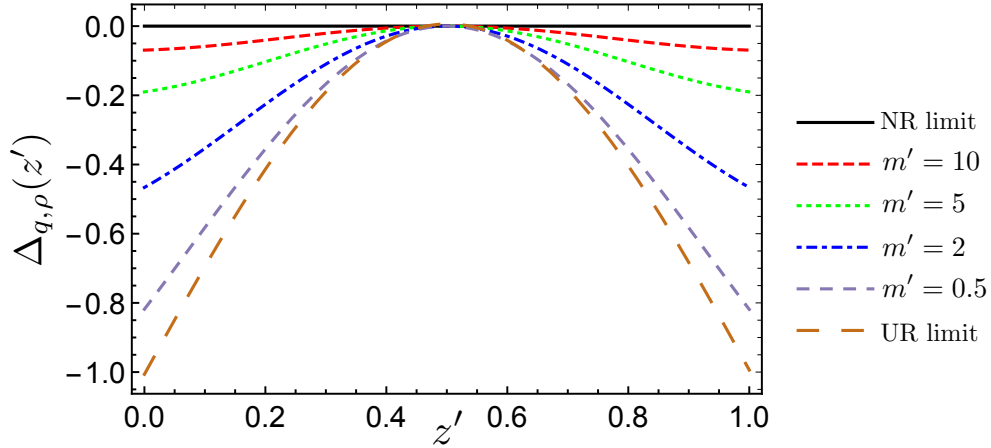
FIGURE 6.9: The difference between the curves of the probability density (Fig. 6.5) and scalar density (6.8), as defined by $\Delta_{q,\rho}(z') \equiv \rho_{k'_{3n},s}(z') - q_{k'_{3n},s}(z')$ for certain values of the parameter m' in the non-chiral case. The difference becomes larger as the decreases of the parameter m'. In contrast, the differences becomes smaller as the increases of the parameter m'.

in a 1D box with $m' = 0.5, 2, 5$, and 10 in the non-chiral case, in comparison with the significantly nonrelativistic and ultrarelativistic limits. This figure shows that the scalar density for all states n vanishes at the boundary surfaces. This behavior can be understood as a consequence of the non-chiral case of the chiral MIT boundary condition. Similar to the behavior of probability density, the scalar density approaches the nonrelativistic limit at larger m' and approaches the ultrarelativistic limit at smaller m'. From this figure, we can also see that the distribution of the scalar density inside a box is symmetrical, which is generated by the non-chiral case.

When one tries to compare the probability density in Fig. 6.3 with the scalar densities in Fig. 6.6, the two densities look to give the same distributions inside the box. This is because we used the parameter $m' = 10$, which is relatively close to the nonrelativistic limit [26, 27]. In addition, in Figs. 6.5 and 6.8, we can see that the probability and scalar densities in the case of the nonrelativistic limit produce the same approximation. However, for certain values of the chiral angle, their behaviors around the boundary surface differ. The probability density for the relativistic particle under the BC-chiral MIT does not vanish at the boundary surface. Instead, its scalar density vanishes when the chiral angle takes the values of the parameter $\Theta = 0, \pi$. In the case of the parameter $m' = 10$, the order of the difference between the probability and scalar densities is relatively small. If we choose smaller values of parameter m', the difference becomes significant (see Fig. 6.9). In the nonrelativistic limit, both the probability and scalar densities exhibit a similar curve (see Fig. 6.9 and Eqs. (6.52) and (6.60)). However, the curve of probability density in the ultrarelativistic limit differs from its scalar density in the same limit. The behavior of the

ultrarelativistic limit of probability density in the non-chiral case resembles the relativistic probability density in the case $\Theta = \frac{\pi}{2}$, which becomes constant along the z' axis. Meanwhile, this property does not arise for the scalar density in the ultrarelativistic limit of the case $\Theta = 0$. Its behavior inside the box for $m' = 0$ and $\Theta = 0$ is described by the sine function, $\sin(2k_{3n}'^{\text{UR}} z')$, rather than a constant along the z' axis.

Chapter 7

Summary and Conclusion

We studied quantum states in an external gravitational field. Quantum systems under the influence of a gravitational field are interesting to discuss because quantum mechanics and relativity operate simultaneously within them. One phenomenon that can be observed in the laboratory is the existence of gravitationally quantum bound states of the UCN [14–20], which are consistent with the theoretical predictions for the quantum bouncer problem of the Schrödinger equation in a linear gravitational potential under a perfectly reflecting mirror (see e.g., Refs. [3–12]). In such situations, the quantum bouncer exhibits discrete energy levels associated with the normalizable wave function.

In this thesis, we revisited the quantum bouncer problem, focusing on the relativistic effects in gravitational quantum states. Using the equivalence principle [22], the system can be seen as a free particle repeatedly bounced off by a uniformly accelerated mirror in Minkowski space. Alongside the scenario, we discussed the properties of the Klein–Gordon and Dirac equations in Rindler coordinates under the mirror boundary conditions. As shown in Refs. [23], in the nonrelativistic limit, the energy levels of relativistic bouncing particles reduce to familiar eigen-energies for the Schrödinger equation in a linear gravitational field under a perfectly reflecting mirror.

For the Schrödinger equation, we adopted the Dirichlet boundary conditions to represent the barrier step Fermi-pseudo potential, where a bouncing particle is assumed to see an infinite potential around the mirror. The main feature of this boundary condition is that it requires a vanishing wave function around the mirror. The same boundary condition is applied for the Klein–Gordon equation, where a free massive scalar field in Rindler coordinates was imposed to vanish at the floor [24]. However, if one imposes the Dirichlet boundary conditions upon the Dirac equation, the solution will vanish trivially everywhere [23] (see

also Ref. [26]). As an alternative, in the present study, we adopted the BC-MIT [28–30] to represent the finite fermi pseudo potential barrier while avoiding the Klein paradox problem. This boundary condition guarantees a vanishing normal probability current and scalar densities at the boundary surfaces. In this discussion, it was unnecessary to discuss the Dirac equation using the boundary condition from the chiral bag model [33–42], despite its being more general than the MIT one.

Using the above analysis, we compared the energy levels of all bouncing particles. We found that the energy level of a Klein–Gordon bouncer always exceeds its nonrelativistic limit for all states, while the energy levels of Dirac and Majorana bouncers are lower than their nonrelativistic limits for the lowest few states and are shifted to exceed that limit for sufficiently large states. The differences in values from the relativistic to the nonrelativistic can be understood as relativistic corrections associated with the specific boundary conditions.

The parameter of the shift of the energy spectrum is not detectable in the laboratory. However, one can measure the parameter of the transition frequencies between two energy eigenstates of the bouncing particles, for example, by using gravitational resonance spectroscopy [118–122]. From our analysis of the quantum bouncers, we found that the transition frequencies between the two energy eigenstates of all relativistic bouncers exceeded their nonrelativistic limits for all states, where the transition frequencies for Dirac and Majorana particles exceeded those of the Klein–Gordon ones. We applied the obtained analytic solutions to both the UCN and Ps atoms. The energy levels of the quantum bouncer for the Ps atom were smaller than those of the UCN. In contrast, the relativistic corrections to the transition frequency of the Ps atom exceeded those of the UCN. However, the relativistic corrections of the transition frequencies for both UCN and Ps atoms were too small to be detectable with present technology.

The different behaviors of the energy levels for bouncing particles may be associated with the behavior of their wave functions, in particular around the boundary surface. Therefore, in the present study, we also discussed the density functions for the bouncing particles: the probability, normal probability current, and scalar densities. The distribution shows that the probability densities of nonrelativistic and Klein–Gordon bouncers exhibit the same behavior: that of vanishing at the mirror surface. This behavior is a consequence of the Dirichlet boundary condition. We also found that the probability densities of both nonrelativistic and Klein–Gordon bouncers are time-independent. The probability density of a Dirac bouncer does not vanish at the mirror surface, in contrast to those of nonrelativistic and Klein–Gordon bouncers. In addition, the probability density of a Dirac bouncer

is also time-independent. The probability density of a Majorana bouncer includes a factor that rapidly oscillates as a function of time. This factor corresponds to the *Zitterbewegung* and depends on the spin orientation. For example, when the spin orientation is in the $\pm z$-directions, the *Zitterbewegung* vanishes for all states. In the condition of vanishing *Zitterbewegung*, the probability density of a Majorana bouncer coincides with that of a Dirac bouncer. The *Zitterbewegung* also appears in the normal probability current density of a Majorana bouncer. When the *Zitterbewegung* in the normal probability current density of a Majorana bouncer vanishes for all states, its distributions coincide with that of a Dirac bouncer, which vanishes everywhere. The presence of the *Zitterbewegung* does not come from the BC-MIT, rather from the interference between the positive- and negative-energy components of the Majorana wave function. The scalar density of a Dirac bouncer does not vanish in general; however, it vanishes at the floor as a consequence of the BC-MIT (see Fig. 5.2). In contrast, the scalar density of a Majorana bouncer vanishes everywhere because the charge conjugation of the Majorana wave function is completely identical to itself. The normal probability current density of a Dirac bouncer vanishes everywhere while that of the Majorana particle does not. The normal probability current density of a Majorana bouncer vanishes at the mirror surface, as required by the BC-MIT.

Note that one can also introduce more general boundary conditions that retain the vanishing normal current density around the boundary surface [42]. A general form of the BC-MIT, which includes the chiral angle, is the BC-chiral MIT [42, 64, 65]. In the non-chiral case, the BC-chiral MIT reduces to the BC-MIT. For the reflection system of the wave function comprising incident and reflected components, one can discuss the interaction between the particle and boundary surface, e.g., the changes of spin orientations under the boundary conditions [25].

To investigate the roles of boundary conditions in more detail, we revisited the system of a Dirac particle confined to a 1D box, using the BC-chiral MIT in describing the properties of the boundary surfaces of the box. A similar confinement system has been previously discussed in Ref. [26] (cf. Ref. [27]), though they used the BC-MIT. The results show that the Dirac particle has discrete momentum and energy levels; generally, these depend on the chiral angle but not on the spin orientation. In the non-chiral case, the results reduce to the results in Refs. [26, 27]. In the significantly nonrelativistic limit, the energy levels of a Dirac particle reduce to the results for the problem of the Schrödinger equation in a box.

For this confinement system, we also discussed the change of spin orientation produced by reflections between the particle and mirrors for the confinement system under the BC-chiral MIT (cf. Ref. [25]). We found that the changes of spin orientation depend on the

chiral angle. For the non-chiral case, we found that the spin orientation does not change. This may explain the reflection for the above Dirac and Majorana bouncing particles under the BC-MIT. The obtained results show that in the confinement system, the reflected wave component at the second mirror exactly matches the incident wave component at the first one, which means that the spin state is in a consistent state to repeat the reflections at both mirrors.

We further discussed the behavior of the density functions for a Dirac particle confined in a 1D box. The results show that the distribution of the probability and scalar densities can be asymmetric, depending on the chiral angle and initial spin orientations. In contrast, the normal probability current density of the Dirac particle vanishes everywhere. As shown in Refs. [26, 27], the box's size determines whether the system approaches the ultrarelativistic or nonrelativistic limits. A study into the boundary conditions for the confinement system might also be helpful in related topics such as the finite volume effect (cf. Refs. [66, 69]).

Acknowledgements

Appendix A

Dirac Equation in Minkowski Coordinates

The Dirac equation for a particle with mass m in Minkowski coordinates is given by

$$(i\gamma^\mu \partial_\mu - m)\Psi_{\boldsymbol{k}s}(t, \boldsymbol{x}) = 0, \tag{A.1}$$

where s denotes the spin orientation and γ^μ are gamma matrices in the Dirac representation given in Eq. (4.4). To proceed, we introduce the general solution to the Dirac equation as

$$\Psi_{\boldsymbol{k}s}(t, \boldsymbol{x}) = u_{\boldsymbol{k}s}e^{-iEt}e^{i\boldsymbol{k}\cdot\boldsymbol{x}}, \tag{A.2}$$

where $E = \sqrt{m^2 + |\boldsymbol{k}|^2}$ is the energy of the Dirac particle and $u_{\boldsymbol{k}s}$ is a four-component Dirac spinor. Then, the Dirac spinor $u_{\boldsymbol{k}s}$ can be decomposed into the upper two-component spinor ξ_s and lower two-component spinor χ_s as

$$u_{\boldsymbol{k}s} = \begin{pmatrix} \xi_s \\ \chi_s \end{pmatrix}. \tag{A.3}$$

Substituting back the Dirac spinor (A.3) to the Dirac equation (A.1), we obtain the following two coupled equations

$$(E - m)\xi_s - \boldsymbol{\sigma}\cdot\boldsymbol{k}\chi_s = 0, \tag{A.4}$$

$$(E + m)\chi_s - \boldsymbol{\sigma}\cdot\boldsymbol{k}\xi_s = 0, \tag{A.5}$$

where Eqs. (A.4) and (A.5) are associated with the negative- and positive-energy solutions, respectively. Herein, we focus on the solution for positive-energy, which implies that the Dirac solution can be written explicitly as

$$\Psi_{\boldsymbol{k}s}(t, \boldsymbol{x}) = \mathcal{N}_{\boldsymbol{k}s} \begin{pmatrix} \xi_s \\ \frac{\boldsymbol{\sigma}\cdot\boldsymbol{k}}{(m+E)}\xi_s \end{pmatrix} e^{-iEt} e^{i\boldsymbol{k}\cdot\boldsymbol{x}}, \tag{A.6}$$

where ξ_s is the normalized two-components spinor $\xi_s^\dagger \xi_s = 1$, and $\mathcal{N}_{\boldsymbol{k}s}$ is the normalization constant obtained by

$$(\Psi_{\boldsymbol{k}s}, \Psi_{\boldsymbol{k}'s'}) = \int d^3\boldsymbol{x}\, \Psi_{\boldsymbol{k}s}^\dagger \Psi_{\boldsymbol{k}'s'} = \delta(\boldsymbol{k} - \boldsymbol{k}')\delta_{ss'}. \tag{A.7}$$

Appendix B

Alternatives Boundary Conditions for Dirac Equation from MIT Bag Model

In this chapter, we briefly review the alternative boundary conditions for the Dirac equation that we use in this study, namely, the BC-MIT [28–30] and BC-chiral MIT [34, 64, 65]. The BC-chiral MIT is a generalization of the BC-MIT, which includes the contribution of the chiral angle. Therefore, we start with a discussion on the BC-chiral MIT for the wavefunction of a relativistic spin-1/2 particle ψ at the boundary surface [64], expressed as

$$iN_\mu\gamma^\mu\psi = e^{-i\gamma^5\Theta}\psi, \tag{B.1}$$

where $\Theta \in [0, 2\pi)$ denotes the continuous chiral angle. Here, N_μ is an inward normal unit vector perpendicular to the boundary surface. At the boundary surface, the BC-chiral MIT ensures a vanishing probability density as

$$
\begin{aligned}
iJ_N = iN_\mu\bar{\psi}\gamma^\mu\psi &= \bar{\psi}e^{-i\gamma^5\Theta}\psi \\
&= -\bar{\psi}e^{-i\gamma^5\Theta}\psi \\
&= 0, \tag{B.2}
\end{aligned}
$$

where the first line comes from the multiplication of both the left- and right-hand sides of BC-chiral MIT (B.1) with $\bar{\psi}(\equiv \psi^\dagger\gamma^0)$ from the left, and the second line comes from the Hermition conjugate of BC-chiral MIT (B.1) multiplyed by $\gamma^0\psi$ from the right [65]. The relations in Eq. (B.2) also indicates that the scalar density $\bar{\psi}\psi$ vanishes when then chiral angle takes values of $\Theta = 0, \pi$, where $\Theta = 0$ represents the non-chiral case. For the non-chiral

case, the boundary conditions (B.1) reduces to BC-MIT [28–30]:

$$iN_\mu\gamma^\mu\psi = \psi. \tag{B.3}$$

Here, the normal probability current and scalar densities vanish at the boundary surfaces (see Eq. (B.2)), as stated above.

Bibliography

[1] S. W. Hawking, Commun. Math. Phys. **43**, 199 (1975).

[2] W. G. Unruh, Phys. Rev. D **14**, 870 (1976).

[3] P. W. Langhoff, Am. J. Phys. **39**, 954 (1971).

[4] R. L. Gibbs, Am. J. Phys. **43**, 25 (1975).

[5] H. Wallis, J. Dalibard, and C. Cohen-Tannoudji, Appl. Phys. B **54**, 407 (1992).

[6] R. Onofrio and L. Viola, Phys. Rev. A **53**, 3773 (1996).

[7] J. Gea-Banacloche, Am. J. Phys **67**, 776 (1999).

[8] H. C. Rosu, Phys. Scr. **65**, 296 (2002).

[9] L. D. Landau and E. M. Lifshitz, *Quantum Mechanics: Non-Relativistic Theory*, 3rd edn. (Butterworth-Heinemann, Oxford, England, 1981).

[10] J. J. Sakurai and J. J. Napolitano, *Modern Quantum Mechanics*, 2nd edn. (Addison Wesley, San Fransisco, 2010).

[11] J. Schwinger, *Quantum Mechanics: Symbolism of Atomic Measurements*, edited by B.-G. Englert (Springer-Verlag, Berlin, 2001).

[12] J. L. Martin and P. Strange, Eur. J. Phys. **42**, 045409 (2021).

[13] A. Martín-Ruiz, A. Frank and L. F. Urrutia, Phys. Rev. D **92**, 045018 (2015).

[14] V. V. Nesvizhevsky *et al.*, Nature **415**, 297 (2002).

[15] V. V. Nesvizhevsky *et al.*, Phys. Rev. D **67**, 102002 (2003).

[16] V. V. Nesvizhevsky *et al.*, Eur. Phys. J. C **40**, 479 (2005).

[17] A. Westphal *et al.*, Eur. Phys. J. C **51**, 367 (2007).

[18] V. V. Nesvizhevsky, F. Nez, S. A. Vasiliev, E. Widmann, P. Crivelli, S. Reynaud, and A. Yu. Voronin, Eur. Phys. J. C **80**, 520 (2020).

[19] G. Ichikawa, S. Komamiya, Y. Kamiya, Y. Minami, M. Tani, P. Geltenbort, K. Yamamura, M. Nagano, T. Sanuki, S. Kawasaki, M. Hino, and M. Kitaguchi, Phys. Rev. Lett. **112**, 071101 (2014).

[20] Y. Kamiya, G. Ichikawa, and S. Komamiya, Adv. High Energy Phys. **2014**, 859241 (2014).

[21] H. Abele, S. Baessler and A. Westphal, Lect. Notes Phys. **631**, 355 (2003).

[22] C. Anastopoulos and B. L. Hu, Class. Quant. Grav. **35**, 035011 (2018).

[23] N. Boulanger, P. Spindel, and F. Buisseret, Phys. Rev. D **74**, 125014 (2006).

[24] A. Saa and M. Schiffer, Phys. Rev. D **56**, 2449 (1997).

[25] N. Nicolaevici, Eur. Phys. J. Plus **132**, 21 (2017).

[26] P. Alberto, C. Fiolhais, and V. M. S. Gil, Eur. J. Phys. **17**, 19 (1996).

[27] P. Alberto, S. Das, and E. C. Vagenas, Phys. Lett. A **375**, 1436 (2011).

[28] A. Chodos, R. L. Jaffe, K. Johnson, C. B. Thorn, and V. F. Weisskopf, Phys. Rev. D **9**, 3471 (1974).

[29] A. Chodos, R. L. Jaffe, K. Johnson, and C. B. Thorn, Phys. Rev. D **10**, 2599 (1974).

[30] K. Johnson, Acta Phys. Polon. B **6**, 865 (1975).

[31] A. Rohim, K. Ueda, K. Yamamoto, and S.-Y. Lin, Int. J. Mod. Phys. D **30**, 2150098 (2021).

[32] A. W. Thomas, Adv. Nucl. Phys. A **13**, 1 (1984).

[33] A. Chodos and C. B. Thorn, Phys. Rev. D **12**, 2733 (1975).

[34] S. Théberge, A. W. Thomas, and G. A. Miller, Phys. Rev. D **22**, 2838 (1980); **23**, 2106(E) (1981).

[35] G. E. Brown and M. Rho, Phys. Lett. B **82**, 177 (1979).

[36] A. Hosaka and H. Toki, Phys. Rept. **277**, 65 (1996).

[37] J. W. Holt, M. Rho, and W. Weise, Phys. Rept. **621**, 2 (2016).

[38] K. Tsushima, T. Yamaguchi, M. Takizawa, Y. Kohyama, and K. Kubodera, Phys. Lett. B **205**, 128 (1988).

[39] G. E. Brown, M. Rho, and V. Vento, Phys. lett. B **84**, 383 (1979).

[40] V. Vento, M. Rho, and G. E. Brown, Phys. Lett. B **103**, 285 (1981).

[41] S. Théberge and A. W. Thomas, and G. A. Miller, Nucl. Phys. A **393**, 252 (1983).

[42] A. W. Thomas, S. Théberge, and G. A. Miller, Phys. Rev. D **24**, 216 (1981).

[43] M. H. Al-Hashimi and U. J. Wiese, Annals Phys. **327**, 1 (2012).

[44] R. N. Mohapatra, J. Phys. G: Nucl. Part. Phys. **36**, 104006 (2009).

[45] R. N. Mohapatra and R. E. Marshak, Phys. Lett. B **94**, 183 (1980).

[46] M. Baldo-Ceolin *et al.*, Z. Phys. C **63**, 409 (1994).

[47] K. S. Babu and R. N. Mohapatra, Phys. Rev. D **91**, 096009 (2015).

[48] S. Gardner and E. Jafari, Phys. Rev. D **91**, 096010 (2015).

[49] S. Gardner and X. Yan, Phys. Rev. D **93**, 096008 (2016).

[50] S. Gardner and X. Yan, Phys. Rev. D **97**, 056008 (2018).

[51] Z. Berezhiani and A. Vainshtein, Phys. Lett. B **788**, 58 (2019).

[52] P. Crivelli, V. V. Nesvizhevsky, and A. Yu. Voronin, Adv. High Energy Phys. **2015**, 173572 (2015).

[53] G. Dufour, D. B. Cassidy, P. Crivelli, P. Debu, A. Lambrecht, V. V. Nesvizhevsky, S. Reynaud, A. Yu. Voronin, and T. E. Wall, Adv. High Energy Phys. **2015**, 379642 (2015).

[54] A. P. Mills and M. Leventhal, Nucl. Instrum. Methods Phys. Res. Sect. B **192**, 102 (2002).

[55] D. B. Cassidy and S. D. Hogan, Int. J. Mod. Phys. Conf. Ser. **30**, 1460259 (2014).

[56] L. L. Foldy and S. A. Wouthuysen, Phys. Rev. **78**, 29 (1950).

[57] E. Eriksen, Phys. Rev. **111**, 1011 (1958).

[58] A. J. Silenko, J. Math. Phys. **44**, 2952 (2003).

[59] A. J. Silenko, Phys. Rev. A **77**, 012116 (2008).

[60] F. W. Hehl and W. T. Ni, Phys. Rev. D **42**, 2045 (1990).

[61] A. J. Silenko and O. V. Teryaev, Phys. Rev. D **71**, 064016 (2005).

[62] S. Ulbricht, R. A. Müller, and A. Surzhykov, Phys. Rev. D **100**, 064029 (2019).

[63] F. Kottler, Ann. Phys. **349**, 701 (1914); **350**, 481 (1914).

[64] C. A. Lütken and F. Ravndal, J. Phys. G: Nucl. Phys. **10**, 123 (1984).

[65] R. L. Jaffe and A. Manohar, Ann. Phys. **192**, 321 (1989).

[66] M. N. Chernodub and S. Gongyo, Phys. Rev. D **95**, 096006 (2017).

[67] V. E. Ambrus and E. Winstanley, Phys. Rev. D **93**, 104014 (2016).

[68] M. N. Chernodub and S. Gongyo, J. High Energy Phys. **01**, 136 (2017).

[69] M. N. Chernodub and S. Gongyo, Phys. Rev. D **96**, 096014 (2017).

[70] A. Rohim and K. Yamamoto, Prog. Theor. Exp. Phys. **2021**, 113B01 (2021).

[71] P. Alberto, S. Das, and E. C. Vagenas, Eur. J. Phys. **39**, 025401 (2018).

[72] M. Alkhateeb and A. Matzkin, arXiv:2103.06538.

[73] V. Alonso and S. De Vincenzo, J. Phys. A: Math. Gen. **30**, 8573 (1997).

[74] G. Menon and S. Belyi, Phys. Lett. A **330**, 33 (2004).

[75] F. M. Toyama and Y. Nogami, Phys. Rev. A **81**, 044106 (2010).

[76] F. M. Toyama and Y. Nogami, Phys. Lett. A **374**, 3838 (2010).

[77] Yu. A. Sitenko, Phys. Rev. D **91**, 085012 (2015).

[78] M. H. Al-Hashimi, A. M. Shalaby, and U. J. Wiese, Phys. Rev. D **95**, 065007 (2017).

[79] Z. Zhang, C. Shi and H.-S. Zong, Phys. Rev. D **101**, 043006 (2020).

[80] I. M. Frank, in *Proceedings of International Conference on Nuclear Study with Neutrons*, Budapest, 1972, p.285.

[81] A. I. Frank, Sov. Phys. Usp. **34**, 980 (1991) [Usp. Fiz, Nauk **161**, 95 (1991)].

[82] A. I. Frank, P. Geltenbort, G. V. Kulin, D. V. Kustov, V. G. Nosov, and A. N. Strepetov, JETP Lett. **81**, 427 (2005).

[83] A. I. Frank, V. I. Bodnarchuk, P. Geltenbort, I. L. Karpikhin, G. V. Kulin, and O. V. Kulina, Phys. Atom. Nucl. **66**, 1831 (2003).

[84] A. I. Frank, P. Geltenbort, G. V. Kulin, and A. N. Strepetov, JETP Lett. **84**, 105 (2006).

[85] A. I. Frank, P. Geltenbort, M. Jentschel, D. V. Kustov, G. V. Kulin, V. G. Nosov, and A. N. Strepetov, Phys. Atom. Nucl. **71**, 1656 (2008).

[86] G. V. Kulin, A. N. Strepetov, A. I. Frank, P. Geltenbort, S. V. Goryunov, M. Jentschel, and D. V. Kustov, Phys. Lett. A **378**, 2553 (2014).

[87] A. I. Frank, JETP Lett. **100**, 613 (2014).

[88] F. V. Kowalski, Phys. Lett. A **182**, 335 (1993).

[89] Y. N. Pokotilovski, arXiv:1805.05292.

[90] K. Tanaka, Phys. Rev. A **25**, 385 (1982).

[91] V. I. Lushchikov, Yu. N. Polotilovskii, A. V. Strelkov, and F. L. Shapiro, Pis'ma v ZhETF **9**, 40 (1969); JETP Lett. **9**, 23 (1969).

[92] A. Steyerl, Phys. Lett. **B 29**, 33 (1969).

[93] V. V. Nesvizhevsky, A. K. Petukhov, K. V. Protasov, and A. Yu. Voronin, Phys. Rev. A **78**, 033616 (2008).

[94] V. V. Nesvizhevsky, A. Yu. Voronin, R. Cubitt, and K. V. Protasov, Nature Phys. **6**, 114 (2010).

[95] E. Fermi, Ricerca Scientifica **7** 1352 (1936), English translation in E. Fermi, *Collected Papers, vol. I, Italy 1921-1938*, (University of Chicago Press, Chicago, 1962) pp. 980-1016.

[96] P.A. Zyla *et al.*, (Particle Data Group), Prog. Theor. Exp. Phys. **2020**, 083C01 (2020); https://pdg.lbl.gov/2020/listings/rpp2020-list-n.pdf

[97] M. Abramowitz and I. A. Stegun, *Handbook of Mathematical Functions with Formulas, Graphs, and Mathematical Tables*, ninth Dover printing, tenth GPO printing (Dover, New York, 1964).

[98] T. Kawai, Acta Phys. Polon. A **96**, 19 (1999).

[99] G. L. Squires, *Introduction to the theory of thermal neutron scattering* (Cambridge University Press, 1978); (Dover edition, Mineola, New York, 1996)

[100] L. C. B. Crispino, A. Higuchi, and G. E. A. Matsas, Rev. Mod. Phys. **80**, 787 (2008).

[101] A. Higuchi, S. Iso, K. Ueda, and K. Yamamoto, Phys. Rev. D **96**, 083531 (2017).

[102] E. M. Ferreira and J. Sesma, J. Comput. Appl. Math. **211**, 223 (2008).

[103] H. Lass, Am. J. Phys. **31**, 274 (1963).

[104] N. D. Birrell and P. C. W. Davies, *Quantum Fields in Curved Space* (Cambridge University Press, Cambridge, UK, 1982).

[105] G. E. A. Matsas and D. A. T. Vanzella, Phys. Rev. D **59**, 094004 (1999).

[106] D. A. T. Vanzella and G. E. A. Matsas, Phys. Rev. Lett. **87**, 151301 (2001).

[107] H. Suzuki and K. Yamada, Phys. Rev. D **67**, 065002 (2003).

[108] K. Ueda, A. Higuchi, K. Yamamoto, A. Rohim, and Y. Nan, Phys. Rev. D **103**, 125005 (2021).

[109] A. Aste, Symmetry **2**, 1776 (2010).

[110] P. B. Pal, Am. J. Phys. **79**, 485 (2011).

[111] W. Greiner, *Relativistic Quantum Mechanics: Wave Equations*, 3rd edn. (Springer-Verlag, Berlin, 2000).

[112] C. Itzykson and J.-B. Zuber, *Quantum Field Theory* (McGraw-Hill, New York, 1980).

[113] D. Oriti, Nuovo Cim. B **115**, 1005 (2000).

[114] P. Longhi and R. Soldati, Int. J. Mod. Phys. A **28**, 1350109 (2013).

[115] R. B. Mann and M. B. Young, Class. Quant. Grav. **24**, 951 (2007).

[116] D. J. Griffiths, *Introduction to Quantum Mechanics* (Prentice Hall, New York, 1995).

[117] S.-Y. Lin, Phys. Rev. D **101**, 124001 (2020).

[118] H. Abele, Prog. Part. Nucl. Phys. **60**, 1 (2008).

[119] T. Jenke, P. Geltenbort, H. Lemmel, and H. Abele, Nat. Phys. **7**, 468 (2011).

[120] G. Cronenberg, P. Brax, H. Filter, P. Geltenbort, T. Jenke, G. Pignol, M. Pitschmann, M. Thalhammer, and H. Abele, Nat. Phys. **14**, 1022 (2018).

[121] R. I. P. Sedmik *et al.,* EPJ Web Conf. **219**, 05004 (2019).

[122] G. Pignol, S. Baessler, V. V. Nesvizhevsky, K. Protasov, D. Rebreyend and A. Voronin, Adv. High Energy Phys. **2014**, 628125 (2014).

[123] M. D. Pollock, Acta Phys. Polon. B **41**, 1827 (2010).